INVOLVEMENT OF A SPECIFIC UBIQUITIN LIGASE IN THE ASSEMBLY OF THE DYNEIN MOTOR IN THE FILAMENTOUS FUNGUS *NEUROSPORA CRASSA*

A DISSERTATION IN
Cell Biology and Biophysics
and
Molecular Biology and Biochemistry

Presented to the Faculty of the University
of Missouri-Kansas City in partial fulfillment of
the requirements for the degree

DOCTOR OF PHILOSOPHY

by
RYAN LEE ELSENPETER

M.S., University of Missouri-Kansas City, Kansas City, MO 2007
B.S., University of Wisconsin-La Crosse, La Crosse, WI, 2005

Kansas City, MO
2012

INVOLEMENT OF A SPECIFIC UBIQUITIN LIGASE IN THE ASSEMBLY OF THE DYNEIN MOTOR IN THE FILAMENTOUS FUNGUS *NEUROSPORA CRASSA*

Ryan Lee Elsenpeter, Candidate for the Doctor of Philosophy Degree

University of Missouri-Kansas City 2012

ABSTRACT

Eukaryotic cells utilize multiple molecular motor proteins to accomplish intracellular transport. The two microtubule based motors, kinesin and cytoplasmic dynein, work in concert to move cargoes outward and inward, respectively, in the cell. In polarized cells, molecular motors are of even greater importance due to a need for long distance transport and maintenance of proper polarity. Although there exists numerous forms of kinesin for anterograde transport, only a single cytoplasmic form of dynein carries out the functions of retrograde transport. To accomplish its tasks, dynein makes use of multiple subunits and accessory proteins, including heavy chains, light chains, intermediate chains, light intermediate chains, and dynactin to form a motor complex of several megadaltons. The last two thirds of the dynein heavy chains contain the main motor unit required for force production, while the N-terminal tail region of the dynein heavy chain along, with other dynein components, aid in cargo binding. Force production and microtubule-based movement is accomplished by coordinating ATP hydrolysis in the motor heads with a microtubule-binding domain. The tail domain allows for both homodimerization of motor heads as well as binding of other dynein subunits.

In this work, various genetic, cell biology, and biochemical methods were used to study cytoplasmic dynein in the filamentous fungus, *Neurospora crassa*. Numerous dynein heavy chain mutants were isolated previously from a genetic screen, with a subset located to the C-terminal region, which were the focal point of this work. To explore the mechanism by which these mutations affect dynein function, both intragenic and extragenic suppressors were identified. A novel extragenic suppressor of dynein mutations was discovered, a gene encoding a putative E3 ubiquitin ligase with homologs present in higher organisms, including humans. Mutation or deletion of the suppressor gene results in restoration of wild type-like growth and *in vivo* dynein localization for each of the C-terminal dynein heavy chain mutants, as well as certain other dynein heavy chain mutants. Results suggest that the activity of this protein affects interaction of dynein heavy chain with dynein intermediate chain and likely is a regulator of dynein motor assembly.

APPROVAL PAGE

The faculty listed below, appointed by the Dean of the School of Graduate Studies, have examined a dissertation titled, “Involvement of a specific ubiquitin ligase in the assembly of the dynein motor in the filamentous fungus *Neurospora crassa*,” presented by Ryan Lee Elsenpeter, candidate for the Doctor of Philosophy degree, and certify that in their opinion it is worthy of acceptance.

Supervisory Committee

Michael Plamann, Ph.D., Committee Chair
Cell Biology and Biophysics

G. Sullivan Read, Ph.D.
Cell Biology and Biophysics

Thomas Menees, Ph.D.
Cell Biology and Biophysics

Leonard Dobens, Ph.D.,
Molecular Biology and Biochemistry

Stephen King, Ph.D.,
Burnett School of Biomedical Sciences

CONTENTS

ILLUSTRATIONS

Figure Page

TABLES

Table Page

AKNOWLEDGEMENTS

This dissertation is about much more than the research described in these pages. My gratitude for the hard work and sacrifice of so many involved over the last handful of years cannot be expressed in simple words. Without the dedication of my advisor, Dr. Mike Plamann, I would have fallen flat on my face early on. But through numerous chalk board sessions and lab discussions, my abilities were sharpened and ideas were launched that brought forth meaningful results and successes, even amongst times of stress and disappointment. Beyond just science, my time in his lab was rewarding and I greatly appreciate the opportunity to complete this project under his advising. I would not have had any success in the lab if it were not for the aid of Rob Schnittker. Not only was he instrumental in completing numerous experiments and maintaining the almost infinite number of strains needed for this research, but he was always willing to listen to my frustrations and share in my accomplishments, both science related and not.

I am grateful for excellent committee members Dr. Steve King, Dr. G. Sullivan Read, Dr. Len Dobens, and Dr. Tom Menees. Without their help throughout the project, many ideas would have never been brought forth and the research would not have come as far as it did. I would like to thank the members of Dr. Steve King's lab, especially Drs. Senthilkumar Sivagurunathan and David Razafsky, who aided in many purifications and biochemical experiments.

To all of my family and friends, I am eternally grateful for your support, not only over the last several years of this research, but from day one. My parents, Robert Elsenpeter and Tim and Jill Puff, deserve much praise and thanks. They saw something in me before I did and their help and encouragement through the years was a real

cornerstone to my life's successes. All of my friends through the years, too many to name, I give my thanks for your help, in school and in life in general. Through good times and bad, my family and friends were always there to offer a hand, whether in assistance or congratulations.

My wife, Celesta Elsenpeter, deserves more credit than I for this dissertation. She is the real foundation of this work, having the uncanny ability to know when to let me rant and complain and when to encourage me to keep pushing. Without her love and support, I would not be who I am today. I love you dearly. Thank you.

CHAPTER 1

INTRODUCTION

To function properly and remain well organized, eukaryotic cells depend on molecular motor systems to transport various cargoes throughout their cellular space. To accomplish their tasks, molecular motors utilize the energy from ATP to travel upon cytoskeletal tracks of either actin filaments or microtubules, which not only provide roadways for molecular motors but also overall structure and support for the cell. For more efficient movement of cargoes, different classes of molecular motors will bind to a cargo, allowing for both bi-directional movement as well as movement between the two cellular track systems (105, 166).

For shorter movements, myosin motors utilize the actin cytoskeleton, while dynein and kinesin motors move along microtubules for longer range, more processive trips (133, 96). Myosin most often functions as a dimer of heavy chains along with a pair of light chains, although certain myosins can function as a single motor head (61). Various classes of myosin exist with the major class involved in transport along actin filaments being myosin V (180). In filamentous fungi, four different myosin motors are utilized for actin-based motility (153).

The bulk of cargo transport occurs along the microtubule lattice by the kinesin and dynein motors. Microtubules have inherent polarity, with the plus-end near the cell periphery and the minus-end at the cell center, and movement along these tracks can occur bi-directionally. Kinesin moves anterograde toward the plus-end, while dynein moves retrograde toward the minus-end of the microtubule (133). Kinesin often exists as a dimer of heavy chains with motor heads, albeit without the aid of light chains. Both

multi-headed kinesins, such as kinesin-5, which is a homotetramer of four motor heads, as well as single headed varieties, do exist (153, 104). Much is understood of the kinesin family of motors, comprising over forty genes in mammals and over ten in the filamentous fungi (153, 110, 68).

Dynein, the most complex of the motor proteins, functions as a dimer of heavy chains in concert with various accessory proteins, including light chains, dynactin complex, and lissencephaly 1 (Lis1) (184, 71, 60). Only three different varieties of dynein exist, axonemal dynein found in cilia and flagellum, and two cytoplasmic forms, one of which carries cargoes in the flagellum and the other in the cytoplasm along microtubules (hereafter referred to as dynein). Dynein works in concert with kinesin to move various cargoes throughout the cell along microtubules. Unlike kinesin, less is understood of the overall function and mechanochemistry of dynein based cytoskeletal movements.

Cellular Roles of Dynein

Various cellular roles of the dynein motor complex include trafficking of cargoes along microtubules, nuclear and organelle positioning, and spindle orientation during mitosis. Discussed at further length on later pages, the dynein complex accomplishes its various cellular roles through the coordination of numerous subunits. Three main subunits are of greater importance to this research: dynein heavy chain (DHC), dynactin, and lissencephaly 1 (Lis1).

The DHC is composed of six ATPases associated with diverse cellular activites (AAA) domains. The largest subunit of the overall dynein complex, DHC contains

ATPase enzymatic activities that drive the complex along the microtubule tracks carrying with it various cargoes throughout the cell. It contains sites for attachment of the various accessory proteins that assist DHC in accomplishing its tasks. A major accessory protein of DHC is dynactin, which is made up of various subunits that aid the dynein complex in both cargo binding and processivity toward the microtubule minus end. The other DHC accessory protein of relevance to this research is Lis1. Lis1 is a DHC interactor that acts as a regulator of dynein via its ATPase activity and also aids in microtubule affinity of dynein (201). In humans, Lis1 mutations can lead to lissencephaly, or smooth brain disorder. (141)

Cargo Trafficking

A major role of the cytoplasmic form of dynein is to transport cargoes toward the minus end of microtubules. There exist a wide variety of cargoes that are transported by the dynein complex, which includes various organelles (168), neurofilaments (187), RNA (82), receptor tyrosine kinases (19), and Doc2, which is involved in neurotransmitter release (123). Dynein carries out transport through various interactions, either directly to cargoes or through its various associating protein partners. Dynein plays a critical role in the process of endocytosis (35). During endocytosis, extracellular materials are internalized into the cytoplasm, forming vesicles. Upon formation of the vesicles by invagination of the plasma membrane, further processing results in the formation of late endosomes, which can then be transported along microtubule tracks to various locations. The Rab GTPases, proteins associated with endosomal vesicles, interact with the dynein complex to carry out transport throughout the cell (79). When dynein function is

perturbed by various means, endosomal transport is also disrupted, indicating a direct role of dynein in vesicle transport (35, 87).

Cell Division

During mitosis, dynein localizes to the cell cortex, spindle poles, and kinetechores. Dynein is involved in orientation of the mitotic spindle, as dynein/dynactin has been found at cortical spots and along astral microtubules (18, 129). Although there is not a consensus on the role of dynein at the kinetochore, dynein is thought to aid in microtubule attachment, movement of chromosomes, and regulation of the spindle assembly checkpoint (135, 170, 200, 194). Numerous mutational and disruption studies have further solidified dynein's role in various aspects of mitosis. These studies include changes to mitotic spindles in normal rat kidney (NRK) cells (129), inactivation of spindle checkpoints and inhibition of kinetochore disassembly in *D. meanogaster* (196), disruption of LIS1 binding to kinetochore by over expression of the dynactin subunit dynamitin (p50) (176), and mutations in ZW10 eliminating dynein localization to the kinetechores in *D. melanogaster* (167). When a dynein light chain member of Tctex1 (DYNLT3) was knocked down by siRNA, progress through mitosis was slowed, indicating dynein is required for effective progression through the cell cycle (101).

Nuclear Migration and Positioning

Without proper positioning of nuclei, cells cannot properly undergo numerous activities, including mitosis, cell differentiation, cell migration, and establishment of polarity. Of relevance to this dissertation is the role of the dynein complex in nuclear

migration and positioning in filamentous fungi. A hallmark of *N. crassa* ropy mutants containing mutations in dynein/dynactin/Lis1 genes is their inability to properly distribute nuclei in the hypha (136, 9). The Lis1 complex of the dynein motor is required for nuclear movements in *A. nidulans* (132). Recent studies in *A. gossypii* implicated dynein as the single motor unit responsible for prevention of nuclear clustering (56). In *C. albicans*,normal morphogenesis is dependent on proper nuclear division and nuclear distribution within budding yeast cells and the filamentous forms and is reliant on functional dynein complexes (42). Various studies in multiple organisms have revealed interactions between the nuclear envelope and subunits of the dynein complex (158, 106, 100, 19). These studies strongly support a role for dynein in nuclear migration and positioning.

Organelle Positioning

To carry out their proper functions, organelles must be located at various places in the cell and must be able to be moved if needed. The dynein complex is intimately involved in this process. When antibodies against dynein intermediate chain (DIC) were injected into *X. laevis* oocytes, organelle movement was eliminated (167). Bidirectional movement of organelles along microtubules, moved by kinesin and dynein, is facilited by p150 of dynactin, as discovered in *Xenopus* (30). The transport and alignment of endosomal vesicles is also dependent upon the dynein complex (73). In *N. crassa*, a loss of distinct cytoplasmic regions near the hyphal tip was seen in dynein mutant strains as well as changes to motility and positioning of mitochondria (144). Together, these data indicate the importance of dynein's role in organelle positioning.

Cell Quality Control

Data is accumulating that links the dynein complex with recycling of misfolded proteins in the cell (46, 169, 188). If proteins cannot be properly refolded following denaturation, they are marked for degradation by the ubiquitin-proteasome degradation pathway. This turnover is especially important in neurons, as denatured proteins can form neurofibrillary tangles that have been implicated in various brain diseases. When the systems in place to recycle misfolded peptides are overwhelmed, aggresomes are formed. These complexes consist of various aggregates of misfolded proteins are formed with the help of the dynein complex (46). Bap31, an endoplasmic reticulum (ER) protein implicated in ER-associated degradation, has a normal cycling pattern between the ER and Golgi during ER's quality control. ER quality control and subsequent cycling of Bap31 was disrupted when microtubules were depolymerized or when the dynein complex was disrupted (186). Recently, the Gβ protein, involved in cell signaling, was shown to bind the Lis1 complex of the dynein motor during ubuqitin-mediated turnover or aggresome development (188). From these studies, dynein is implicated as an important participant in cell quality control.

Dynein dysfunction and connections to disorders

Dynein is involved in numerous cellular activities and any mutations in the members of the complex can lead to disorders and diseases. Due to its roles during mitosis, dynein mutations may lead to cases of aneuploidy and possibly cancer (128, 137, 11). Other issues with improper chromosomal disjunction can produce various disorders like Turner's or Down syndrome.

Defects in nuclear migration due to mutations in the *lis1* gene cause Lissencephaly. This disease is characterized by a smooth brain lacking the normal folds and grooves and is due to a lack of proper migration of neural progenitor cells during fetal development. Lissencephaly leads to severe neurological issues and often death at a very young age (141).

In neurons, dynein activity is necessary for the long-range transport of cargo from axonal termini to the neuronal cell body. A disruption to the dynein complex leads to limitations or elimination of this important role of dynein in polarized neurons. Numerous neurological disorders are linked to the inability of dynein to aid in the movement of protein aggregates, including Parkinson's disease (177), Huntington's disease (24), and Alzheimer's disease (84). Recent studies found that a decrease in dynein activity via siRNA increased the population of Rab GTPases involved in membrane trafficking in a monkey brain. Further, β-amyloid precursor protein aggregates increased in these brains, suggesting a role for dynein based recycling in both Alzheimer's disease and general aging of the brain (84, 12). Changes in overall behavior due to altered neuronal development were first seen in a mouse model with mutation in the dynein light intermediate chain, DLIC1. A point mutation leading to an amino acid change of N235Y led to a marked increase in anxiety in the mouse carrying the mutation (2). Another study found that drop in the expression of DIC (dynein intermediate chain) in the frontal cortex of Alzheimer's disease patient's brains. Changes to the frontal cortex lead to changes in behavior, motor skills, and problem solving abilities (117).

The accumulation of protein aggregates in transmissible neurodegenerative disorders is of great interest due to the effects on both humans and important animal

species. These so called prion diseases are caused by an accumulation of aggregates of the host specimen's cellular prion protein (PrPC). This build up of PrPC is the hallmark of Creutzfeld-Jacob disease in humans (23) and chronic wasting disease (CWD) in deer, elk, and moose (38). Molecular motors mediate the transport of these prion aggregates and disruptions in one or both of kinesin and dyneincan lead to accumulation of these protein complexes and advancement of the disease (38).

Charcot-Marie-Tooth disease, consisting of axonal degeneration leading to distal sensory loss, skeletal deformities, and deep tendon reflex abnormalities has been linked to dynein mutations. A recently completed pedigree of a family with numerous members stricken with the disease revealed a single base change in DHC, H306R (192). This mutation is located in the homodimerization domain of DHC, which has been shown to be the location of mutations in mouse models that lead to various neurodegenerative disorders (59, 25).

Besides the various neurological diseases that dynein disruption contributes, viruses are known hijackers of the dynein complex for transport through the cell and efficient infection. Studies have revealed connections between viral proteins and dynein complex members, including the light chains, LC8 and Tctex1 (140, 8). When p50 of dynactin is overexpressed or infected cells are incubated with peptides that outcompete viral proteins for dynein, retrograde transport of viral components is hindered (108). It is clear from the above studies that greater understanding of dynein function and activity is of utmost importance for better treatment of various human diseases and disorders.

Dynein Studies in Various Model Organisms

Different model systems have been used recently to study the function, structure, and mechanochemistry of the dynein motor complex. Studies from *D. melanogaster* and *X. laevis* have revealed the role of dynein during embryonic development in mRNA positioning for axis polarity as well as the role of dynein in various cargo movements (12, 86, 111). Early studies of the structure and powerstroke of DHC were completed using axonemal dynein from the model organism *C. reinhardtii* (14). More recent high-resolution crystal structures have been completed for DHC from both *S. cerevisiae* and *D. discoideum* (20, 91). Along with studies in *S. cerevisiae*, other fungal systems serve as models for the study of the dynein complex. Work in *A. nidulans* first identified the dynein regulatory factor nudE (Lis1) and work is ongoing to elucidate more detail on the functional role of nudE/Lis1 in the filamentous fungus (185, 37).

This work utilized the filamentous fungus *N. crassa* to study dynein function because of its advantages as a model organism. Due to its filamentous growth, the fungus serves as a good model for long-range transport by dynein along microtubules and mimics both neuronal growth and maintenance. Many components of the dynein complex are conserved between *N. crassa* and higher eukaryotes and dynein functions in numerous activities that are common between many species as well. Dynein is not required for cell viability in *N. crassa*, thus any developmental defects or embryonic lethality issues do not come into play during study. Dynein mutants display a very distinct and unique growth phenotype that allows for their easy identification and isolation in the fungus. Lastly, because *N. crassa* has a haploid genome, mutations that arise in a single locus of a dynein gene will lead to a homogenous population of motors.

Dynein Structure and Organization

Dynein is a 1.6 mega Dalton protein complex comprises numerous protein subunits. The major component is the dynein heavy chain (DHC), which consists of approximately 4300-4600 amino acids depending upon the organism of origin. The DHC contains different regions, an N-terminal tail, a ring of AAA (ATPases associated with diverse cellular activities) domains, and a microtubule-binding domain (Figure 1). Structures garnered from electron microscopy on *C. reinhardii* flagellar dynein showed the motor ring structure with an external diameter of 10-14 nm, a central cavity of 2.5 nm, and seven total lobes (Figure 2) (15). Image analysis and model fitting using structural data from studies on cytoplasmic dynein from *D. discoideum* indicated that six of the lobes from the EM images represent the six AAA domains of DHC with the seventh being that of the globular C-terminal domain (116, 152). These studies also revealed two projections from the AAA ring portion, representing the N-terminal tail (20-30 nm) and the microtubule-binding stalk (13-15 nm). The overall length of DHC as determined from these data is approximately 50 nm.

Recent crystal structures completed on both yeast and *D. discoideum* cytoplasmic dynein provide further detail of the overall structure and organization of the DHC, including the newest structure with a resolution of 2.8 Å (Figure 3) (91, 21, 20). These data provide further insight into the structures and proposed mechanisms of specific regions of the DHC and will be discussed in further detail in later sections.

Two individual DHC peptides interact through the N-terminal tail region to form DHC homodimers (14, 146). The tail region of the DHC is needed for proper cargo binding and for proper interaction of the dynein motor complex subunits, including the

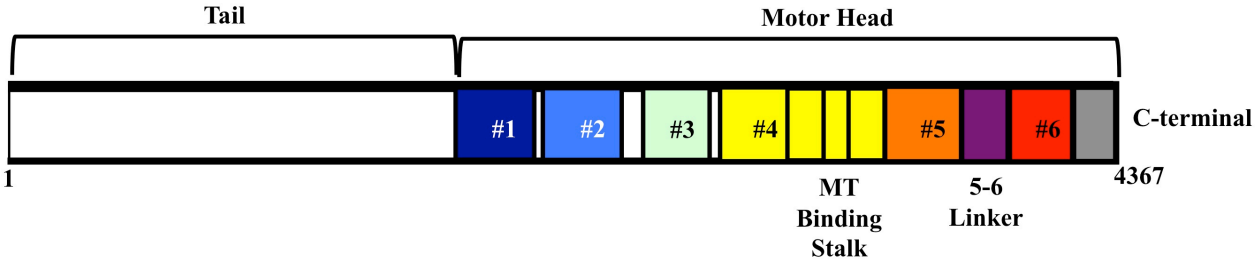

Figure 1. Linear depiction of the DHC subunit of the dynein complex. The cartoon was produced using *N. crassa* dynein heavy chain (DHC) (accession number XP_962616.1) as template and domain boundaries determined from *S. cerevisiae* structural data (PDB 3QMZ). AAA domains are numbered 1-6 followed by a grey C-terminal domain. This C-terminal domain is truncated in relation to mammalian DHC.

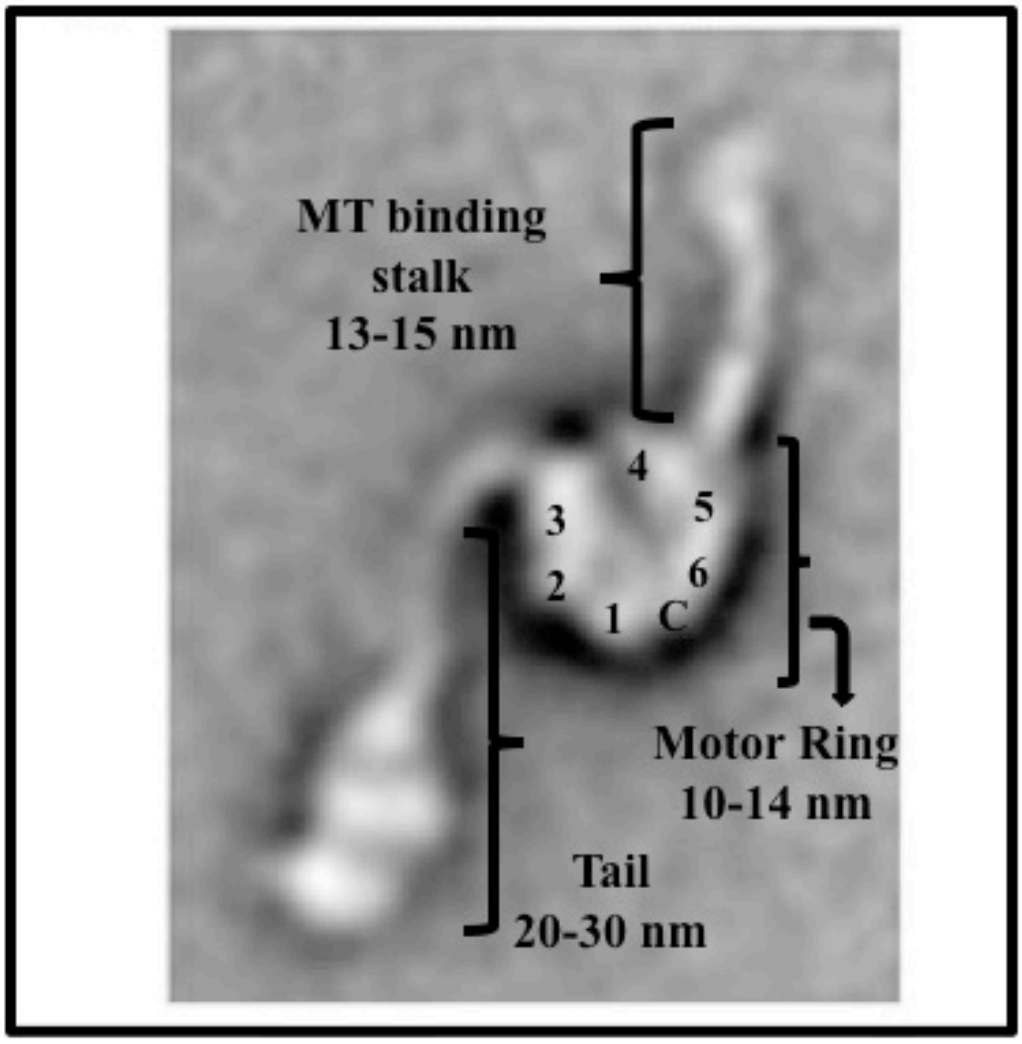

Figure 2. Electron micrograph of DHC. Dyenin heavy chain (DHC) is shown in a nucleotide bound state (ADP.Vi) with visible projections from the central ring of AAA domains (Labeled 1-6, C). Below the AAA ring is the N-terminal tail and above the microtubule binding stalk. In the middle of the AAA ring is a central cavity (2.5 nm) that is not visible, possibly due to the linker portion of the N-terminal tail. (Adapted from reference 14)

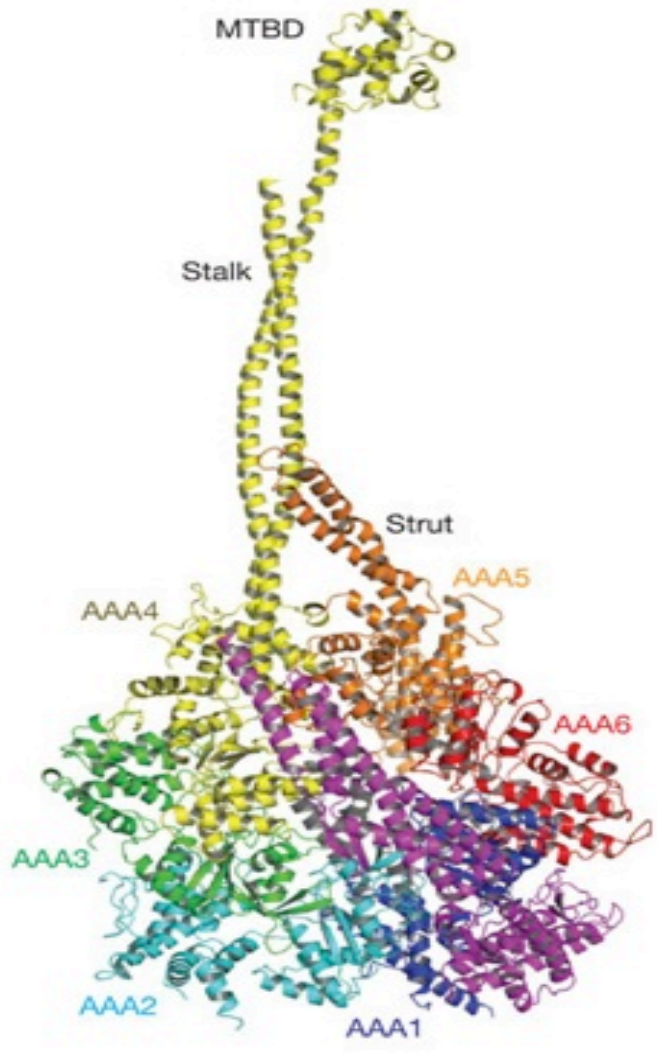

Figure 3. Crystal structure of DHC from *Dictyostelium discoideum*. A recent structure of the 380-kDa dynein motor from *D. discoideum* solved to a resolution of 2.8 Å (PDB 3VKH) with AAA domains, stalk and strut, and microtubule binding domain (MTBD) labeled. The pink structure in front is the linker portion of the N-terminal tail. On the opposite side of the ring lies the C-terminal domain (not shown). Missing is the remaining structure of the N-terminal tail. (Adapted from reference 91)

joining of the two DHC monomers (15). Studies suggest a flexible region of the N-terminal tail that moves during the ATPase powerstroke of the DHC. This flexible portion of the tail is thought to shift its position across the AAA ring structure during the power stroke, changing contacts near the C-terminal area to contacts in and around AAA2/3 (146). When the tail region is eliminated, a loss of unidirectional movement and ATP dependent microtubule release is seen for the dynein complex (77). A change in overall enzymatic behavior was seen for a dynein motor that was missing the N-terminal tail region. This recombinant form of the motor had both a 6-fold increase in ATP hydrolysis compared to the full-length peptide and had a loss of sensitivity to vanadate-mediated inhibition of ATPase activity (72).

The heart of the dynein complex is the motor head, a member of the oligomeric AAA superfamily, composed of six AAA domains, AAA1 through AAA6, each with differing abilities as ATPases (124, 78). A characteristic model of a typical AAA family member is shown in Figure 4. Each AAA domain shares both structural and sequence similarity to other domains in the AAA family. Each module contains signature features that participate in the mechanochemical cycle of the dynein complex. The first is the Walker A motif, containing the signature P-loop, which is involved in both magnesium ion coordination and ATP binding. The actual hydrolysis of the bound phosphate is achieved by the Walker B motif (51, 52, 129, 92, 115). The Sensor 1, found between Walker A and B in the SRH (second region of homology), is a conserved polar residue, often asparagine, that interacts with the ATP γ-phosphate and is involved in discerning between ADP and ATP bound states (83, 64). Near the C-terminal end of the AAA

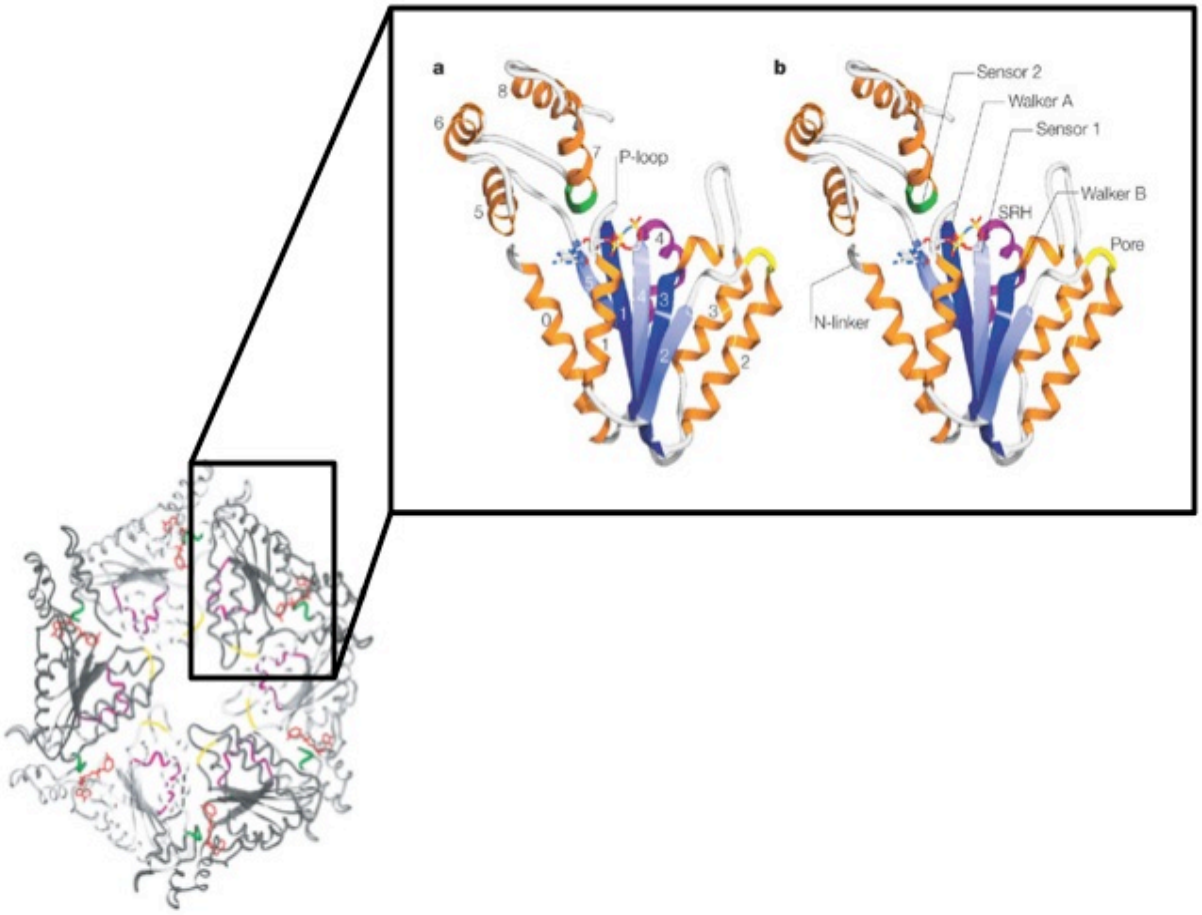

Figure 4. Structure of typical AAA domain from NSF. Both the AAA hexameric ring and an individual AAA domain are shown from N-ethylmaleimide sensitive factor (NSF103) (PDB 1D2N). Labeled are the major structural elements in the AAA domain. SRH is the second region of homology. Bound nucleotide is shown in stick form with the Mg^{2+} not shown. (Adapted from reference 62)

domain lies the sensor 2. An arginine in sensor 2 is also involved in binding of ATP in the pocket (64). Arginine fingers in the SRH help to stabilize the ATP while aiding in communication of nucleotide binding and hydrolysis between neighboring AAA domains (131, 189).

Dynein contains AAA domains of similar architecture to the standard motifs found in typical AAA proteins. Recent model data from *D. discoideum* dynein found that each AAA domain consists of a larger and smaller subdomain. The large subdomain is composed of five α-helices arranged around a five-stranded β-sheet while the smaller subdomain contains five α-helices with the two subdomains connected by a linker (Figure 5) (91).

AAA 1-4 Domains

Although DHC contains six AAA modules, only AAA1-4 contain the needed motifs for ATP binding and hydrolysis. AAA1 contains a P-loop that is conserved between both the cytoplasmic and axonemal forms of dynein and has been shown to be the primary site of ATP hydrolysis from both *in vitro* vanadate-mediated photocleavage experiments (52) and *in vivo* DHC mutational analyses (47). Although the main site of hydrolysis is in AAA1, adjacent elements present in AAA2 are a needed part of ATPase activity (176). In addition to the P-loop in AAA1, AAA3 has a well conserved P-loop as well. Mutational studies in *Drosophila* indicated that changes to P-loop 3 alter the ATP-dependent release of dynein complex from microtubules while not changing ATP binding or hydrolysis at AAA1 (160). Studies in yeast also indicated a role of the ATP binding

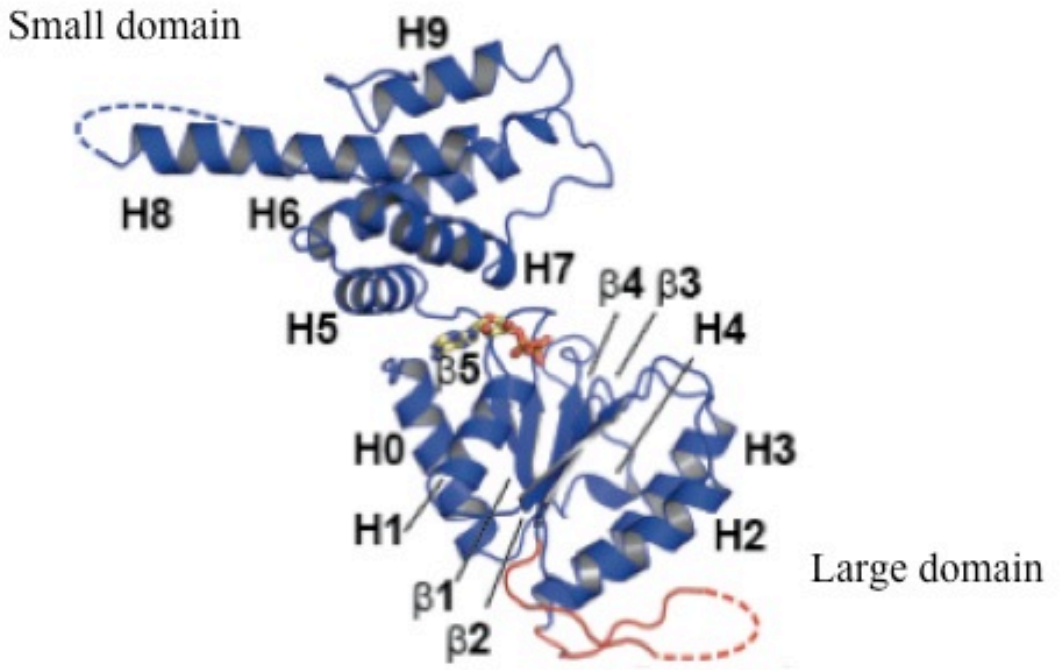

Figure 5. AAA1 domain of DHC. Shown is a crystal structure in ribbon form of DHC AAA1 from *Dictyostelium discoideum*. Labeled are the large domain (helices H0-4 and β-strands β1-5) and small domain (helices H5-9). Bound nucleotide is shown in stick form between the two domains. (Adapted from reference 91)

site in AAA3 in microtubule binding and overall dynein force production and processivity (26). The most recent structure indicated that AAA1, AAA3, and AAA4 all contain the needed motifs to hydrolyze ATP, while AAA1 was determined to be the primary site for hydrolysis based on microtubule-stimulated ATPase assays (91). Other elements in AAA1-4 are seemingly involved in overall dynein complex communication during the ATPase cycle and movement along microtubules. EM studies revealed a change in the orientation of the linker portion of the N-terminal tail across the face of the AAA ring, between AAA2 and the stalk base (146). Another recent crystal structure of the dynein motor domain revealed a gap between AAA1 and AAA2 at the ATP binding site (20). It is thought that binding of ATP into this pocket may induce a change in structural conformation of the dynein ring and is involved in communication across the ring face and up to the MTBD (20). Since each of the AAA1-4 domains contain consensus Walker motifs, it has been proposed that sites other than those of AAA1 and AAA3 have a role in regulation of dynein function (51, 114). In agreement, based on the most recent structure, it was found that the characteristic motifs of the other AAA domains are changed in AAA2 and that the arginine fingers from AAA3 make contact with bound nucleotide in AAA2 (91). This suggests that AAA2, while able to bind nucleotide, does not hydrolyze it, but may be involved in overall ATPase cycle regulation.

Microtubule-binding Domain

The dynein motor complex makes contact with microtubule tracks via a microtubule binding domain (MTBD) situated at the end of an approximately 10 nm long antiparallel coiled-coil protruding from the AAA ring between AAA4 and AAA5 (47, 88,

92, 146, 90, 20). The MTBD was discovered after deletions of the region containing it rendered dynein unable to bind microtubules (47, 92). When ATP is present in the AAA1 binding site, affinity for microtubules is reduced and when the MTBD rebinds to a microtubule, the ATPase powerstroke is activated (75). Recent work, including crystal structure data, indicates that conformational changes along the coiled coil domain are important for communication between the MTBD and the AAA ring (49, 21, 146, 20).

AAA5-6 Domains

Although both AAA5 and AAA6 do not contain consensus Walker sequences and most likely are not required for DHC enzymatic activity (130, 124), when this region of DHC is eliminated, changes in overall dynein activity occur (72). This region of the dynein motor is likely important for overall structure of the AAA ring as well as communication throughout the ATPase cycle and movement along microtubules. Recent structures include the addition of a buttress or strut coiled-coil protruding from AAA5, which conceivably serves as a physical support to the MTBD stalk coiled-coil during times of load and force generation (Figure 3) (90, 20). The newest crystal structure supports the idea that the strut is not only important for support, but is involved in communication between the MTBD and the main site of ATP hydrolysis in AAA1 (91). This structure also contained a new globular structure on AAA5, termed the AAA5 extension. Thus far, its functional role is unknown (91).

C-terminal Domain

A globular C-terminal domain of about 300-600 residues, depending on the organism, follows AAA6 and closes the motor ring with AAA1 (72). Seemingly, the C-terminal domain takes part in regulation of dynein function. Studies removing a 32 kDa portion of the C-terminal region of DHC resulted in a reduction of the ATPase activity in AAA1 and the elimination of vanadate-mediated photocleavage in AAA1 (47, 72). Additionally, in the truncated DHC lacking the C-terminal region of the peptide, the protein no longer displayed vanadate-mediated inhibition of ATPase activity and had a 6-fold increase in overall ATPase activity as compared to a full-length motor (72). These results suggest the C-terminal domain of DHC is playing a regulatory role in overall dynein activity. In the newest crystal structure, the C-terminal domain was found to lie on one face of the AAA ring opposite the linker region of the N-terminal tail, making contact with portions of AAA1, AAA5, and AAA6 (Figure 3) (91). Interestingly, the C-terminal domain in fungi, including *N. crassa*, is much shorter than in other higher organisms. This may indicate a different role in overall dynein function in these organisms.

Dynein Heavy Chain Conformational Changes and the Power Stroke

Early EM imaging results led investigators to the conclusion that dynein undergoes a power stroke during the ATPase cycle to generate force for walking along its microtubule tracks (13, 14). Although all of the details regarding the mechanochemistry involved in dynein motility along microtubules are not yet fully elucidated, models can be proposed based on the numerous studies thus far completed. As the nucleotide status

of the AAA ring changes from unprimed (ADP+Pi) to primed (ATP), various changes occur throughout the DHC (Figure 6) (146, 22). With dynein bound to a microtubule, ATP binds in the pocket of AAA1 and is hydrolyzed leading to a weak dynein:microtubule interaction. Upon completion of hydrolysis, this change in nucleotide state is communicated throughout the ring complex and up through the coiled-coil stalk and buttress up to the MTBD. Dynein is now released from the microtubule and is able to move forward along the microtubule where it can rebind. Upon rebinding, dynein:microtubule interaction is strong and the hydrolyzed phosphate is released while ADP remains in the ATP binding pocket during the powerstroke and movement of both the N-terminal tail linker and coiled-coil MTBD. ADP is then released upon the N-terminal tail linker reorienting to a post-powerstroke position. Finally, ATP is able to rebind in the AAA1 binding pocket and the cycle is repeated. Upon ATP binding, the N-terminal tail and linker moves from a position over AAA1, AAA6, AAA5, and AAA4 to a position out from AAA1 over AAA2 and is displaced by approximately 17 nm total. In addition, the coiled-coil stalk also shifts the α-helices to bring about a movement of the MTBD by about 5 nm (146). This sliding of the coiled-coil was further studied and a model for the movement was proposed in a recent article (22). This data, in addition to previous work, led to a model whereby the amino acids contained in the anti-parallel coiled coil slide upon each other during the powerstroke and that these changes in the overall structure of the helices changes the affinity of the MTBD to the microtubule (Figure 7) (21, 22).

The recent crystal structures of DHC are in agreement with the previous data described previous (90, 20, 91). However, even greater detail was elucidated about

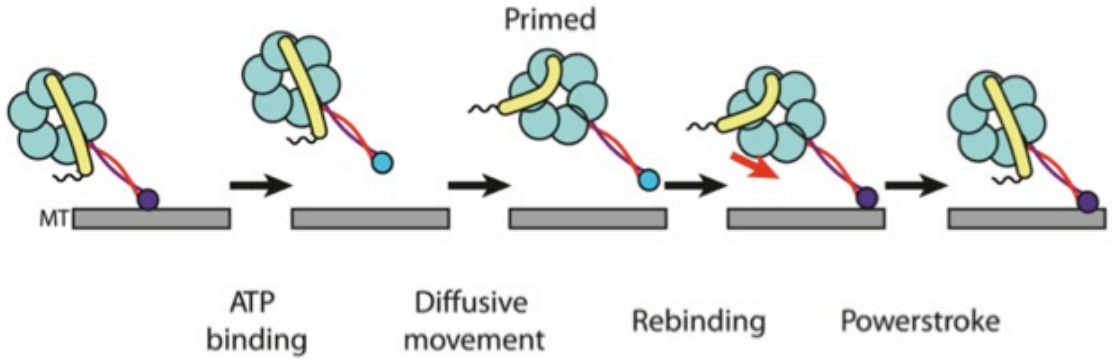

Figure 6. Depiction of the mechanochemical cycle of dynein. Steps of the dynein mechanochemical cycle as it walks along a microtubule (grey). The N-terminal linker (yellow) remains close to the microtubule binding domain during the post-powerstroke state (left side). Upon ATP binding, dynein moves further down the microtubule, the linker swings away from the microtubule binding domain, and dynein is primed (center). Upon hydrolysis, the nucleotide state is communicated throughout the ring structure to the microtubule binding domain, which results in the powerstroke and motor movement. (Adapted from reference 22)

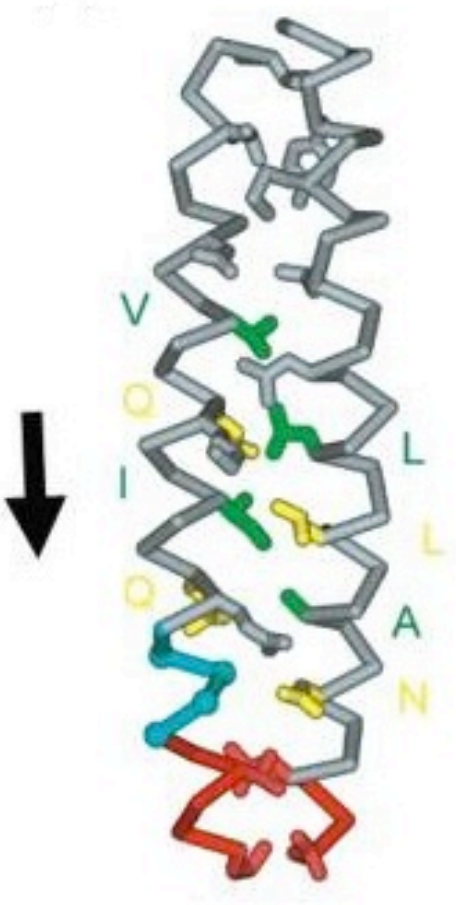

Figure 7. Sliding of the microtubule binding stalk of dynein during the powerstroke. Coiled-coil 1 (left) sliding along coiled-coil 2 (right) during the dynein powerstroke creates a high microtubule affinity state of the microtubule binding domain. As coiled-coil 1 shifts down, as indicated by the arrow, the side chains labeled in yellow and green of each coiled-coil make contact with their binding partner on the opposing coiled-coil. (Adapted from reference 22)

various structures in and around the AAA ring. The linker domain, composed of nineteen α-helices and eight β-strands, was found to make major points of contact with AAA1 at its C-terminal end and AAA4 at its N-terminal end (91). The linker itself was found to lie across the ring surface and center opening similar to a bucket handle.

Dynein Heavy Chain Interactions

Dynein Intermediate Chain

Dynein intermediate chain (DIC) interacts with DHC as a dimer and makes various interactions with dynein and non-dynein subunits. This interaction occurs at the N-terminal tail of DHC. The various combinations of interacting partners increase the potential dynein functions in the cell (Figure 8). DIC, a protein of approximately 75 kda, is believed to interact with DHC through its WD40 repeats (194, 58). DIC exists in various isoforms due to alternative splicing, phosphorylation, and other posttranslational modifications (32, 125). DIC interacts with p150 of dynactin and the dynein light chains (DLCs) through its coiled-coil N-terminal region (116, 183, 87).

Dynein Light Chains

Dynein light chains (DLCs), proteins of 10-20 kda, interact with the dynein complex through interaction with DIC as homodimers. The Tctex1 and LC8 families of DLCs, structurally similar but lacking sequence homology, bind to an unstructured portion of DIC next to the binding site for dynactin (3, 99, 126, 195). LC8 binds both

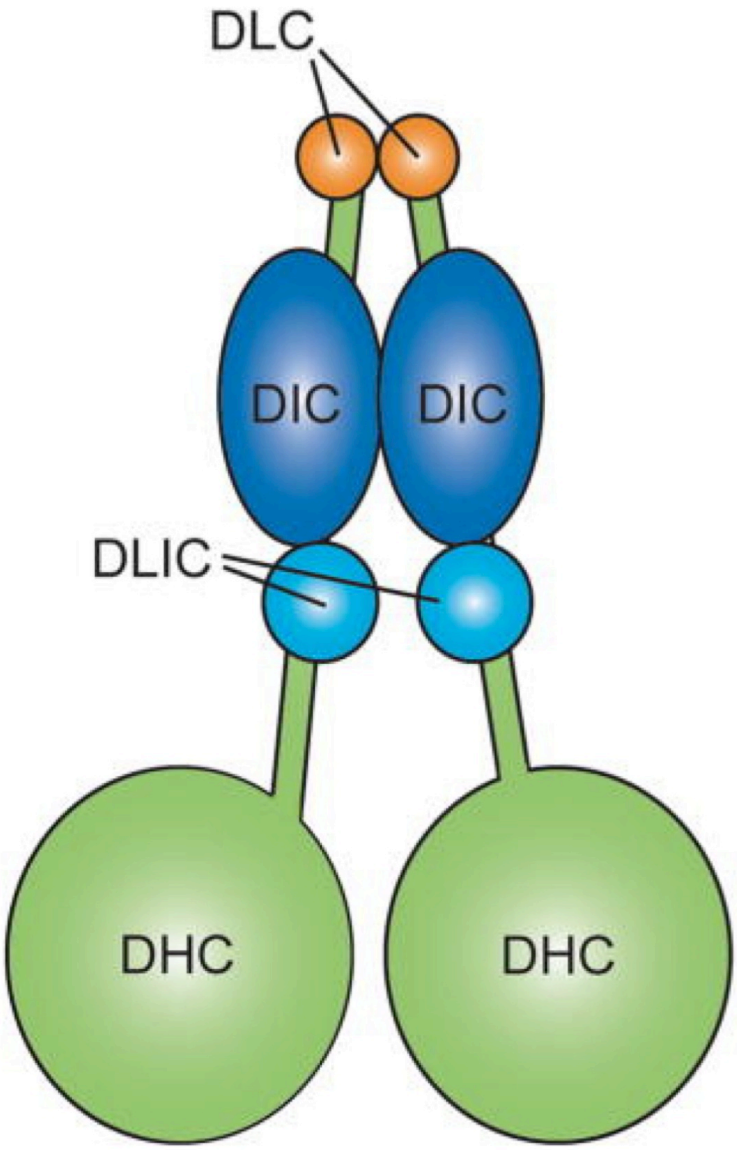

Figure 8. Cartoon depiction of the dynein complex. This image displays the multiple interactions made in the dynein complex, which is composed of two heavy chain molecules (DHC), and pairs of dynein light intermediate chains (DLIC), dynein intermediate chain (DIC), and dynein light chains (DLC). The combination of various dynein subunits allows dynein to carry out multiple cellular roles. (Adapted from 44)

nuclear distribution protein E (NudE) and NudE-like protein (NudEL), which are binding partners of Lissencephaly protein (Lis1) that is discussed in later sections. A third family of DLC with different overall structure, Roadblock, binds to a binding site on DLC that is downstream of both LC8 and Tctex1 (60). The GTPase Rab6 interacts with a DLC and is involved in transport of vesicles between early and late Golgi compartments (191). It is still unknown what specific roles DLCs play in dynein function as both LC8 and Tctex1 bind various non-dynein protein partners like myosin V, Rabies virus P protein, and rhodopsin (40, 140, 174). It was thought these various interactions of DLC leads to the connection with the dynein complex, but recent data has refuted this theory because DIC interacts with both LC8 and Tctex1 in the same location as the various non-dynein proteins (99, 195).

Dynein Light Intermediate Chain

Dynein light intermediate chain (DLIC), a 52-61 kda protein, is unique to the cytoplasmic form of dynein, which implies intracellular transport specific functions (53). Numerous studies have implicated DLIC in dynein cargo attachment, including interactions with Rab4 and other members of the Rab GTPases that are involved in endosomal transport (4). DLIC may also play a role in dynein:centrosome interactions as determined by studies in *C. elegans* where depletion of DLIC led to disruptions in pronuclear migration, centrosome seperation, and attachment of the pronuclear envelope to the centrosome (106). DIC interacts with both DLICs and DLCs in various combinations that can lead to different dynein subcomplexes (87). These different

subcomplexes suggest that dynein exists in various forms inside the cell that may explain how dynein is able to ineract with different cargoes.

Dynactin

Dynactin is a complex of over 1 MDa that contains multiple protein subunits and aids dynein processivity and cargo binding. It can be segmented into three parts: 1) cargo binding 2) motor (dynein) binding and 3) microtubule binding (Figure 9).

The major portion of the cargo binding segment is the actin-related protein, Arp1 (96). Multiple Arp1 peptides combine into a filament-like structure and are thought to bind acidic lipid head groups of membranes via a region of basic side chains (121). The Arp1 filament is capped on one end with the CapZ protein, while the other end interacts with the pointed end complex. This complex consists of Arp11, p25, p27, and p62 and may aid in the binding to various cargoes (36). The recruitment of dynein to kinetochores during mitosis is thought to occur through the interaction of the mitotic checkpoint protein Zeste white 10 (ZW10) with dynactin p50, also known as dynamitin (165, 182).

The second major portion of the dynactin complex is involved in dynein binding. The p150 subunit, composed of approximately 1300 amino acids and a molecular weight of 150 kDa, is the primary subunit that makes contact with the dynein complex (Figure 9). A coiled-coil region of p150 interacts with DIC and this portion of p150 has been shown to be inhibitory to the dynein:dynactin interaction when injected into cells (138, 88).

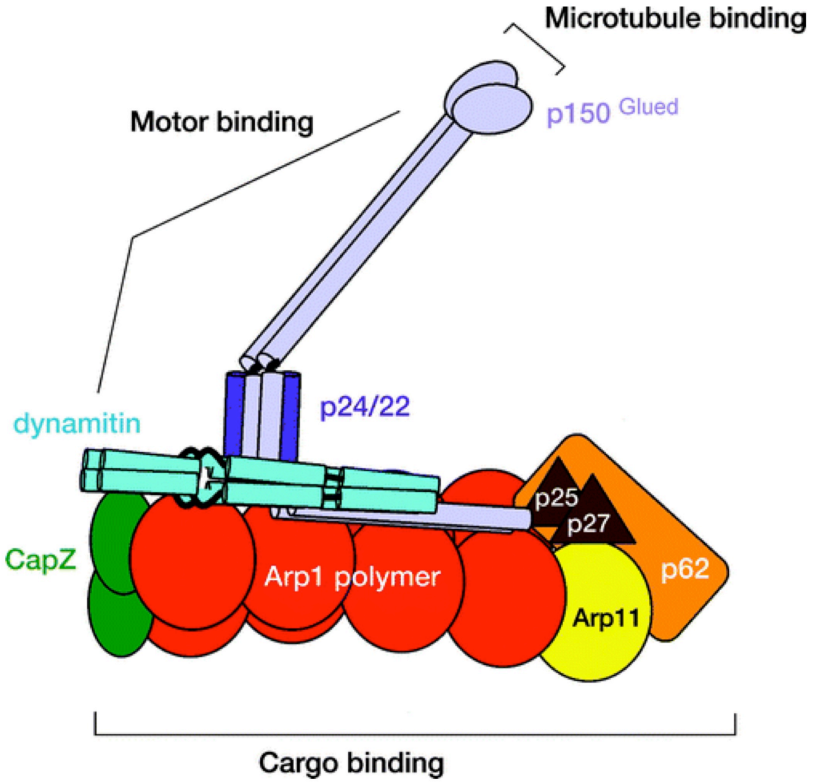

Figure 9. Cartoon depiction of the dynactin complex. Shown are the various subunits of the dynactin complex, with major roles and corresponding sections of dynactin labeled. Roles of various subunits are discussed in the text. (Adapted from reference 154)

The p150 subunit of dynactin is also involved in the third role of dynactin, microtubule interaction. Contained within the N-terminal end of p150 are two different microtubule-binding domains. The CAP-Gly domain, or cytoskeleton-associated protein-glycine-rich domain, is followed by a basic domain with a small collection of basic residues (142). These two domains exhibit varying affinity for microtubules, with CAP-Gly seemingly having a stronger affinity and the basic domain displaying a weaker interaction to the microtubule. These two separate domains for microtubule binding has been hypothesized to account for a "skating" like behavior of dynactin along the microtubule that aids in overall dynein processivity (29).

Lissencephaly 1 (LIS1)

LIS1, a protein of 45 kDa, contains a WD repeat at its C-terminal end that allows for the LIS1 interaction with DHC at both the AAA1 domain and the N-terminal tail (162, 175). LIS1 alters the ATPase activity of the dynein complex, thus LIS1 can be considered a regulator of dynein (109). Mutations in *lis1* have been linked to the human neurological disorder, lissencephaly or smooth brain disease. LIS1 has orthologs in numerous organisms, including both mammals and fungi and is functionally and structurally conserved between various species (141, 198).

NUDE (Nuclear distribution protein E) and NUDEL (Nude-like) proteins are interacting partners with LIS1 that form a tripartite complex with the dynein motor (41, 178). Upon binding to LIS1, the NUDE/NUDEL complex directs LIS1 to bind with dynein (57, 168). Recent data suggests that LIS1 alone or bound with NUDE aids in the transport of cargoes by increasing dynein microtubule affinity (107). In addition, like

p50 of dynactin, LIS1, NUDE and NUDEL are binders of ZW10, a kinetechore interactor (99). The LIS1/NUDE/NUDEL complex has been shown to be important for dynein's role in nuclear and centrosomal trafficking in neurons, orientation of mitotic spindles and alignment of chromosomes, and cell migration (168, 33).

Ubiquitin Ligases

During the course of this dissertation research, it was discovered that mutations in a gene encoding a putative E3 ubiquitin ligase were able to bring about suppression of specific DHC mutants of *N. crassa*. Therefore it is necessary to introduce ubiquitin enzymes and provide a general summary of their known activity in the cell.

E1 Ubiquitin-activating Enzyme

The ubiquitin ligase system, in concert with the proteasome complex, is intimately involved in maintaining protein homeostasis by selectively marking misfolded or damaged proteins for subsequent degradation. In addition, ubiquitin ligases also aid in spatial and temporal regulation of normal proteins. To accomplish this task, a cascade exists whereby a ubiquitin-activating enzyme (E1) charges a ubiquitin-conjugating enzyme (E2) with ubiquitin, which then pairs with a ubiqutin-protein ligase (E3) to specifically transfer ubiquitin (Ub) peptides to a chosen protein (149) (Figure 10).

The initial step in the process is the activation of the 76 amino acid Ub protein by the ubiquitin-activing enzyme, E1. This enzyme, highly abundant in the cell, uses ATP to produce the more highly reactive form of Ub, a Ub thioester which is then attached to E1 to be transferred onto a ubiquitin-conjugating enzyme, E2 (149). Attachment to other

Ub molecules is mediated by a glycine residue in the C-terminus of the Ub protein as well as numerous lysine residues that aid in polyubiquitin formation (27). The majority of organisms have one main E1 enzyme responsible for Ub activation (164, 163). *N. crassa* has four possible E1 enzymes based on sequence homology, but the exact number of functional gene products is unclear (6).

E2 Ubiquitin-conjugating Enzyme

After an E1 enzyme activates Ub, the next step is transfer of the Ub thioester from E1 to a cysteine residue on the ubiquitin-conjugating enzyme, E2 (Figure 10). The E2 is a smaller enzyme with a conserved 16-kD core that holds the cysteine with which the Ub forms the thioester bond (149). E2s then interact with a specific ubiquitin-protein ligase (E3) to transfer Ub to the proper protein target. Depending on the type of E3, the Ub can either be transferred directly from the E2 to the target protein or first to the E3 then to the target protein (149). Interaction between E2 and E3 is dependent on the type of E3 involved in each case, however E2s do contain regions of homology in their N- or C-terminal regions that mediate interaction with both E1s and E3s (181). Data suggest that it is in fact the E2 that determines the eventual fate of target proteins as the E2 is involved in the choice of lysine residue on the target protein where Ub will be attached (70, 16). In comparison to E1, there are multiple E2 enzymes encoded by cells, thirty-five total in the human genome (181). In *N. crassa*, there are approximately twenty-five E2 enzymes predicted to exist (6).

E3 Ubiquitin-protein Ligase

The Ubiquitin-protein ligase E3 is the final enzyme in the Ub pathway. With over a thousand different E3 ligases in higher mammals, this enzyme allows for the Ub pathway to target and coordinate the transfer of Ub from E2 to targets throughout the cell (164). *N. crassa* has approximately 60 E3 enzymes based on sequence homology (6). There exists three main classes of E3s based on structure and activity: HECT, U-box, and RING (54, 74). HECT enzymes are monomeric units that contain a conserved C-terminal domain with a cysteine side chain that allows a thiodiester bond to form between the enzyme and Ub (66, 149). In contrast, U-box enzymes facilitate Ub attachment to targets by either directly binding the target to recruit an E2 or by binding to a Ub chain already linked to the target. U-box enzymes do not initiate Ub chains, but rather associate with elongating chains (74, 163). The third class, RING E3 enzymes, do not form thioester bonds with Ub. RING enzymes act as a scaffold for both the target protein and the E2 to facilitate the transfer of Ub from E2 to target and can function as monomers or in complex with other proteins (54, 31). Other types of E3 enzymes exist, varying in the way in which they bind target, E2, and Ub. It is thought that the various combinations allow for not only Ub tagging of proteins destined for degradation, but also the other Ub activities present in the cell (74).

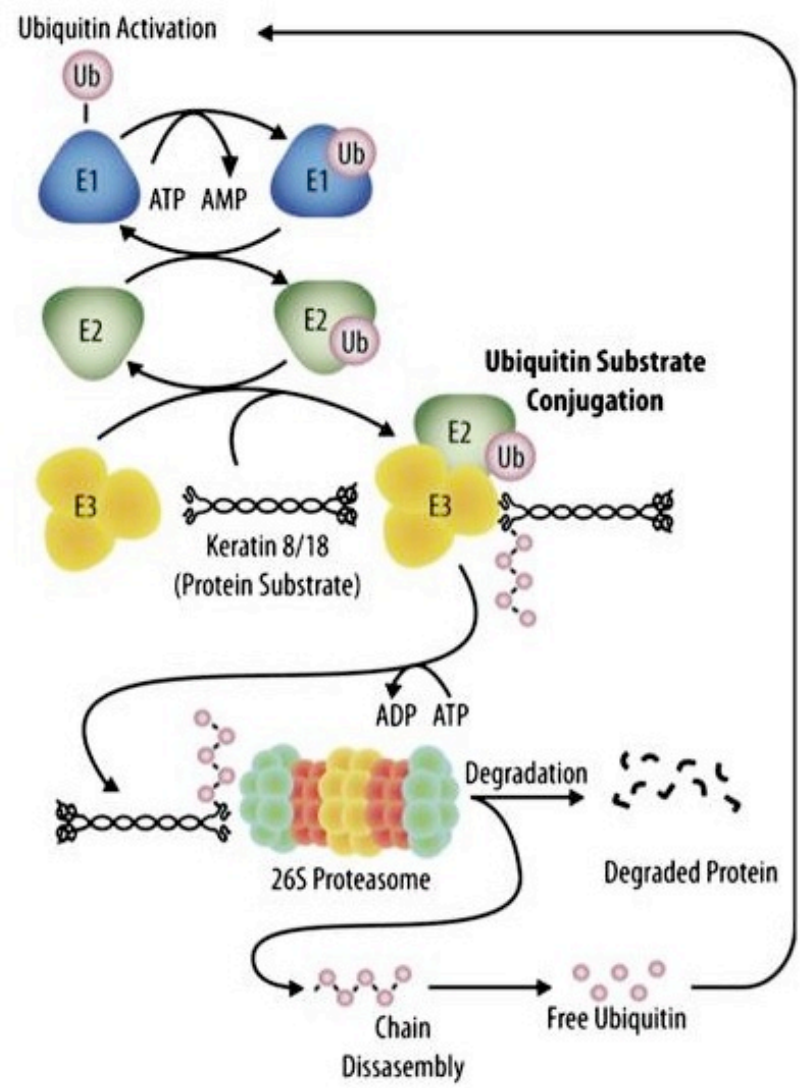

Figure 10. Ubiquitin ligase pathway leading to protein degredation.
Figure 10 depicts a summary of protein degradation via the ubiqutin ligase pathway. Activated ubiquitin is transferred from ubiquitin-activating enzyme (E1) to ubiquitin-conjugating enzyme (E2). The ubiquitin is then conjugated to the substrate protein by coordination of E2 with ubiqutin-protein ligase (E3). This ubiquitin marked protein is then directed to the proteasome for degradation and the ubiquitin chain is recycled back into free monomers. (Adapted from 149)

Examples of E3 Ubiquitin-protein Ligases in Cellular Activities

Due to the significant number of E3 ligases that exist, it is of little surprise that they are involved in the control of numerous cellular activities. Table 1 provides a summary of a small subset of E3 ligases and their general function in the cell.

One activity that E3 ligases regulate is the progression through the cell cycle. The anaphase promoting complex (APC) is a multiprotein complex with E3 ligase activity. Found in complex with other mitotic proteins, APC aids in the degradation of cyclins and other mitotic proteins (1).

ITCH functions in the activation and signaling of T cell receptors by ubiquitinating multiple proteins. One of those protein targets is Foxp3, a transcriptional repressor of T cell receptor. ITCH controls the levels of Foxp3 to aid in proper immune response by T cells (171, 172).

The response to DNA damage is controlled by E3 ligases. HUWE1 regulates the degradation of Mcl-1, which promotes cell survival under normal conditions. Upon severe DNA damage, HUWE1 ubiquitinates Mcl-1, allowing apoptosis to occur (203).

P53 is a well studied tumor suppressor protein and many E3 ligases are involved in regulating its levels. Both Pirh2 and TOPORS are E3 ligases that are have been shown to bind and ubiquitinate p53, leading to its degradation (98, 199). Pirh2 and p53 act in an autoinhibitory feedback loop, as p53 controls Pirh2 expression (98).

MARCH-II is an E3 ligase that interacts with syntaxin6 in endosomes and aids in the regulation of vesicle trafficking. MARCH-II and other MARCH family proteins regulate movement between the trans-Golgi network and endosomes (122).

Monoubiquitination by E3 Ubiquitin Ligases

E3 ubiquitin ligases not only polyubiquitinate proteins to be targeted for degradation, they also can add a single Ub to a protein as a means of protein regulation. The earliest demonstration of this ability was with monoubiquitination of histones (17). This modification has been linked to the transcription of meiotic genes in yeast and histones lacking the sites required for monoubiquitination prevent proper yeast sporulation (147).

In addition to histone modification by E3 ubiquitin ligases, monoubiquitination has been shown to regulate protein activity associated with the plasma membrane (67). Whether a membrane protein will be internalized or not is determined by the presence of a single Ub peptide on its cytoplasmic domain (67, 5). This phenomenon is most common for those proteins bound for the endocytic pathway and eventual degradation.

Deubiquitinating Enzymes

Protein ubiquitination is not a one way street and deubiquitinating enzymes, DUBs, exist to allow for the removal of Ub from proteins. Interestingly, DUB-1, a growth-regulating DUB, has been linked to the regulation of DHC levels in murine cells (95). In this study, it was found that not only was DHC polyubiquitinated, conceivably leading to degradation by the proteasome, but that DUB-1 directly interacts with DHC and removes Ub from the protein. When DUB-1 was overexpressed, the ubiquitination level of DHC was greatly reduced and when MG132, a proteasome inhibitor, was added to the cells, Ub levels on DHC was restored (95). Although it was shown that a DUB exists to help control levels of DHC in cells, no E3 ligase has been identified that binds DHC.

Studying Dynein Function in the Model Organism *Neurospora crassa*

With a haploid genome, *N. crassa* displays both an asexual and sexual phase of growth (Figure 11). As an ascospore germinates and develops, it forms a series of multinucleated tubular cells (hyphae) that represent the mycelium. During the asexual phase, the fungus will develop either microconidia (uninucleate) or macroconidia (multinucleate) that are able to germinate and continue the cycle of mycelial growth. Upon the mixture of two colonies of opposite mating type, the sexual phase is initiated. When fusion of the two hyphae takes place, the protoperithecium beings to develop. This mass serves as a protective covering for the development of the sexually-derived spores. As the products of meiosis develop, they line up together as an octad into an ascus. Many asci develop within the mature fruiting body which is called the perithecium. These perithecia release the mature spores that are able to germinate and restart the process of hyphal growth. Although many studies have focused primarily on the hyphal stage of the asexual cycle, the worked contained herein took advantage of both the asexual and sexual phases of fungal growth. As the multinucleate hypahe develop and extend at about four mm/hour, septation occurs in the fungus. However, there is not a complete separation, but rather septal pores are formed that still allow materials to move throughout the hyphae. Full separation occurs during conidial development. Microtubules also extend through septal pores and thus molecular motors are able to freely pass throughout the septated cytoplasm (43). Overall, the tubular hyphae have an average diameter of 4-10 μM with branches occurring every 15-150 μM in wild type strains (151).

Table 1. Examples of E3 ubiquitin ligases and cellular functions.

Ligase	Cellular Function	Reference
APC	Degradation of cyclins and mitotic proteins	1
Cbl	Down regulation of signaling proteins (Ex. T cell receptor)	152
CHFR	Mitotic stress checkpoint protein	7
HACE1	Tumor suppressor (Wilms' tumors and colorectal cancer)	202
HECTD3	Cytoskeletal regulation, actin remodeling, and vesicle trafficking	149
HERC3	Membrane trafficking	69
HUWE1	DNA damage induced apoptosis	203
HYD	DNA damage response	120
ITCH	T cell receptor activation	171, 172
MARCH-II	Vesicle trafficking	122
NEDD4L	TGF-β signaling	45
Pirh2	p53 degradation	98
RFWD2	DNA damage response	34
TOPORS	p53 stability	199
UHRF2	Cell cycle progression	118

(Adapted from Cell Signaling Technology)

N. crassa is able to grow with such speed and efficiency due to the rapid synthesis of the cell wall at the hyphal tip. Because of the hyphal branching and subsequent elongation, the fungus relies on long range polarized transport from molecular motors for exocytosis to and endocytosis from the hyphal apex (63, 179). Various studies utilizing both light and electron microscopy provided greater understanding of the organization and dynamics occurring at hyphal tips (103, 143, 144, 179). Emerging from these types of studies was the importance of the Spitzenkörper organelle at hyphal tips (Figure 12). The Spitzenkörper exists as a cytoskeletal matrix with various elements present both spatially and temporally, including ribosomes and secretory vesicles (179). It serves a role as a vesicle supply center and aids in organizing and regulating tip extension, morphogenesis, and exocytosis and signaling (76, 179). The dynein complex has been shown to be a vital part of Spitzenkörper function as dynein and dynactin mutants had a smaller Spitzenkörper and changes to hyphal morphologies due to an erratic trajectory of the Spitzenkörper compared to wild type. These changes to the Spitzenkörper in dynein mutants add to the ropy growth phenotype seen in mutant strains (143). In *N. crassa*, mutations resulting in elimination or reduction in the function of DHC (*ro-1)*, dynactin (*ro-3)*, or Lis1 (*ro-11)* lead to a change in growth phenotype from wild type with straight growth and extensive and straight branches to a more curly or ropy growth phenotype (Figure 14).

Microtubule Organization in *Neurospora crassa*

As in other organisms, the microtubule cytoskeleton serves numerous roles in *N. crassa* including control of cellular movement, intracellular transport of cargoes, cell

shape and support, and cell division (136, 119, 43, 145). Their dynamic structural changes aids in the efficient and fast growth of the fungus (119, 179). The microtubule meshwork in *N. crassa* is complex consisting of a braided network of filaments that run longitudinally along the hyphal length in the cytoplasm (119, 139). Although they are braided together, cytoplasmic microtubules tend to exist solitarily or as small bundles of less than four filaments. At the growing hyphal tip, microtubules extend to the apex and intertwine into the Spitzenkörper and exist in a mixed polarity population. It was observed that as hyphae grow, microtubules rotate along the hyphal axis indicating they may advance and spin to aid in cytoplasmic flow (119, 145). As is the case in other fungi, microtubules in *N. crassa* originate from the spindle pole body (SPB), a fungal version of the centrosome. The SPB is associated with the nuclear envelope and permits any of numerous nuclei to function as a microtubule organizing center (MTOC) in the fungus, allowing microtubules to extend easily throughout the hyphal length (76, 127, 145).

Due to the numerous roles microtubules play in *N. crassa* and their intimate relationship with dynein, it is of no surprise that mutations to members of the dynein complex lead to changes in microtubules in the hyphae. Dynein heavy chain mutants not only display changes in growth, but microtubules changes include: loss of microtubule arrays focused at the SPB, failure of SPB to anchor nuclei during interphase, modification of microtubule based nuclear movement, and overall less abundant numbers of microtubules (76, 144).

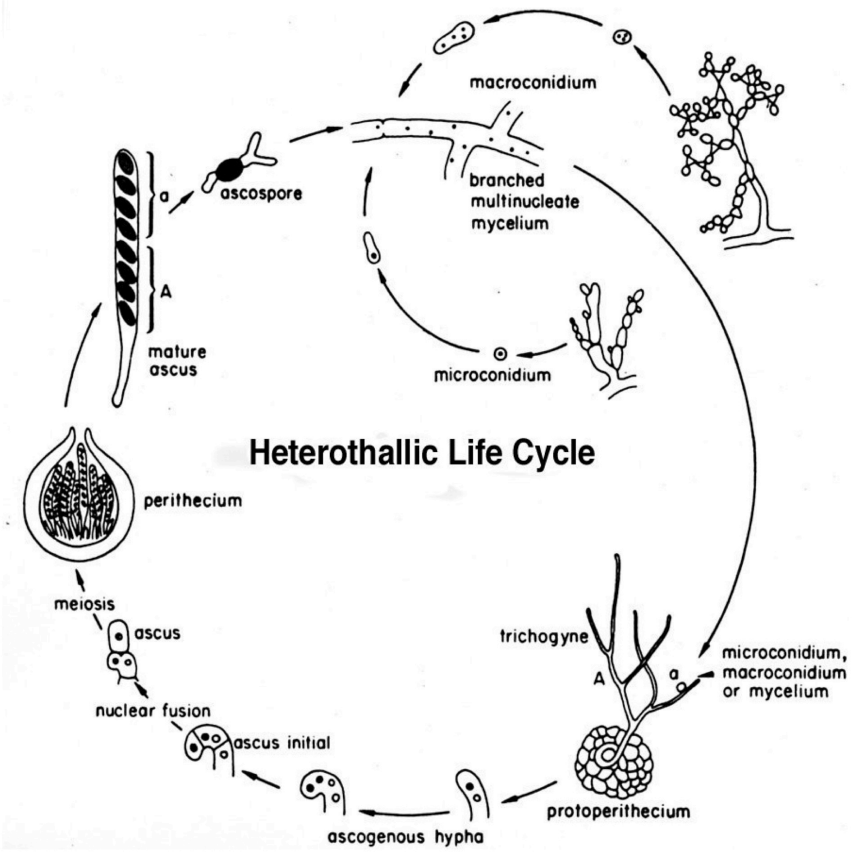

Figure 11. Life cycle of *Neurospora crassa*

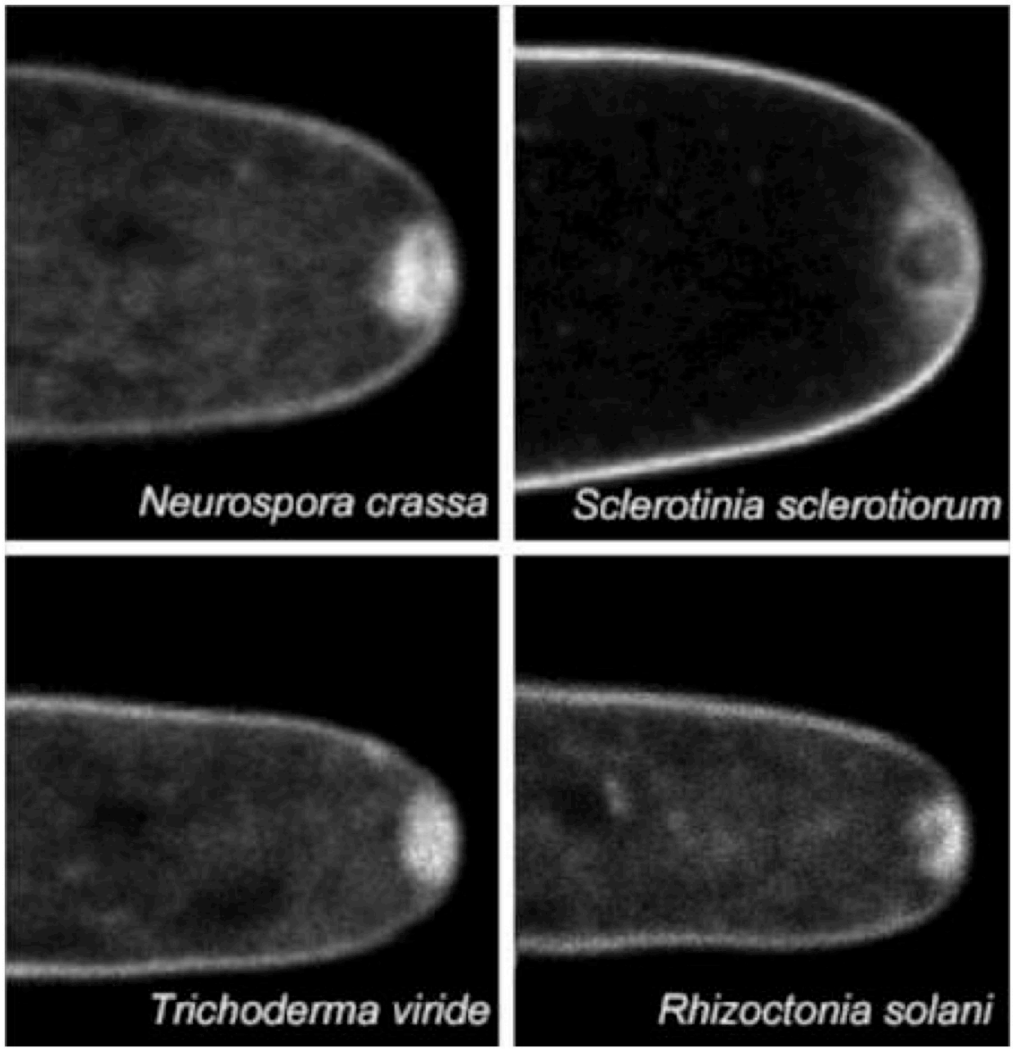

Figure 12. Spitzenkörper in various fungal species. The Spitzenkörper of different fungal species is shown via dye labeling with FM-464 and is visible at the tip of the apex. The organelle at hyphal tips serves as a vesicle organizing center for the growing fungus. (Courtesy of Fisher-Parton *et al*., The University of Edinburgh)

Nuclear Positioning and Migration in *Neurospora crassa*

Due to the expansive and rapid growth of hyphae, *N. crassa* utilizes asynchronous and closed nuclear division (intact nuclear envelope) without cytokinesis. This mode of nuclear division allows for multinucleate cytoplasmic environment or syncytia (150, 148). This syncytial state allows for rapid supply of cell wall growth materials for the actively growing hyphal tips. To avoid clustering of nuclei and changes to needed cellular processes, the nuclei are distributed fairly evenly across the hyphal length (145). Because dynein serves as a nuclear distributing protein complex, mutant forms of dynein alter this distribution of nuclei in the growing hyphae (136, 148) (Figure 13). In dynein mutants, nuclei no longer distribute properly and cluster near the start of the hyphae instead of extending out toward the growing tip. Although C-terminal DHC mutants that are the focus of this study have a ropy growth phenotype, they have slightly better growth than dynein null mutants and their nuclear distribution is only mildly affected. Similar defects have been seen in other fungi including *A. nidulans*, *U. maydis,* and *S. cerivisiae* (39, 158, 173, 76, 197).

Examination of C-terminal DHC Mutants and Revertants

Although numerous studies have been published on the dynein complex, very few have been focused on the C-terminal region of DHC. In fact, only two recent articles have studied or commented on the importance of this area of DHC. One study found that a DHC motor missing a portion of the protein containing the C-terminal region had a six fold increase in ATPase activity (72), while the other created a model whereby the N-terminal tail of DHC slides during the ATPase powerstroke, making and breaking

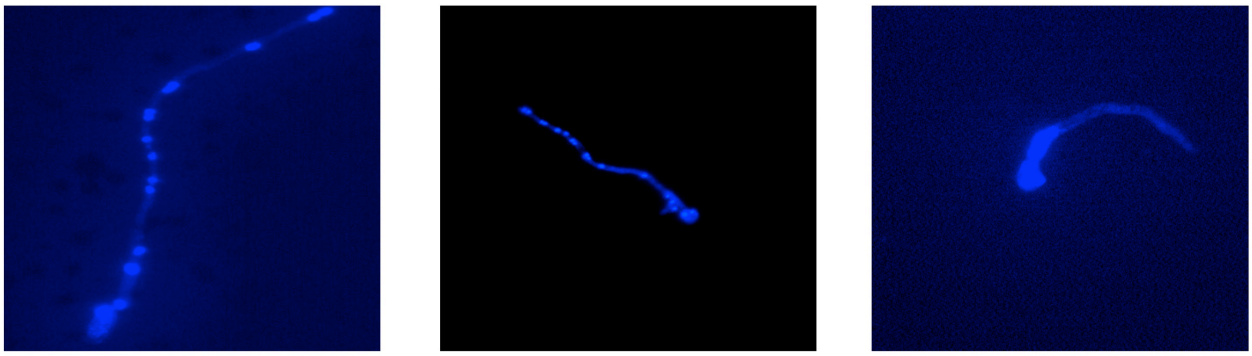

Wild type G4146A Δ DHC

Figure 13. Nuclear distribution of wild-type , C-terminal mutant, and dynein null strains. DAPI staining of nuclei was used to visualize nuclear distribution patterns in growing hyphae of *Neurospora crassa*. In wild type (left), nuclei are evenly distributed along the hyphal length, while a lack of dynein heavy chain (right) results in clumping of nuclei and lack of even distribution in the hypha. A C-terminal DHC mutant (center) is mildly affected and has fairly even distribution of nuclei along the hyphal length.

contacts between AAA1/2 and the C-terminal domain (113). With the newest structures recently completed (20, 91), some conjecture has been put forth regarding the workings of the C-terminal domain/region, but thus far no new data has been presented on that front.

In addition to the lack of data for the C-terminal region of DHC, initial data from this work suggests an interesting role of the C-terminal region of DHC in *N. crassa*. Upon completion of classification of suppressor mutations from revertant analysis screens, it was found that the C-terminal DHC mutants were the only mutants that when subjected to reversion analysis had certain suppressor mutations mapped to a gene or genes other than *ro-1*. Up until this screen, no other DHC mutants from the *N. crassa* DHC reversion analysis had this particular characteristic. Also striking was the mild ropy phenotype seen for this class of DHC mutants and lack of any major change to nuclear distribution.This preliminary information guided the direction of this study to explore not only the C-terminal DHC mutants and their intragenic suppressors, but also to identify and begin to characterize the extragenic suppressor(s). By gathering data on both classes of suppressors, both intragenic and extragenic, the goal of this dissertation research was to better understand the role of the C-terminal region of DHC in the dynein complex.

CHAPTER 2

MATERIALS AND METHODS

cot-1^{ts} Screen for Dynein Heavy Chain Mutants in *N. crassa*

The *N. crassa cot-1* gene encodes a serine/threonine protein kinase required for proper hyphal tip elongation (156, 200). A temperature-sensitive *cot-1* strain grows in a compact, colonial form at 37°C, while at 25^{o} C, the colonies have a wild type growth phenotype (Figure 14). Previous studies determined that mutations that result reduce or eliminate dynein/dynactin/Lis1 function partially suppress the *cot-1^{ts}* growth phenotype at 37^{o} C (9). In brief, to isolate spontaneous dynein gene mutants, ~ 2 x 10^{5} *cot-1^{ts}* conidia were plated on sucrose minimal media plates and incubated at 37^{o} C for 4-6 days. Plates were screened for colonies that displayed a larger diameter of growth (1-5 mm) than that of the original *cot-1^{ts}* (~0.1mm), indicating the presence of a dynein gene mutation. Those colonies picked were purified through crosses with wild type and those displaying ropy phenotype after crossing were used for further study. Complementation assays were performed to identify the respective dynein/dynactin/Lis1 gene that was mutated leading to suppression of the *cot-1^{ts}* growth phenotype. Heterokaryons, mycelial cells containing multiple but genetically unique nuclei, were created between unknown ropy mutants from the screen and strains with known deficiencies in dynein genes and plated at 25^{o} C. Complementation was defined by the presence of straight hyphal growth for a pair of strains. Non-complementation was indicated by the presence of ropy growth for the pair upon plating.

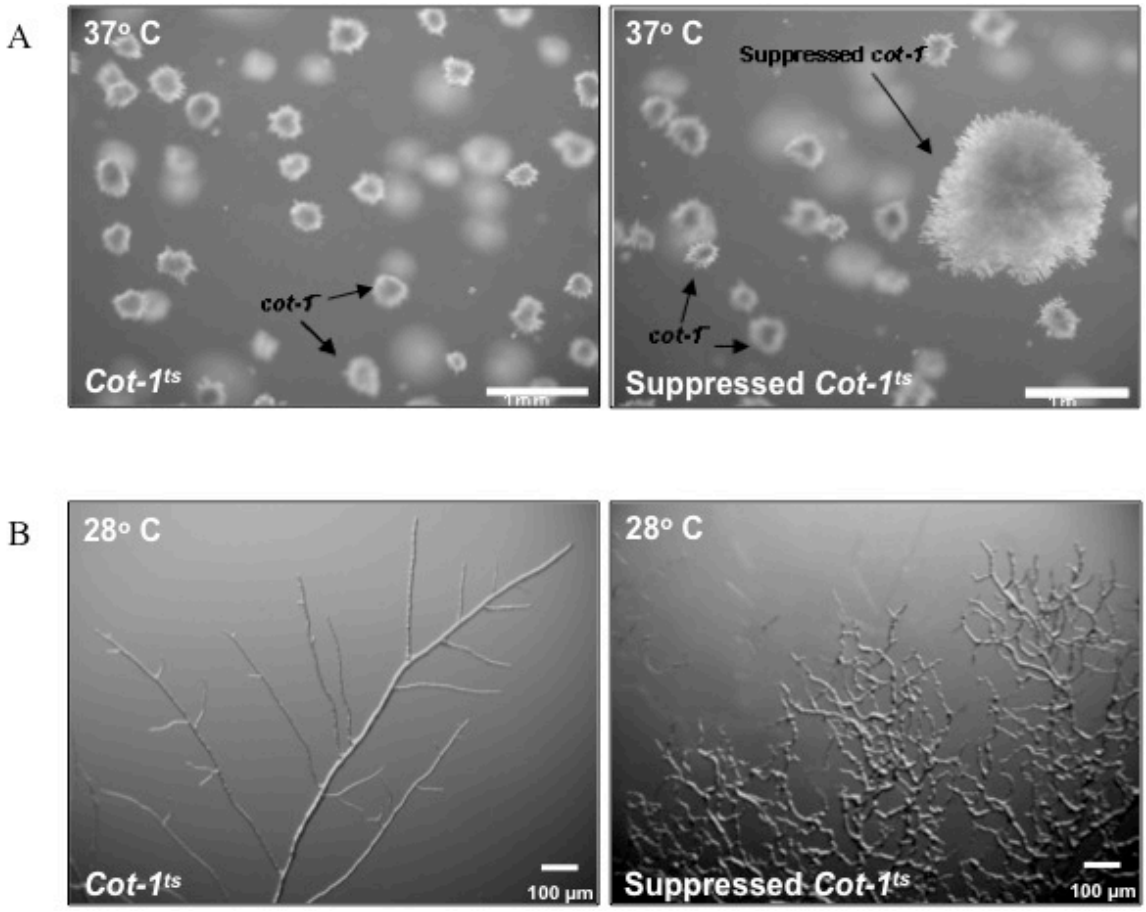

Figure 14. *Neurospora crassa* colony morphology. (A) *cot-1*^{ts} colonies (left) grown at the restrictive temperature (37°C) form tight colonies with little to no outgrowth. When a spontaneous mutation occurs in a *ropy* gene, the colony displays more extended and curly outgrowth (right).
(B) At the permissive temperature (28°C), *cot-1*^{ts} colonies grow with the wild type phenotype (left). In contrast, *ropy* mutants isolated from panel (A) display the common ropy growth phenotype (right).

Assessment of Dynein Heavy Chain Mutant Protein Levels by Western Blot

Dynein heavy chain mutants purified from the cot-1 screen described previously were assayed to check for the presence of full length, or nearly full length, dynein heavy chain and to determine the relative levels of dynein heavy chain protein present in each strain compared to wild type. Overnight cultures were prepared by inoculation of 25 ml of sucrose minimal media with a small loop of conidia and placed at 28^{o}C shaking at 250 rpm. Cultures were filtered by vacuum manifold set up to remove media and 0.5 g of wet hyphal mass from each strain was used to produce cell extracts. One ml of extraction buffer pH 7.0 (35 mM KOH, 35 mM PIPES, 5 mM $MgSO_4$, 1 mM EGTA, 0.5 mM EDTA, 0.5 mM ATP, 1 mM DTT) was added to each tube and the hyphal mass subjected to sonication using a Fischer Scientific Sonic Dismembrator (Waltham, MA) at a setting of15 for three separate 15 second pulses while on ice. Each sample was subjected to centrifugation in a tabletop centrifuge for 10 minutes at maximum speed. The supernatent was removed and placed in an epitube with SDS-PAGE loading buffer (250 mM Tris-HCl pH 6.8, 5% SDS, 30% glycerol, 2-Mercaptoethanol, bromophenol blue) and boiled for 5 minutes. Samples were then loaded onto a 6% SDS-PAGE gel and run at 150 V until the dye front ran off the bottom of the gel. Proteins were electrophoretically transferred to a nitrocellulose or PVDF membrane overnight at room temperature at a setting of 30 mA. The membrane was then blocked with 1% BSA in TBST for 1 hour with gentle shaking. After a brief wash with TBST, the membrane was incubated for one hour in diluted, anti-DHC antibody solution (1:1000 dilution in TBST). The anti-DHC antibody was raised in rabbit against the AAA1/AAA2 region of the *N. crassa* DHC (112). The membrane was then washed with TBST for 30 minutes with

three buffer changes. Next, the membrane was incubated in secondary antibody (Goat anti-Rabitt IgG AP conjugated) for 30 minutes, diluted 1:5000 in TBST. Another set of washes in TBST for 30 minutes with three buffer changes was done and then the membrane briefly washed twice in TBS to remove tween. For development, 66 μl NBT (nitro-blue tetrazolium chloride) and 82.5 μl BCIP (5-bromo-4-chloro-3'-indolyphosphate p-toluidine salt), dissolved in 70% formamide at 20 μg/μl, were added to 10 ml alkaline phosphatase buffer (100 mM Tris-Cl pH 9.5, 100 mM NaCl, 5 mM $MgCl_2$) and added to the membrane. Upon sufficient color development, the membrane was washed 5 times in H_2O and scanned to generate a photographic image.

Identification of Dynein Heavy Chain Mutants by DNA Sequencing

To identify the respective mutations in the *ro-1* (dynein heavy chain gene) mutants, total genomic DNA was isolated from each mutant and the DNA sequence was determined for the entire *ro-1* structural gene. Genomic DNA was isolated from the *ro-1* mutants as follows: 5 ml of Vogel's minimal media (500 mM sodium citrate, 1.8 M monopotassium phosphate, 1.25 M ammonium nitrate, 40 mM magnesium sulfate, 30 mM calcium chloride, 2 mM citric acid, 3 mM zinc sulfate, 60 μM ferrous ammonium sulfate, 10 μM copper sulfate, 30 μM manganese sulfate, 80 μM boric acid, 20 μM sodium molybdate, and 2 mM biotin) was placed in a 48 well polypropylene plate and inoculated with the appropriate strain of *N. crassa.* The plate was placed at 28° C shaking at 220 rpm for 2-3 days. Cultures were briefly sonicated (2-3 seconds) on the #10 setting to disrupt the hyphal walls. Each culture was then brought to 1% SDS, 100 mM Tris pH 8.8, 10 mM EDTA, and 0.1 μg RNAse and incubated at 75° C overnight.

The following day, the plate was brought to room temperature, 100 μg Protease K was added to each culture well and the plate is incubated at 37° C shaking for 2 hours. Plates were then spun at 3K rpm for 30 minutes at 4°C to remove cell debris. The cleared lysate was transferred to a fresh 48 well plate and isopropanol was added to a 33% concentration. The plate was spun for additional 30 minutes at 4° C to pellet DNA. The supernatant was discarded and the pellets washed twice with 70% ethanol and centrifugation at 3K rpm 4° C. The plate was then spun upside down at 700 rpm to remove residual ethanol and the plate was air dried for 15 minutes. The DNA was then re-suspended in 1 ml TE and placed at 4° C overnight. The next day, 1 ml of 6 M potassium iodide was added to each well and the mixture transferred to a glass fiber filter plate and spun at 2K rpm at room temperature for 5 minutes. The filter plate was then washed with 70% ethanol and 2K rpm spins twice. The plate was then briefly (2 minutes) spun dry at 3K rpm. After drying, 350 μl of warm TE was added to each well and the DNA was eluted with spinning at 2K for about 1 minute.

The genomic DNA from above was then used as template for PCR amplification to prepare samples for DNA sequencing. For a 25 μl reaction, 20.7 μl H_20, 2.5 μl 10x NEB PCR buffer (Ipswich, MA), 200 μM (each) NEB dNTP mix, 0.4 μM (each) IDT primer (Coralville, IA), 1 unit NEB Taq polymerase, and 100 ng genomic DNA template was added. Samples were run on a Biorad thermo cycler (Hercules, CA) for 30 cycles of 95°C 30 seconds, appropriate annealing temperate 20 seconds, and 72°C for 1-2 minutes based on length of desired product. After completion of PCR amplification, samples were purified using 6M potassium iodide and glass fiber filter plates as described above. Estimation of concentration of samples was completed by agarose gel electrophoresis.

Samples were compared to a known concentration of λ HindIII digested DNA marker (NEB, Ipswich, MA). Briefly, 20 μl of purified PCR was loaded alongside 5 μl of molecular weight marker and the gel run at 100V for approximately 40 minutes. 25 ng of DNA diluted appropriately was then added to a sequencing cocktail consisting of 1 μl Master Mix (ABI, Carlsbad, CA), 3.5 μl 5x Buffer (ABI, Carlsbad, CA), 0.3 ul appropriate primer, and sterile water to a volume of 20 μl. Sequencing program on Biorad thermo cycle was used: 94^{o}C 15 seconds, 57^{o}C 15 seconds (decrease 0.5^{o}C per cycle), 60^{o}C 3 minutes, repeat 4x, 94^{o}C 15 seconds, 54.5^{o}C 15 seconds, 60^{o}C 3 minutes, repeat 26x. Upon completion, samples were washed with 250 μl 70% ethanol and collected by centrifugation (4000 rpm, 4^{o} C, 1 hour). Ethanol was removed and the samples air-dried for 30 minutes. After drying, 18 μl of formamide was added to each sample and the plate was heated to 85^{o} C for 20 minutes to release DNA pellet into solution and denature DNA to single strands for sequencing. Plates were processed on an ABI Prism 3100 Genetic Analyzer (Carlsbad, CA) using the manufacturers suggested protocol. Sequence reads were analyzed using both the SeqScape (ABI, Carlsbad, CA**)** and Sequencing Analysis (ABI, Carlsbad, CA) programs to check for the presence of mutation(s).

Classification of Dynein Heavy Chain Mutant Phenotypes

DAPI Staining for Nuclear Distribution

Since dynein function is necessary for proper nuclear distribution in early germlings, DAPI (4', 6-diamidino-2-phenylindole) staining of nuclei was performed on the dynein heavy chain mutants and compared to wild type. To complete DAPI staining,

2 ml of sucrose minimal media (1.5% sucrose, 10 ml Vogel's supplement per 500 ml H_2O) was inoculated with a small loop full of conidia in a small snap cap tube and placed at 4°C overnight. The next morning, the tubes were transferred to a 28°C shaking incubator at 250 rpm. After approximately 4 to 5 hours, the samples were transferred to Eppendorf (Hauppauge, NY) tubes and spun in a bench top centrifuge for 5 minutes at 1200 rpm. The supernatants were then removed and the pelleted germlings resuspended in 0.5 ml fixative (9:1 mixture 70% ethanol:formaldehyde). After fixing, the germlings were collected by centrifugation (table top centrifuge, 5 minutes at 1200 rpm). The supernatants were discarded and pellets were resuspended in 0.5 ml PBS buffer and again spun for 5 minutes at 1200 rpm. The supernatants were discarded and 40 μl (0.1 μg/ml) of DAPI stainwas added to each pellet. 6 μl of sample was then placed on a slide and observed using an Olympus BX50 stereomicroscope (Center Valley, PA) at an exposure of 60 ms and gain of 8 using the UV filter setting. Images were taken using a SPOT RT SE digital camera (Sterling Heights, MI) mounted to the microscope.

In vivo Dynein Localization

Recombinant dynein intermediate chain (DIC) and dynactin (p150) were used for *in vivo* dynein localization. Senthilkumar Sivagurunathan created both constructs in a separate study (161). In brief, the mCherry gene was fused to the 3' end of a previously constructed DIC-HMS (his-myc-strep) gene, tagged dynactin p150 genes were constructed by fusing the mCherry or EGFP genes with the 5' end of the p150 structural gene (Figure 15). These constructs were then crossed into strains of interest as needed. For imaging, standard glass microscope slides were covered with sucrose minimal agar

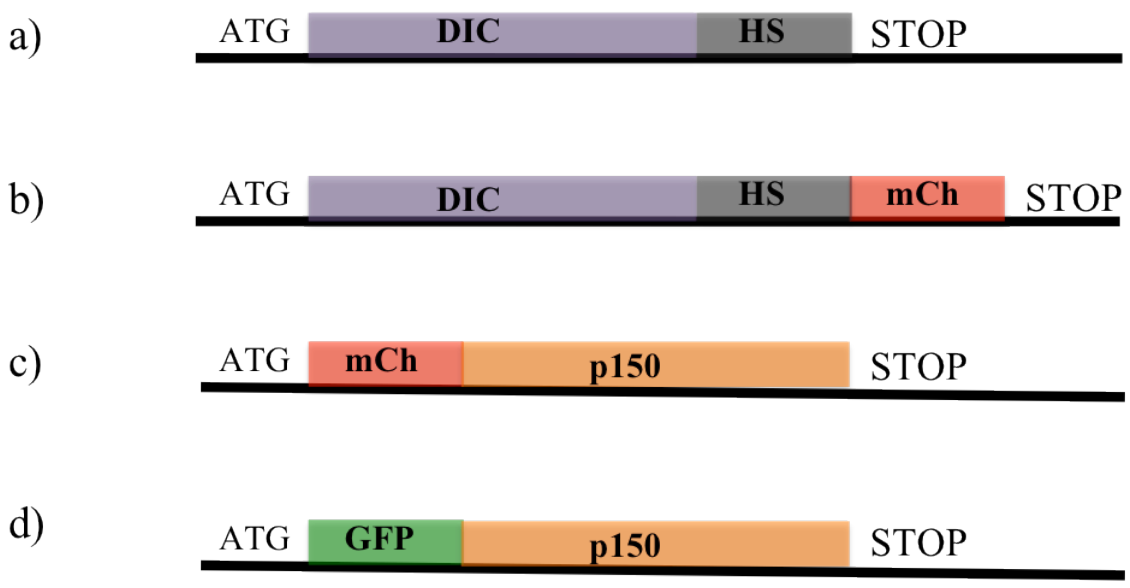

Figure 15. Fluorescently tagged gene constructs for *in vivo* dynein localization. A DIC-mCherry tagged strain (b) was constructed from the framework of a DIC-HS (hexahistidine and Strep II) strain (a) used for dynein protein preps. Additional p150 constructs were created for *in vivo* dynein localization studies as well, a p150-mCherry (c) and a p150-GFP (d).

by dipping them in a tube of liquid media. Slides were placed in a Petri dish over two toothpicks for drying. Slides were then inoculated in the center with a small loop of conidia and placed at 28^{o}C overnight (~16-18 hours). Slides were imaged using the Olympus BX50 stereomicroscope (Center Valley, PA) at an exposure of 800, binning of 3x3, and a gain of 4. Images were taken using a SPOT RT SE digital camera (Sterling Heights, MI) mounted to the microscope.

Reversion Analysis

UV Mutagenesis Screen for Revertants

To identify mutations that suppress the effects of specific DHC mutations, *ro-1*mutants were exposed to UV light, plated in minimal agar medium, incubated overnight and survivors examined for revertants displaying wild-type or near wild-type hyphal growth. In brief, conidial suspensions were made in 25 ml sterile water to a count of ~4-5 x 10^{6} conidia/ml. These suspensions were poured into Petri dishes, placed on a table top tray shaker at 150 RPM, and exposed to UV light for 30 seconds which was determined to result in 80-90% killing. Next, 110 μl samples of the suspensions were placed into a standard 50 ml screw cap tube and mixed with 30 ml of warm (~50^{o}C) agar. This mixture was then poured into a standard Petri dish and placed at 25^{o}C overnight. Plates were observed under a Olympus SZ-11 Stereozoom Microscope (Center Valley, PA) and any colonies showing wild-type growth (i.e., those with suppressor mutations) were picked to sucrose minimal slants and incuated at 25^{o}C. These revertants were then streaked out for purity and backcrossed to wild type to eliminate extraneous mutations resulting from UV light exposure.

Reversion Analysis of AAA6 Nonsense Mutant as Proof of Concept

One of the DHC mutants found from the original DHC mutant screen has a nonsense mutation that eliminates 55 amino acids from the C-terminal end of the peptide. This mutant has a mild ropy growth phenotype and a DICmch signal that is hazy and disperse, similar to other C-terminal DHC mutants. Because the last portion of the C-terminal domain is missing from this mutant, reversion analysis was done to explore if the end of the protein is necessary for overall function or if *N. crassa* can go without and bypass the need for that portion of DHC. Out of 14 pure revertant strains, DNA sequence was able to be determined for 8 samples. Of those 8, all had suppressor mutations that modified the codon of the original DHC mutation either back to a WT codon or a codon conferring a different amino acid than WT (Table 2). From this screen, there were no extragenic suppressors found and no intragenic suppressors that modified any other codon than the one at the original DHC mutant location. Results from this pilot experiment indicated that the reversion analysis scheme developed was able to modify a very small and distinct target codon and would be prudent for further use with the four C-terminal DHC mutants.

Identification of Intragenic and Extragenic Suppressors

Revertants deemed pure after UV mutagenesis screening and purification streaking were crossed with wild type to determine the general location of the suppressor mutation(s). Ascopores were gathered after ~10-14 days in 1 ml of water and heat-shocked by incubating at 60^{o}C for 30 minutes. The ascospore were then plated on sucrose minimal media plates, incubated at 25^{o}C overnight, and then observed under a

Table 2. Reversion analysis results for a DHC C-terminal nonsense mutant

Revertant Number	Reversion Mutation
1	Stop4311L
4	Stop4311W (WT)
6	Stop4311W (WT)
7	Stop4311W (WT)
9	Stop4311E
11	Stop4311W (WT)
18	Stop4311Q
26	Stop4311W (WT)
30	Stop4311Q
34	Stop4311L

Olympus SZ-11 Stereozoom Microscope (Center Valley, PA) the following day. Strains were separated into sets of intragenic or extragenic suppressor mutations following the screen by backcrossing with wild type. The entire *ro-1* stuctural gene was DNA sequence for those revertants containg intragenic suppressor mutations.

Single Nucleotide Polymorphism (SNP) Mapping of Extragenic Suppressors

The Neurospora Genome Group at Dartmouth developed a novel approach to the discovery of a mutation of interest in the *N. crassa* genome (94). The screen was based on tracking single nucleotide polymorphisms (SNPs) that exist between different laboratory strains of *N. crassa*. *N. crassa* Oakridge, the strain used for experimentation throughout this dissertation containing the C-terminal DHC mutations, and *N. crassa* Mauriceville, another standard laboratory strain, have known genomic sequences and numerous SNPs exist between the two strains. 96 SNPs scattered throughout the genome were selected and primer sets created to produce PCR generated products of approximately 500 bp with the SNP being present near the middle of the respective product. Depending on the identity of the SNP, whether Oakridge or Mauriceville, a restriction enzyme cut site would either be created or destroyed. To identity which of the SNPs were linked to the mutations that suppressed C-terminal DHC mutants, we crossed the revertants, which are in the Oakridge background, with a wild-type Mauriceville strain. Ascospores were collected and plated using the standard protocol and progeny showing ropy growth were isolated. These ropy progeny contained the C-terminal DHC mutation, but did not contain the suppressor mutation (Oakridge) and were thus were *sup*$^{+}$(Mauriceville) (Figure 16). DNA was isolated from each progeny using the methods

previously described. For the first set of screens, progeny DNA was pooled and used as template for PCR using the set of 96 primer pairs previously described. PCR was completed with the following mixture (per reaction): 16 μl water, 2 μl 10x PCR buffer, 0.5 μl 10 mM dNTPs, 0.5 μl primer mix, 0.1 μl Taq polymerase, 1 μl gDNA template (~100 ng/μl). Samples were run under the following conditions: 94°C 5 minutes, 94°C 30 seconds, 54°C 30 seconds, 72°C 1 minute repeated for 30 cycles, 72°C 10 minutes. PCR samples were then used as template for restriction enzyme digests under standard conditions and protocol using the proper enzyme based on the SNP present in each PCR product (Tsp509I, TaqI, BstUI, ApoI, HaeIII, AluI, MboI, NlaIII, MspI, BfaI, Eco0109I, AccI, HhaI, RsaI, MseI). Digested samples were compared via gel electrophoresis using standard protocol. Any unlinked samples had two bands present after electrophoresis due to being a mixed population of DNA between Oakridge and Mauriceville, while linked samples had a single band, indicating the presence of only Mauriceville DNA. Any SNPs with samples in lanes that had fully uncut or cut samples were examined further. In the second round of screening, individual progeny DNA samples were used and the protocol just described repeated.

Three Point Crosses

To better isolate the region in the *N. crassa* genome containing the extragenic suppressor of C-terminal DHC mutants that was located to linkage group II, a three point cross was developed. An *arg-5*$^{-}$ strain was crossed with various strains that contained a hygromycin phosphotransferase gene deletion in the area of linkage group II predicted to contain the C-terminal DHC suppressor by SNP mapping as previously described.

Progeny were plated on sucrose minimal media with added arginine via standard protocol and progeny picked. After conidiation, progeny were spotted on media containing hygromycin and *arg-5*$^{-}$, hygromycin resistant progeny were used for subsequent crossings. This strain (*ro-1*$^{+}$; *arg-5*$^{-}$; hyg^{R}) was then crossed with a C-terminal DHC revertant strain (*ro-1*$^{-}$; *arg-5*$^{+}$; hyg^{S}) and the progeny plated on sucrose minimal media with ropy progeny picked, eliminating any *arg-5*$^{-}$; *sup*$^{-}$ progeny and resulting in a *ro-1*$^{-}$; *arg-5*$^{+}$; hyg^{R} strain. After conidiation, progeny were spotted on hygromycin media to determine individual resistance. The percentage of hygromyosin susceptible progeny was calculated with the lowest percentage(s) indicating tight linkage with the suppressor of C-terminal DHC mutants.

DNA Transformation of *N. crassa*

Electroporations of *N. crassa* were performed as follows: conidia were harvested into 25 ml of sterile water and mixed to bring into solution. The conidial solution was centrifuged for 5 minutes at 3000 RPM and the supernatant poured off. 20 ml of 1 M sorbitol was added to the conidial pellet and the solution centrifuged for 5 minutes at 3000 RPM with the supernatent then poured off. This step was repeated three times and after the final spin, 4 ml of 1 M sorbitol was added to the conidia and the solution mixed to bring the conidia into solution. The conidia were counted with a hemocytometer and the proper dilution of ~2.5 x 10^{9} conidia/ml made. 40 μl of conidia was added in an epitube along with 15 μl of DNA, the contents mixed, and the tube placed on ice for 5 minutes. The mixture is then added to a 2mm cuvette and any bubbles removed.

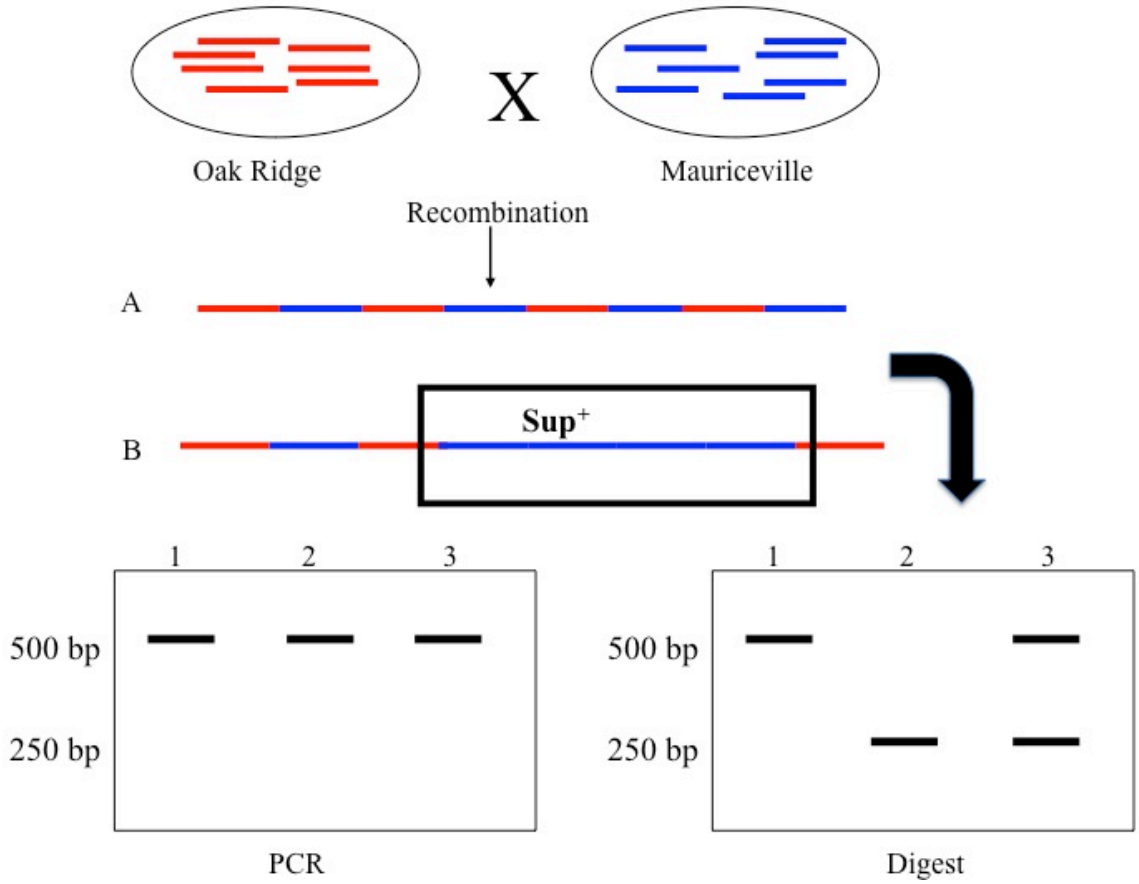

Figure 16. SNP mapping schematic. Using two different wild type strains of *N. crassa*, Oak Ridge (red) and Mauriceville (blue), the region containing a C-terminal DHC suppressor mutation was isolated. Progeny of a C-terminal revertant (Oak Ridge) and a wild type (Mauriceville) strain had either WT (3/4) growth phenotype (A) or ropy (1/4) growth phenotype (B). DNA isolated from strains that were Sup+ and ropy were subjected to multiple rounds of PCR to create a product of about 500 base pairs. This product contained a SNP in the middle of the PCR sequence that either created or destroyed a restriction enzyme site, depending on which strain's DNA was present. Comparison of product after digestion revealed regions of interest (Lanes 1 and 2) where the suppressor mutation could be found by further examination and eliminated other regions due to a mixed PCR population (Lane 3).

The cuvette was pulsed under the "fungal" setting using a Bio-rad Gene Pulser (Hercules, CA). 1 ml of chilled 1 M sorbitol was added to the cuvette and the solution transferred to an epitube. Samples were then plated in sucrose minimal media and placed at 28^{o}C overnight and screened the following morning for any strains with wild type growing conidia. Any gene that when knocked out brought about a return to more wild type growth was then sequenced using a C-terminal DHC revertant strain genomic DNA as template. DNA isolation and sequencing was completed as previously described.

In vitro Dynein Activity Assays

Protein Isolation from *N. crassa*

Conidia from ~7-14 day old plates with strains containing the DIC-HMS tag as shown in Figure X1 were used for protein preparations. The general protein preparation scheme is outlined in Figure 17. 12 ml of minimal media was added to each plate, the plate wrapped in parafilm and gently mixed to bring conidia into solution. After mixing, the conidial suspension was removed and placed into a 50 ml conical tube. This process was repeated until a total of 40 ml of conidial suspension was collected in two tubes. Tubes were then spun at 4000 rpm for 5 minutes and the supernatent poured off. 20 ml of minimal media was then added to each tube and the suspensions combined into one tube. Conidia were then counted using a hemocytometer. Each of the eight (8) 1 L flasks of sucrose minimal medium was inoculated with ~ 1 x 10^{9} conidia and placed in a dark 28^{o}C incubator overnight (~16-18 hours) shaking at 250 RPM.

The following morning, the mycelia were filtered via vacuum filtration using a P8 cellulose filter and the pads ground in grinding buffer pH 7.0 (35 mM KOH, 35 mM

PIPES, 5 mM $MgSO_4$, 1 mM EGTA, 0.5 mM EDTA, 0.5 mM ATP, 1 mM DTT, 40 μg/ml PMSF, 1 μg/ml Leupeptin, 1 μg/ml Pepstatin A, 10 μg/ml TAME, 10 μg/ml TLCK, 10 μg/ml TPCK). On ice, mycelial pads were ground using a mortar and pestle with sea sand until mycelia were ground into a uniform solution. While on ice, solutions were then pulsed for 15 seconds on, 15 seconds off for 8 minutes using a sonic dismembranator at a setting of 18. The solutions were then centrifuged at 8K RPM for 20 minutes at 4°C in an SLA-3000 rotor. The supernatent was then centrifuged at 35K RPM for 30 minutes at 4°C in a Ti45 rotor. The supernatent from the previous spin was loaded at ~ 6 ml/min onto a grinding buffer equilibrated SP Sepharose Fast Flow column (GE Healthcare Uppsala, Sweden) with a bed of approximately 100 ml. After loading was complete, the column was washed with 2 column volumes (CV) of SP wash buffer pH 7.0 (35 mM KOH, 35 mM PIPES, 5 mM $MgSO_4$, 0.5 mM ATP, 40 μg/ml PMSF, 1 μg/ml Leupeptin, 1 μg/ml Pepstatin A, 10 μg/ml TAME, 10 μg/ml TLCK, 10 μg/ml TPCK). Elution was accomplished with SP elution buffer pH 7.0 (35 mM KOH, 35 mM PIPES, 5 mM $MgSO_4$, 500 mM KCl, 0.5 mM ATP, 40 μg/ml PMSF, 1 μg/ml Leupeptin, 1 μg/ml Pepstatin A, 10 μg/ml TAME, 10 μg/ml TLCK, 10 μg/ml TPCK). The protein solution was diluted with an equal volume of dilution buffer pH 7.0 (35 mM KOH, 35 mM PIPES, 5 mM $MgSO_4$, 20% sucrose w/v) then loaded at 3 ml/min onto a 5 mL HiTrap HP column (GE Healthcare Uppsala, Sweden) that was pre-equilibrated with HP load buffer pH 7.0 (35 mM KOH, 35 mM PIPES, 5 mM $MgSO_4$, 250 mM KCl, 0.5 mM ATP, 1 mM imidazole) and charged with a 100 mM $CoCl_2$ solution. After load, the column was washed with HP load buffer using a gradient to remove unbound proteins. Bound proteins were eluted by an increase in imidazole concentration to 250 mM. Eluted

protein was then loaded at 0.5 ml/min onto a 1 mLStrepTrap column (GE Healthcare Uppsala, Sweden) that was pre-equilibrated with Strep load buffer pH 7.0 (35 mM KOH, 35 mM PIPES, 5 mM $MgSO_4$, 1 mM EGTA, 0.5 mM EDTA, 100 mM KCl, 10 μM ATP). After load, the column was washed with 5 CV Strep load buffer. Bound proteins were eluted by 2.5 mM d-Desthiobiotin in Strep load buffer in 250 μl fractions. Fractions were run on an SDS-PAGE gel and visualized by coomassie blue staining. For strains with very low dynein heavy chain yield were further visualized via silver staining using standard staining protocol. Dynein heavy chain concentration was determined by comparison to a known bovine dynein heavy chain standard.

In vitro ATPase Assay

Thin-layer chromatography (TLC) was performed to measure the ATPase activity of purified *N. crassa* dynein. 20 μl of purified protein was added to a 50 μl total mixture in BRB80 buffer (80 mM PIPES, 1 mM EGTA, 1 mM $MgCl_2$). Purified protein was incubated for 60 minutes at 28^{o}C with 10 μCi α-^{32}P ATP (Perkin Elmer Boston, MA) with or without 5 μl taxol stabilized microtubules to compare activities with out without microtubules. Reactions were stopped via addition of 50 μl 5N formic acid and the reaction mixtures centrifuged at maximum speed for 10 minutes in a micro centrifuge. To measure the ATPase rate of the purified dynein, the amount of ADP produced during incubation with or without microtubules was compared. 0.4 μl of each supernatent was spotted onto a PEI-Cellulose TLC plate (EMD Gibbstown, NJ). Plates were then developed in 0.6 M potassium phosphate buffer pH 3.4. ADP and ATP spots were visualized after exposure of the TLC plates to a storage phosphor screen for 60 minutes.

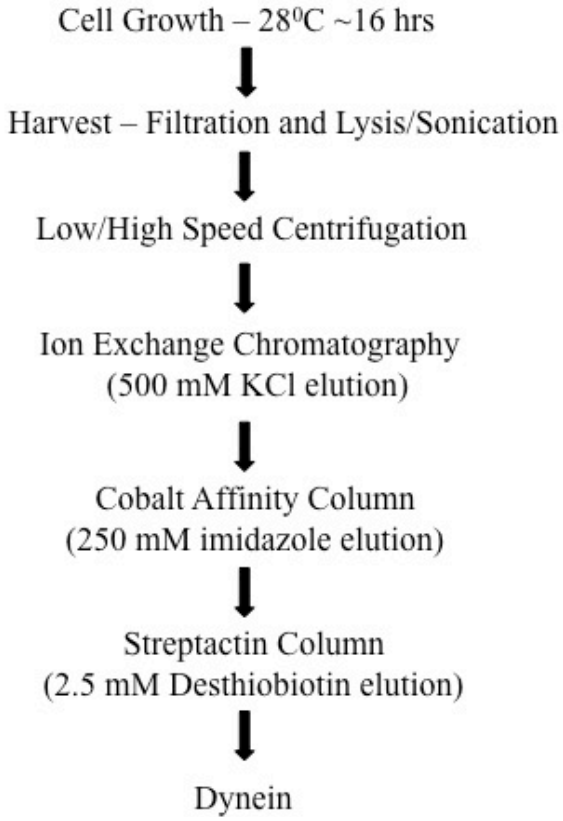

Figure 17. Dynein purification from *N. crassa*. The purification scheme with the steps used completed for isolation of dynein from *N. crassa*. The first column used contained SP-Sepharose cation exchange resin for concentration of protein from lysate. The cobalt affinity column utilized the hexahistidine and while the final column (Streptactin) took advantage of the Strep II tags placed at the C-terminal end of DIC to purify further.

Plates were scanned on a STORM phosphor imager (Molecular Dynamics Sunnyvale, CA) and spots quantified using ImageQuant software (Molecular Dynamics Sunnyvale, CA).

Single Molecule Studies

To gather information for dynein activity on microtubules for each purified strain, single molecule studies were undertaken. Microtubules were made by incubation of purified tubulin with dilution buffer pH 6.9 (100 mM PIPES-NaOH, 2 mM EGTA, 1 mM $MgSO_4$), taxol, and GTP for 15 minutes at 37^{o}C. After completion, microtubules were diluted in dilution buffer pH 6.9, taxol, and GTP. Casein (5 mg/ml), used to inhibit inappropriate binding of beads to the glass slides, was filtered with a 0.22 μm syringe filter and taxol and GTP added after filtering. A flow cell was created by coating a rectangular glass cover slip with a 1/10 dilution of poly-L-lysine in denatured alcohol, double sided tape strips placed parallel and lengthwise on the cover slip, then a standard glass slide placed perpendicular on the cover slip over the tape strips. 25 μl of diluted microtubules were added to the chamber (right to left) and incubated for 15 minutes. Microtubules were then washed with 50 μl dilution buffer and the chamber then blocked with 50 μl filtered casein and incubated 5 minutes. After washing with dilution buffer, sample was added to the chamber. The sample mixture contained 2.5 μl of a 1/25 dilution of 0.2 μm polystyrene beads, 2.5 μl of 10 mM ATP, 1 μl filtered casein, dynein sample of appropriate dilution, and dilution buffer to 25 μl. After addition of sample, the slides were observed under an inverted differential interference contrast microscope and video was recorded using a DVD recorder attached to the microscope. Movies were

analyzed for run length and speed of movements using LVCOR (UCI Software) and Kaleidagraph (Synergy Software, Reading, PA).

CHAPTER 3

RESULTS

Colonial temperature sensitive (*cot-1^{ts}*) gene interactions with dynein

Isolation of dynein complex mutants has been made possible by the development of a genetic screen for partial suppressors of *cot-1^{ts}* mutants (136, 9).

The *cot-1* gene encodes for a serine/threonine protein kinase that has been shown to be important for hyphal growth (200, 157). It is still unclear as to the mechanism of suppression of *cot-1^{ts}* by dynein mutants. In wild-type strains, COT1 is located throughout the hyphal length, while in dynein mutant strains, COT1 is found clustered near the hyphal tip (157). In kinesin mutant strains, COT1 becomes localized to regions distal to the tip. These results suggest that COT1 is transported by both motor populations and in dynein mutants, partially functional COT1 is able to accumulate near the hyphal tip which allows for hyphal growth. Previously, the Plamann lab has developed a screen for the isolation of dynein complex mutants from *cot-1^{ts}* strains (136). Discussed at greater length in materials and methods, briefly, at 28^{o}C, *cot-1^{ts}* colonies grow similar to wild-type, while at 37^{o}C, *cot-1^{ts}* grow in a colonial or restricted growth (Figure 14). The results of this initial screen are compiled in Table 3, which includes the isolation of over 700 independent alleles from various dynein, dynactin, lissencephaly, and non-dynein genes.

Spontaneous mutations were identified in dynein complex genes that allow the *cot-1^{ts}* strain to regain partial hyphal extensive growth. However, when these dynein mutants are isolated and grown at 28^{o}C (permissive temperature for the *cot-1^{ts}*), they exhibit a unique rope-like or curled hyphae growth pattern. Thus, dynein genes in *N.*

crassa are referred to as ropy genes (ex. DHC = *ro-1*). After completion of complementation tests, the initial collection of approximately 700 ropy mutants was separated into 14 gene classes with over 300 representing independent DHC alleles (Table 3).

Identification of DHC mutants producing "full-length" DHC polypeptide

Western blots were completed on protein samples from *N. crassa* to gather information on the general dynein heavy chain protein levels amongst various mutant strains. These experiments revealed varying levels of the dynein heavy chain protein between the mutant strains (Figure 18). Amongst those completed in this initial screen were mutants later revealed to contain mutations in the C-terminal region of the dynein heavy chain. Those strains with "full-length" dynein heavy chain protein were chosen for further study, while those without detectable DHC or those with truncated DHCs (likely the products of frameshift or nonsense mutations) were excluded from further study. This lot of approximately 75 DHC mutants was then DNA sequenced and 34 mutants were determined to have point mutations scattered throughout the DHC gene (Figure 19).

In vivo localization of dynein in *Neurospora crassa*

In vivo localization of dynein in *N. crassa* has been made possible by the development of a mCherry-tagged dynein intermediate chain (DIC) strain created by Senthilkumar Sivagurunathan (161). When the DIC-mCherry is crossed into a wild-type strain, the dynein motor is found to localize to hyphal tips of actively growing fungus (Figure 20). However, in DHC mutants containing mutations in the C-terminal

Table 3 Dynein/dynactin gene designations, size, and alleles.

Subunit	Neurospora gene number	Neurospora designation	Number of amino acids	Number of independent alleles
Cytoplasmic dynein subunits				
Dynein heavy chain	NCU06976.3	*ro-1*	4367	290
Dynein intermediate chain	NCU09142.3	*ro-6*	698	55
Dynein light intermediate chain	NCU09982.3	*ro-13*	546	38
Dynein light chain, LC8	NCU02610.3	*dyn-1*	103	0
Dynein light chain, Tctex1	NCU03882.3	*dyn-2*	161	0
Dynein light chain, Roadblock	NCU09095.3	*dyn-3*	212	0
Dynactin subunits				
p150	NCU03483.3	*ro-3*	1367	62
p50/dynamitin	NCU08375.3	*ro-14*	431	29
p24	NCU10696.3	*ro-10*	217	17
Arp1	NCU04247.3	*ro-4*	380	56
Arp11	NCU03563.3	*ro-7*	644	40
p62	NCU11177.3	*ro-2*	696	31
p25	NCU07196.3	*ro-12*	197	5
p27	NCU04043.3	*dyn-4*	217	0
Lis1 complex				
Lis1-1	NCU04534.3	*ro-15*	451	46
Lis1-2	NCU04312.3	*dyn-5*	474	0
NudE	NCU08566.3	*ro-11*	697	40
Non-dynein genes				
Ascomycete-specific gene	NCU01277.3	*ro-16*	416	5
Plp2, phosducin-like protein 2	NCU00617.3	*plp-2*	256	1

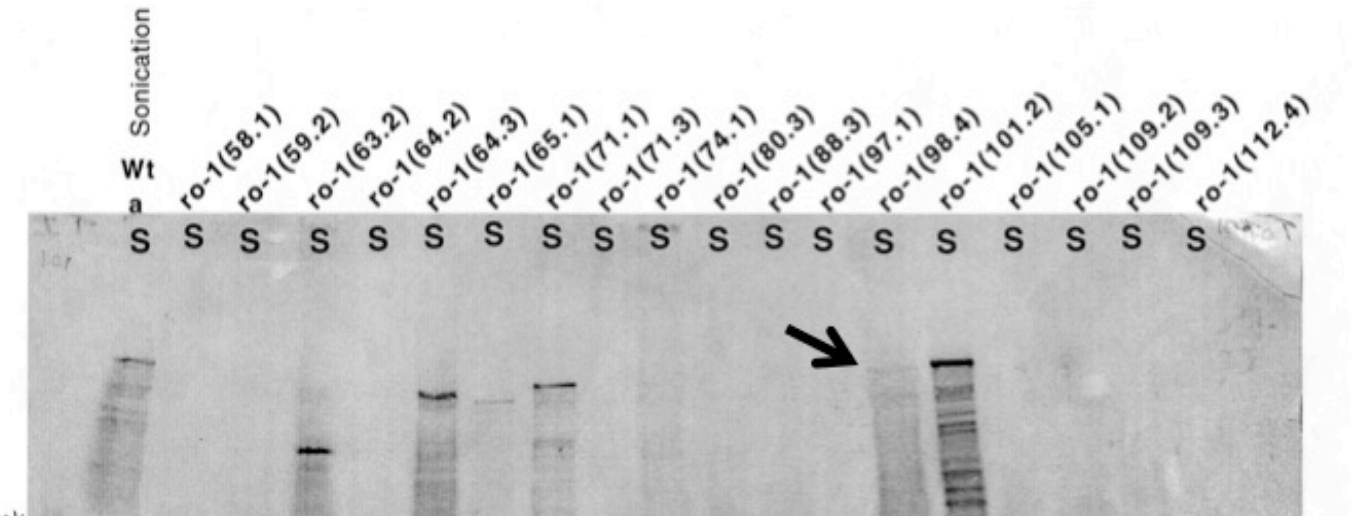

Figure 18. Western blot for *Neurospora crassa* dynein heavy chain. Initial crude Western Blot analysis with ROPY1 antibody revealed varying levels of ROPY1 protein between mutant strains. Of particular interest are the C-terminal dynein heavy chain mutants, including the I4232N mutant, indicated by the arrow. In comparison to the wild-type strain, this C-terminal mutant has a lower overall level of the dynein heavy chain protein.

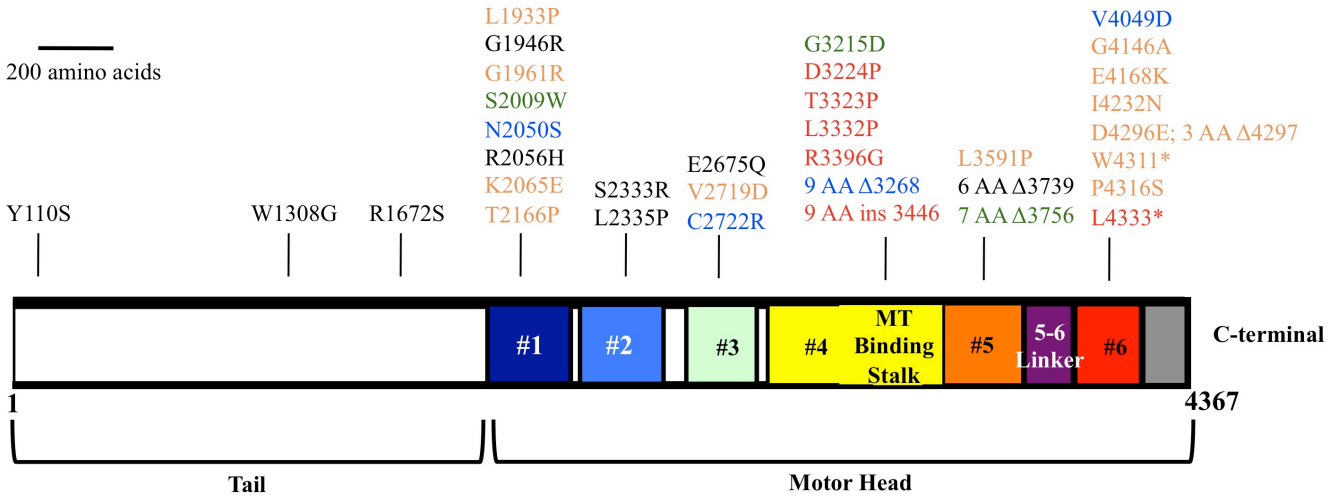

Figure 19. Linear diagram of DHC from *N. crassa* with mutations. The relative placement of DHC mutations are displayed with amino acid changes. Numbers 1-6 represent the AAA domains. Mutations are color coded by classes 1-5.

region of the DHC, dynein localization is no longer concentrated at hyphal tips, but is rather more diffuse along the hypha (Class 5). In contrast, other non-C-terminal DHC mutants display various localization phenotypes, including light distal microtubule localization (Class 1), proximal microtubule localization (Class 2), comet like structures near the hyphal tip (Class 3), or distal punctate aggregates (Class 4). In addition to the C-terminal DHC mutants, other non C-terminal DHC mutants also display a haze or diffuse DICmCherry distribution phenotype.

Dynein Heavy Chain Mutant Phenotypes

Dynein gene mutations display a range of phenotypes, with the strongest being a dynein heavy chain deletion strain and the weakest being mutants with near wild-type growth. Those strains with C-terminal region mutations lie in between these two extremes and can be considered to be mild ropy mutants as opposed to more severe ropies like the dynein heavy chain deletion strain. The difference in growth between wild-type and C-terminal region mutants is more pronounced when observed for colonial growth than it is for growth from an individual ascospore (Figure 21).

Although C-terminal DHC mutants are considered to have a mild ropy growth phenotype and lack any significant differences for nuclear distribution relative to wild-type, when examined for their distribution of dynein in the hyphae, they do display a diffuse or haze pattern (Figure 22 A). This haze distribution is seen for each of the C-terminal DHC mutants examined for this study.

Dynein Heavy Chain Mutant Reversion Analysis Results

To gain a better understanding of the function and role of the C-terminal region of DHC, a reversion analysis experiment was completed with the C-terminal DHC mutants. Briefly, conidia from a C-terminal DHC mutant were suspended in water in a standard Petri plate, placed on a rocking platform, and subjected to thirty seconds of exposure to a hand-held UV light source. Then, the conidia were plated in standard sucrose minimal media and the survivors were allowed to grow for 18 to 24 hours. After this incubation period, the plates were screened for revertants that displayed wild-type or nearly wild-type growth. After completion of UV mutagenesis screening of each of the dynein heavy chain C-terminal region mutants, strains displaying a return to more wild-type growth were isolated and purified from any contaminants. Backcrosses with wild-type strain were completed to determine if the suppressor mutation(s) that arose from exposure to UV light were present in the dynein heavy chain gene or another gene. The results of this screen are presented in Table 4. Genomic DNA from those strains containing intragenic suppressor mutations was prepared and DNA sequencing of the dynein heavy chain was completed to identify the mutation(s) present. DNA sequencing resulted in the identification of seventeen unique suppressor mutations of C-terminal DHC mutants (Table 5).

The majority of the intragenic suppressor mutations are found near to the original C-terminal DHC mutations in the five-six linker region (seven) and C-terminal domain (six). Of interest is a group of intragenic suppressors that are located at the very C-terminal end of the DHC sequence, causing changes within the last dozen amino acids of the peptide (Figure 23). These suppressors are able to independently revert each of the

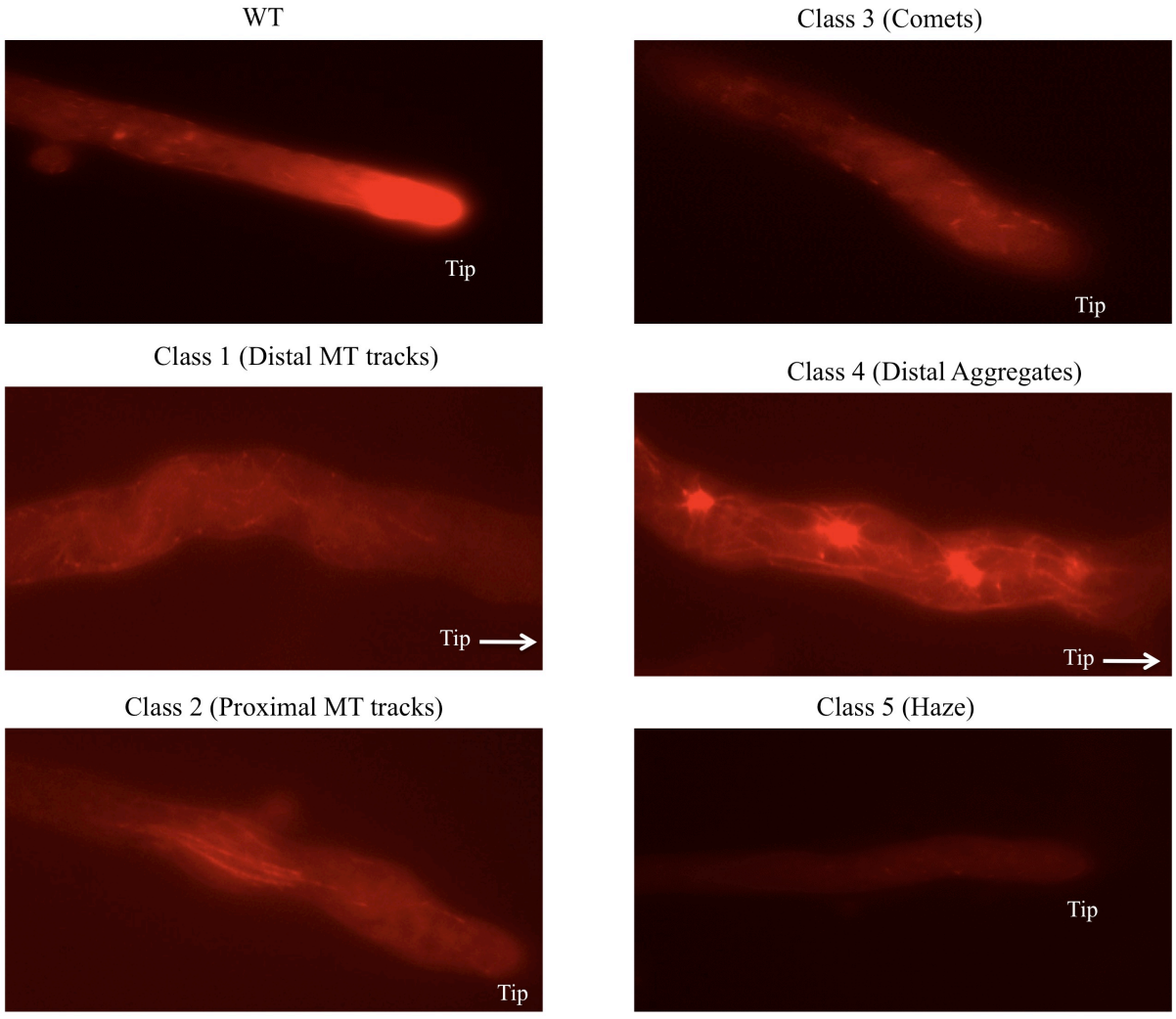

Figure 20. *In vivo* dynein localization of various *Neurospora crassa* strains. Various classes of dynein distribution mutants have been discovered and vary in localization compared to wild-type (WT), which displays a heavy gradient near the hyphal tip. Class 1 has localization along MT tracks distal to the hyphal tip, while class 2 localizes along Mats proximal to the tip. Class 3 has comet like structures near the tip and class 4 exhibits an aggregate distribution of signal in distal regions. Class 5 mutants, which includes the C-terminal DHC mutants, has a haze of mCherry signal with no distinct pattern of localization.

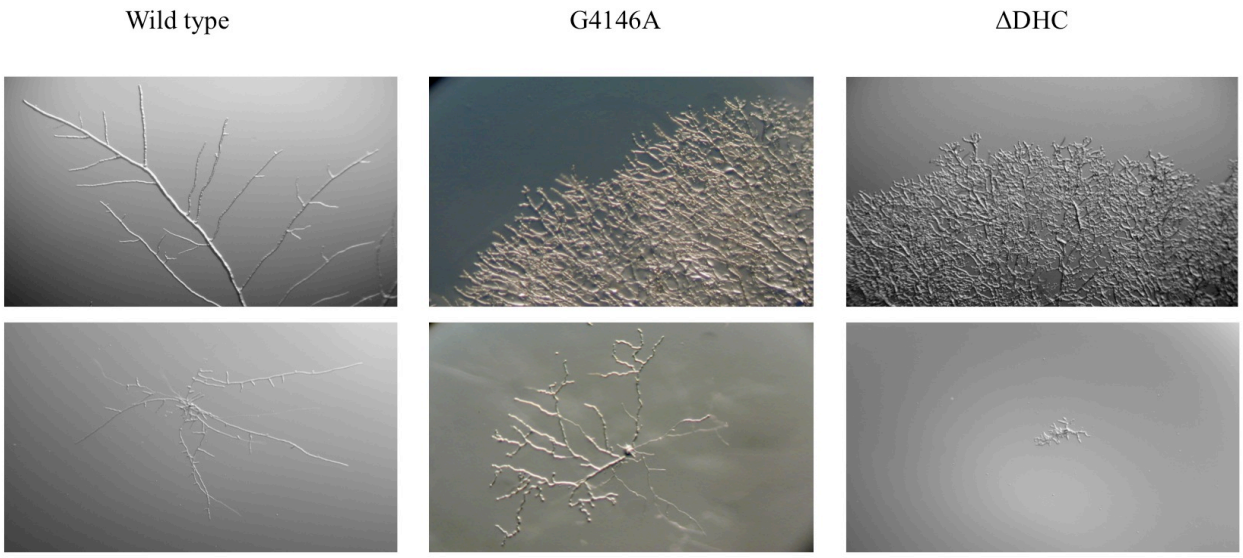

Figure 21. Growth comparison of dynein mutants with wild-type *Neurospora crassa*. Colony edge (top) and individual colony (bottom) images are shown for wild-type (left), a C-terminal DHC mutant (center), and a DHC null strain (right). C-terminal DHC mutants are classified as mild ropy growers as they have a phenotype closer to wild-type than the strain lacking DHC.

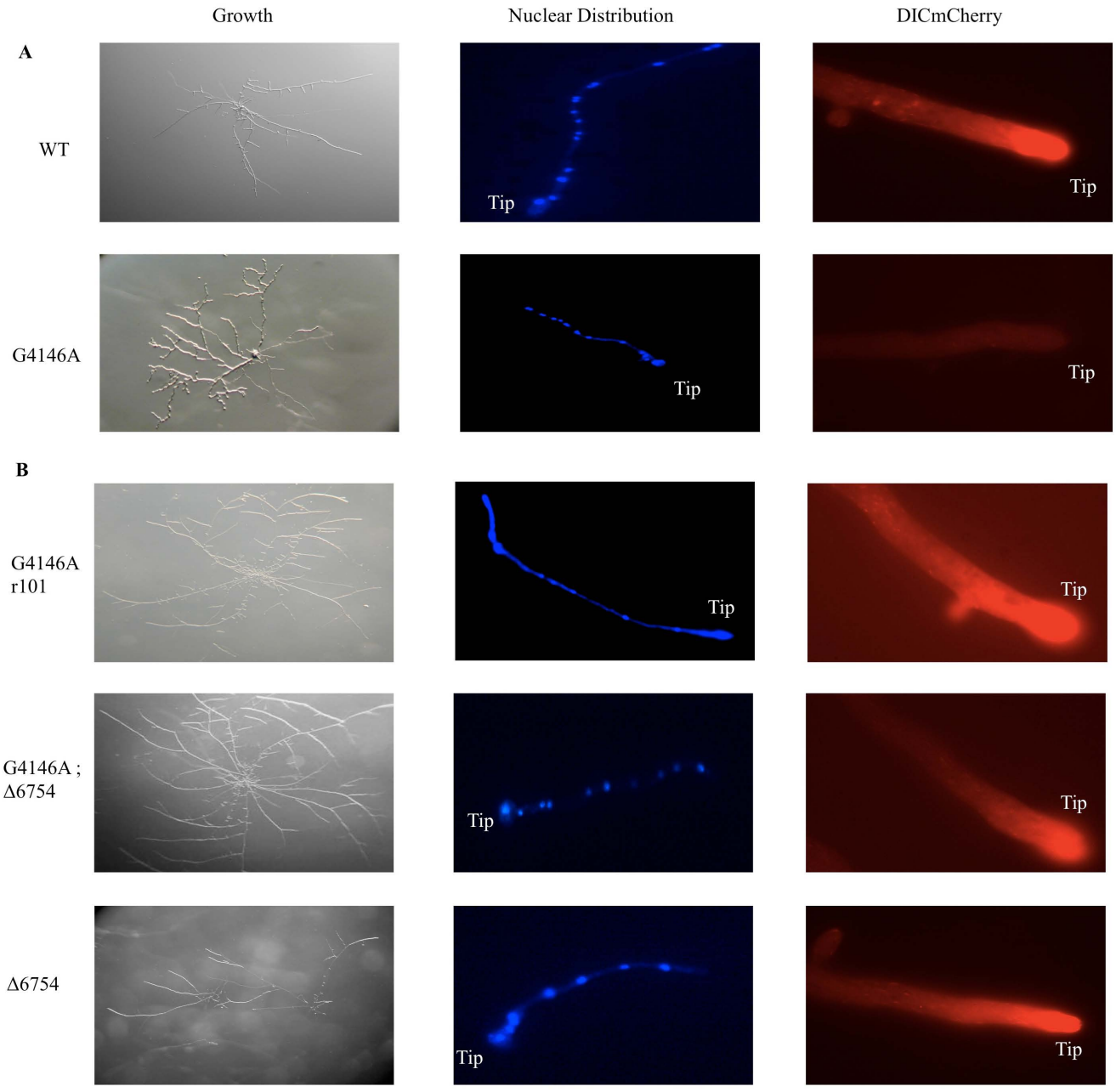
Growth
Nuclear Distribution
DICmCherry
A
WT
Tip
Tip
G4146A
Tip
Tip
B
G4146A
r101
Tip
Tip
G4146A ;
Δ6754
Tip
Tip
Δ6754
Tip
Tip

Figure 22. Growth, nuclear distribution, and *in vivo* DICmCherry compared to WT. A) In comparison to wild-type, the C-terminal DHC mutant (G4146A) has ropy growth phenotype, albeit mild, as well as a mild nuclear distribution phenotype. It differs, however, in the DICmCherry distribution. B) The intragenic suppressed C-terminal DHC mutant (G4146A r101), the extragenic suppressed C-terminal DHC (G4146A; Δ6754), and the ΔNCU06754 strain have growth, nuclear distribution, and DICmCherry distribution similar to wild-type.

four C-terminal DHC mutants and the S4364F suppressor mutation was found for both G4146A and P4316S mutant screens. Interestingly, the remaining four suppressor mutations have been mapped to the N-terminal tail, AAA1, and AAA2 region. This area has been shown to lie in close proximity to the C-terminal region when the dynein heavy chain is properly folded in its functional state (72, 20, 91). By mapping both the original C-terminal DHC mutations and the suppressor mutations to the recent crystal structure of DHC from *D. discoideum* (91) a pattern emerges (Figure 24). The C-terminal DHC mutations are clustered in a region of AAA6 and the C-terminal domain and seemingly perturb local structure and interactions.

Of the seven suppressor mutations found in the C-terminal domain, six are located within the last dozen amino acids of the DHC. Each of the three suppressor mutations, discovered in independent screens, exhibit an identical DNA base change that leads to a serine to phenylalanine change four residues from the C-terminal end. This data suggests that modification of the distal portion of the C-terminal domain can confer a universal suppression in C-terminal region DHC mutants in *N. crassa.*

Reversion analysis of the C-terminal region DHC mutants resulted in both intragenic and extragenic suppressor mutations (Table 4). To determine if a suppressor was intragenic or extragenic, the revertant strain was crossed with wild-type and the spores plated. Any extragenic suppressor strains had a 3:1 ratio of wild-type growth or ropy growth, while intragenic suppressor strains had only wild-type growth. To date, this class of mutants is the only that has been found to revert via extragenic lesion(s). One of the C-terminal region mutants (G4146A) was used as the first strain for reversion analysis, which resulted in a disproportionate number of extragenic suppressors in

comparison to other C-terminal region mutants. When this is taken into consideration, extragenic suppressors account for about 50% of mutations that lead to reversion of the C-terminal DHC mutants. When isolated suppressor mutation strains are crossed with the various C-terminal DHC mutants, suppression of the ropy growth is seen in all cases, suggesting that these extragenic suppressors can act as universal suppressors of the C-terminal DHC mutants, similar to the phenomenon seen with the intragenic suppressors found at the C-terminal end of DHC.

Single Nucleotide Polymorphism (SNP) Mapping Results of Extragenic Suppressors

A SNP mapping scheme was developed to locate the extragenic suppressor mutations elsewhere in the genome that when present bring about suppression of the C-terminal DHC mutants ropy growth (94). Briefly, two standard strains of *N. crassa*, Oak Ridge and Mauriceville, were used to determine the general location of an extragenic suppressor mutation due to their slight genomic differences with varying single SNPs (see Materials and Methods). The Oak Ridge strain contained the suppressed C-terminal DHC mutant (ropy1^{-} ; sup^{-}) and the Mauriceville was wild-type (ropy1^{+} ; sup^{+}). Ropy progeny were selected upon plating of spores from the cross of the two previously described strains. These progeny had a region or regions in their genome that contained Mauriceville DNA, which lacked the suppressor mutation, leaving the progeny with the ropy phenotype. DNA was prepared from these progeny, pooled, and PCR amplification was completed using a set of paired primers for regions throughout the genome. This PCR amplification resulted in a 500 base pair product that contained a SNP in the middle of the sequence. This SNP, whether from Oak Ridge or Mauriceville, would confer or

Table 4. C-terminal DHC mutant reversion analysis results.

DHC C-terminal Region Mutant	Intragenic Suppressor Mutations	Extragenic Suppressor Mutations
G4146A	9	90
I4232N	6	22
D4296E ; del 4297-99	8	61
P4316S	21	9

Table 5. Intragenic suppressors of C-terminal DHC mutants.

C-terminal Mutant	Suppressor Mutation	Location in DHC
G4146A	K1897E	N-terminal tail
	I2047M	AAA1
	E2278K	AAA2
	Y3905S	AAA5-6 linker
	L3916P	AAA5-6 linker
	ΔTE3962-3	AAA5-6 linker
	L3985P	AAA5-6 linker
	K3992E	AAA5-6 linker
	S4364F	C-terminal domain
I4232N	FS 4356	C-terminal domain
D4296E ; del 4297-99	V3826I	AAA5-6 linker
	L3912S	AAA5-6 linker
	V4336A	C-terminal domain
	FS 4357	C-terminal domain
P4316S	E1679A	N-terminal tail
	S4364F	C-terminal domain
	A4366T	C-terminal domain

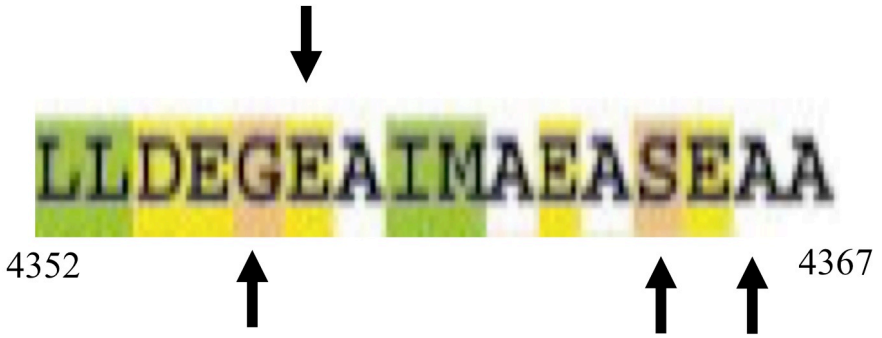

Figure 23. C-terminal mutant intragenic suppressor mutations at the end of the DHC. Shown is the end of DHC, which contains multiple C-terminal DHC mutant suppressor mutations, indicated by arrows. From left to right, the mutations are: FS4356, FS 4357, S4364F, and A4366T. The DNA change that leads to S4364F is able to suppress multiple C-terminal DHC mutants.

eliminate a restriction enzyme cut site at that SNP location. After a restriction enzyme digest, the sample was subjected to agarose gel electrophoresis and those sample lanes with fully cut or uNCUt DNA were further studied (Figure 25). By tracing the locations and identities of SNPs in the *N. crassa* genome in this way, a region on linkage group II was isolated that contains the mutation(s) that lead to suppression of ropy growth for C-terminal DHC mutants (Figure 26). This region spans over 450kb and contains over 150 open reading frames (ORFs).

Identification of Extragenic Suppressors of C-terminal DHC Mutants

Building upon the results of the SNP mapping experiments, further studies utilizing the nutritional marker *arg-5* and a hygromyosin resistant knockout strain were completed. Briefly, two opposing strains of *arg-5*, hygromyosin resistance, and the unknown suppressor were crossed and those progeny exhibiting double recombination events resulting in an *arg-5*+ and hygromyosin sensitive ropy strain without the suppressor present were picked. This three point cross experiment resulted in a 9.5% double recombination rate for strains containing a hygromyosin knockout at NCU06801 and a 0.4% double recombination rate for strains containing a hygromyosin knockout at NCU06746, both on linkage group II. Gene knockouts from this region were then crossed into a C-terminal DHC mutant strain. One, an NCU06754 knockout, brought about suppression of the C-terminal DHC mutant. A total of twenty six revertants showed linkage to this region containing the suppressor and DNA sequencing data was obtained for nineteen different alleles of NCU06754 that act as suppressors of C-terminal DHC mutants (Table 6). A number of these alleles contain mutations that confer amino

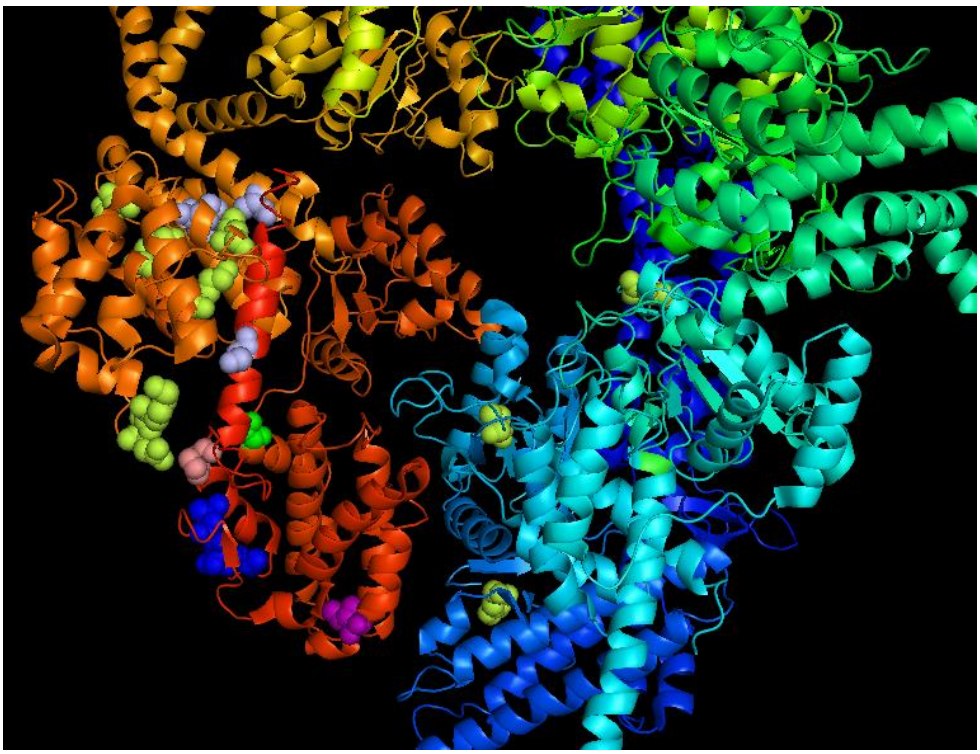

Figure 24. Crystal structure of DHC with C-terminal mutations and suppressor mutations. The four C-terminal DHC mutations are located together in the AAA6/C-terminal domain region. G4146A (green), I4232N (purple), D4296E, del4297-99 (blue), and P4316S (salmon/pink) are seen in the bottom left corner. Suppressor mutations are color coded as follows: light green ,G4146A suppressors and grey, I4232N suppressors. Other suppressors are not shown due to the crystal structure not containing the additional C-terminal domain residues.

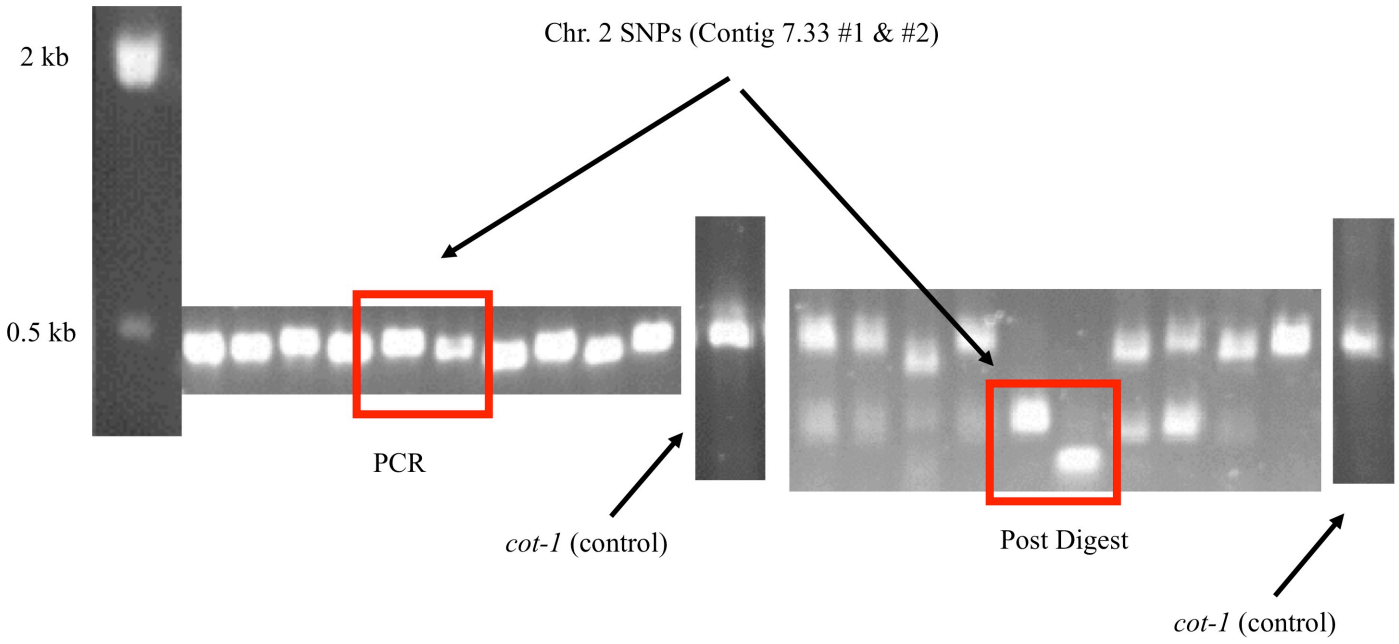

Figure 25. SNP mapping agarose gel for isolation of C-terminal DHC suppressor. An example of a SNP mapping agarose gel is shown for both pre-restriction enzyme digestion (left) and post-digestion (right). Boxed lanes are identical samples for PCR products from contig 7.33 on linkage group II. Both samples were completely digested indicating strong linkage of the C-terminal extragenic suppressor to this region. A control lane (*cot-1*) is shown which is known not to be digested by any restriction enzyme used in the experiment.

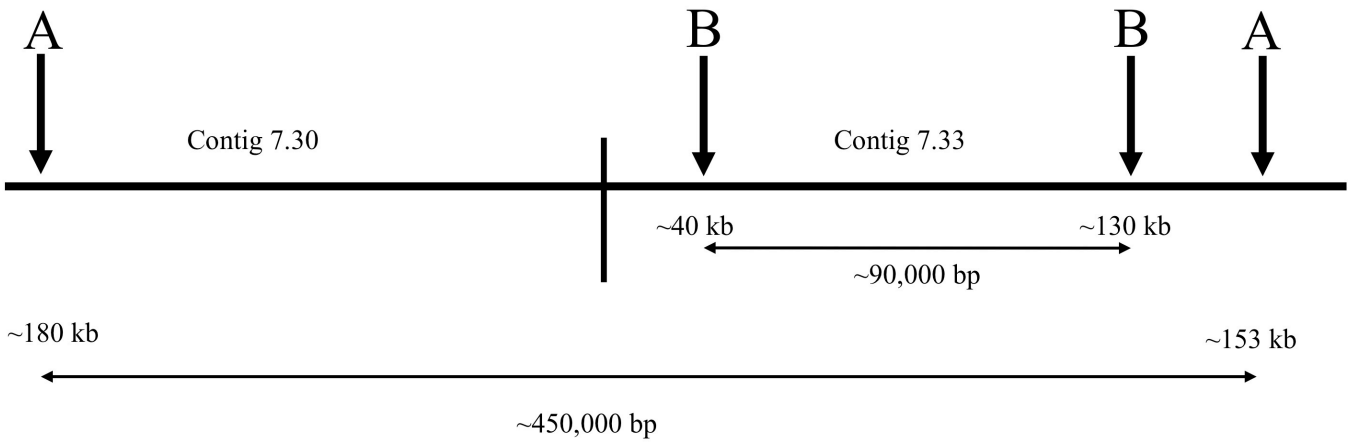

Figure 26. Results from SNP mapping and three point cross experiments. After completion of SNP mapping, a region on Chromosome II containing portions of contigs 7.30 and 7.33 of approximately 450,000 bp was identified that contained an extragenic suppressor mutation of a C-terminal DHC mutant (A arrows). Three point crosses were then completed which further isolated the region containing the suppressor onto contig 7.33, an area covering about 90,000 bp (B arrows).

acid changes in and around the CHY-RING of the NCU06754 protein that has a region of homology to the human E3 ubiquitin ligase PirH2 (Figure 27). This region is involved in the coordination of zinc ions via the CHY-RING zinc finger and the mutations present in *N. crassa* NCU06754 map to residues involved in the zinc coordination in human PirH2. Both the *N. crassa* and human proteins are unique in that they are the only E3 ubiquitin ligases that contain the CHY-RING motif alone without other similar domains (159).

Another minor locus, not linked to this region on linkage group II, has been identified. To date, this locus contains only a single allele. The location of the minor locus has been identified via whole genome sequencing. Initial results revealed 556 non-synonymous SNPs located throughout the genome of the strain. Five ubiquitin-related genes were identified amongst the genes containing non-synonymous SNPs. Because many of these gene candidates are essential in *N. crassa*, the identity of this suppressor was verified by electrporation of a PCR product containing the ORF of one of the ubiquitin-related genes, NCU02289, into a C-terminal DHC mutant resulting in a short term RNAi response bringing about a reversion to more wild-type growth. This phenomenon was not seen for the other genes of interest. The suppressor mutation is located within the NCU02289 gene located on linkage group VII, which encodes a putative E2 ubiquitin ligase (Figure 28). Interestingly, the human homolog of NCU02289 has been shown to interact with Pirh2, the human homolog of NCU06754 (159).

NCU06754 Mutations Suppress All C-terminal DHC Mutants

In the presence of an NCU06754 mutation or deletion, C-terminal DHC mutants have a more wild-type like growth phenotype and DICmcherry *in vivo* localization pattern (Figure 22 B). This suppression is seen for both colony edge and individual ascospore growth. As expected, nuclear distribution remains fairly unchanged from a C-terminal DHC mutant to a suppressed strain, since C-terminal DHC mutant strains do not display errant nuclear distribution. The most striking difference in phenotype is seen for *in vivo* dynein localization from C-terminal DHC mutants to suppressed mutant strains. C-terminal DHC mutants have a haze-like, diffuse pattern of DICmcherry distribution, whereas suppressed strains return to a wild-type like dynein localization pattern with restoration of signal at the hyphal tip.

C-terminal DHC Mutants and Revertants Have Similar Levels of DHC Protein Produced *In vivo*

As a follow up to initial western blots to determine the presence of full length (or nearly full length) DHC in the various mutants, a western blot was completed against DHC with total protein samples from C-terminal DHC mutants, intragenic and extragenic revertants of C-terminal DHC mutants, and a ΔNCU06754 strain, the major locus of extragenic suppression for C-terminal DHC mutants (Figure 29). Each of the strains contains measurable levels of DHC and there are no appreciable differences between C-terminal DHC mutants and revertant strains that contain either intragenic or extragenic mutations.

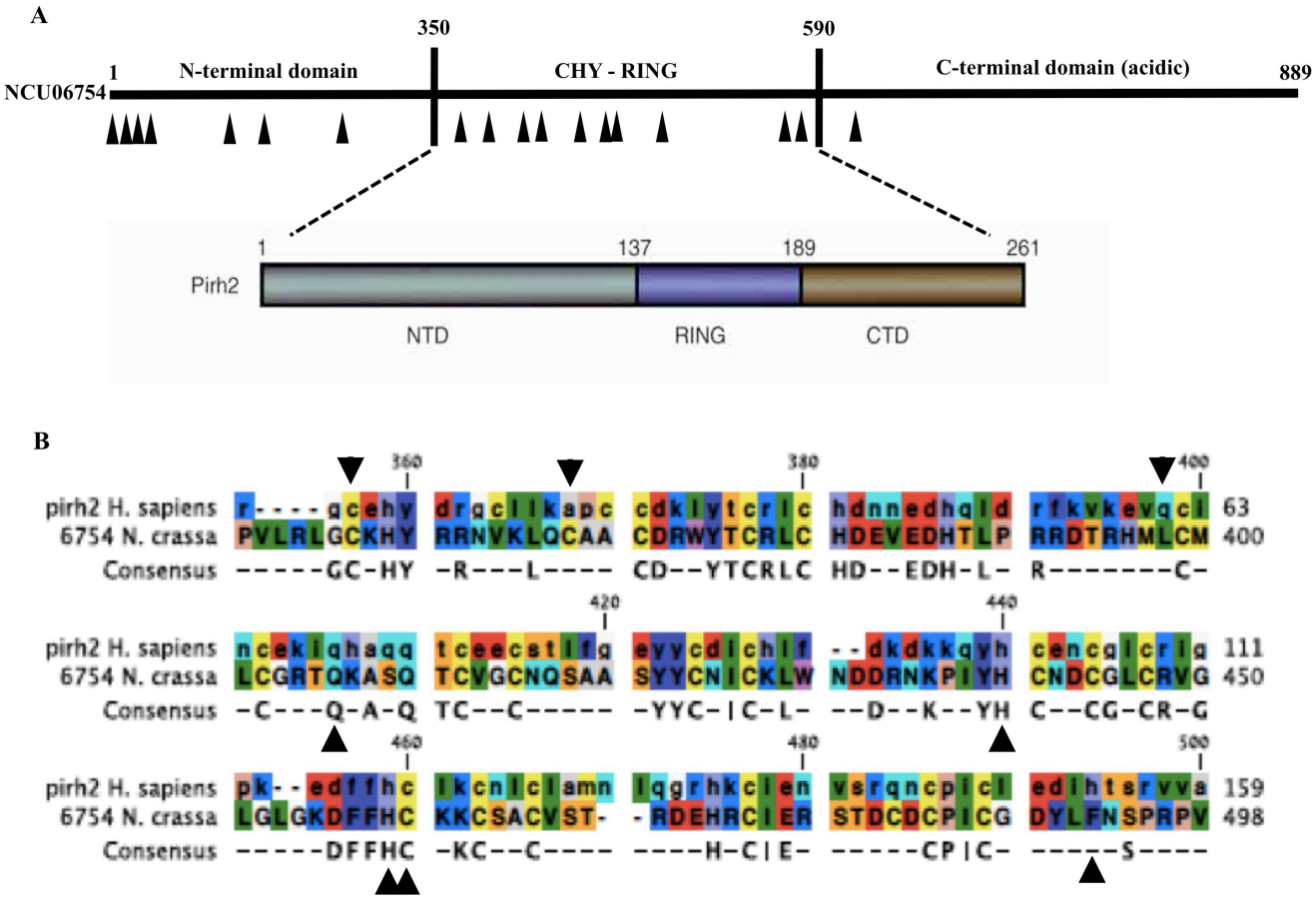

Figure 27. Line diagram of *N. crassa* NCU06754 and *H. sapiens* Pirh2 and BLAST alignment. A) Line diagrams of *N. crassa* NCU06754 and *H. sapiens* Pirh2 depicting region of greatest homology in the CHY-RING portion of NCU06754. Arrow heads indicate approximate positions of mutations found in *N. crassa* NCU06754 during C-terminal DHC mutant reversion analysis. B) BLAST alignment of region of homology between the two proteins. Arrowheads indicate residues changed in *N. crassa* that bring about suppression of C-terminal DHC mutants. Note the number of conserved cysteine and histidine amino acids that are modified.

Table 6. Extragenic suppressors of C-terminal DHC mutants located in NCU06754.

C-terminal DHC Mutant	Amino Acid Change in ncu06754
D4296E, del4297-99	Δ -250-156
D4296E, del4297-99	L4Stop
D4296E, del4297-99	D7Stop
D4296E, del4297-99	D7Stop
P4316S	R17Stop
D4296E, del4297-99	FS 110
G4146A	L138Stop
P4316S	W280Stop
D4296E, del4297-99	C357R
D4296E, del4297-99	C368R
D4296E, del4297-99	L398P
D4296E, del4297-99	Q406Stop
D4296E, del4297-99	H440L
I4232N	H459Y
G4146A	C460R
P4316S	F492L
D4296E, del4297-99	G575R
D4296E, del4297-99	N586H
D4296E, del4297-99	E604K

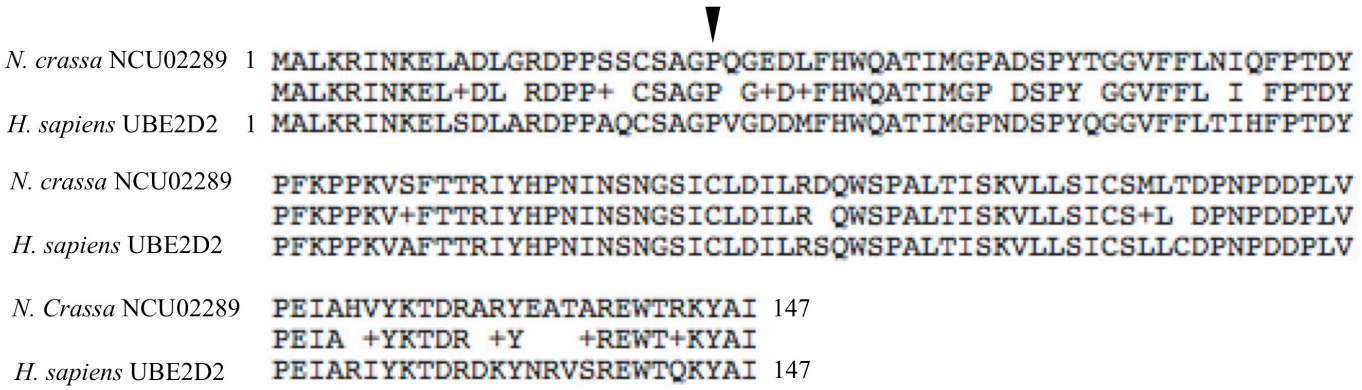

Figure 28. BLAST alignment of *N. crassa* NCU02289 and *H. sapiens* UBE2D2 proteins. These two proteins have an 84% identify between them and UBE2D2 has been shown to interact with the human homolog of NCU06754 in *N. crassa* (159). The arrowhead indicates the amino acid change (P25S) found from the C-terminal DHC mutant reversion analysis that brings about suppression of C-terminal DHC mutants.

D429GE ; del 4297-99
D429GE ; del 4297-99 r18 (I)
D429GE ; del 4297-99 r51 (I)
G414GA
G414GA r101 (I)
I423ZN
I423ZN r14 (I)
P431GS
P431GS r6 (I)
P431GS r12 (I)
ANCU06754
D429GE ; del 4297-99 r11 (E)
G414GA r19 (E)
I423ZN r3 (E)
P431GS r14 (E)
I423ZN r9 (E)

Figure 29. Western blot for DHC levels in C-terminal DHC mutants and revertants. The four C-terminal DHC mutants (D4296E ; del4297-99, G4146A, I4232N, and P4316S) and respective intragenic (I) and extragenic (E) revertants as well as ΔNCU06754 contain similar levels of DHC *in vivo*. Each of the extragenic revertants contain mutations in NCU06754 with the exception of I4232N r9, which contains a mutation in NCU02289.

C-terminal DHC Mutant Strains Have Reduced Levels of DHC Protein After Purification

The dynein protein purification scheme developed by Drs. David Razasfsky and Sethilkumar Sivagurunathan during the initial stages of this project was used to isolate dynein from two C-terminal DHC strains. Initial silver stain gels indicated that the level of DHC protein in these strains was greatly reduced in comparison to a wild-type strain, in direct conflict with previous western blot data (Figures 29, 30). When quantified more accurately, the concentration of DHC from C-terminal mutant strains is approximately 0.001 μg/μl, or about $1/30^{th}$ that of wild-type strains, which averages 0.03 μg/μl (Figures 30, 31).

Suppressed C-terminal DHC Mutant Strains Have Increased Levels of DHC Protein After Purification

Initial silver stain gels indicated that the level of DHC protein in suppressed C-terminal DHC mutants is increased in comparison to the C-terminal mutant strains alone. An intragenic suppressed strain (G4146A ; S4364F) has a concentration of approximately 0.006 μg/μl, or about 20% that of wild-type strains (Figure 30, 31). This increase from the C-terminal DHC mutant strains is sufficient for a return to more wild-type growth. Surprisingly, when the NCU06754 deletion is present in the G4146A C-terminal DHC mutant strain, the DHC protein returns to a level close to wild-type, about 0.03 μg/μl on average. In the I4232N C-terminal mutant strain, the introduction of the NCU06754 deletion leads to a DHC protein level of 0.009 μg/μl on average, or about 33% of wild-type. As is the case for the intragenic suppressed strain, this strain also is suppressed sufficiently enough to return to more wild-type growth, albeit not to the same suppression

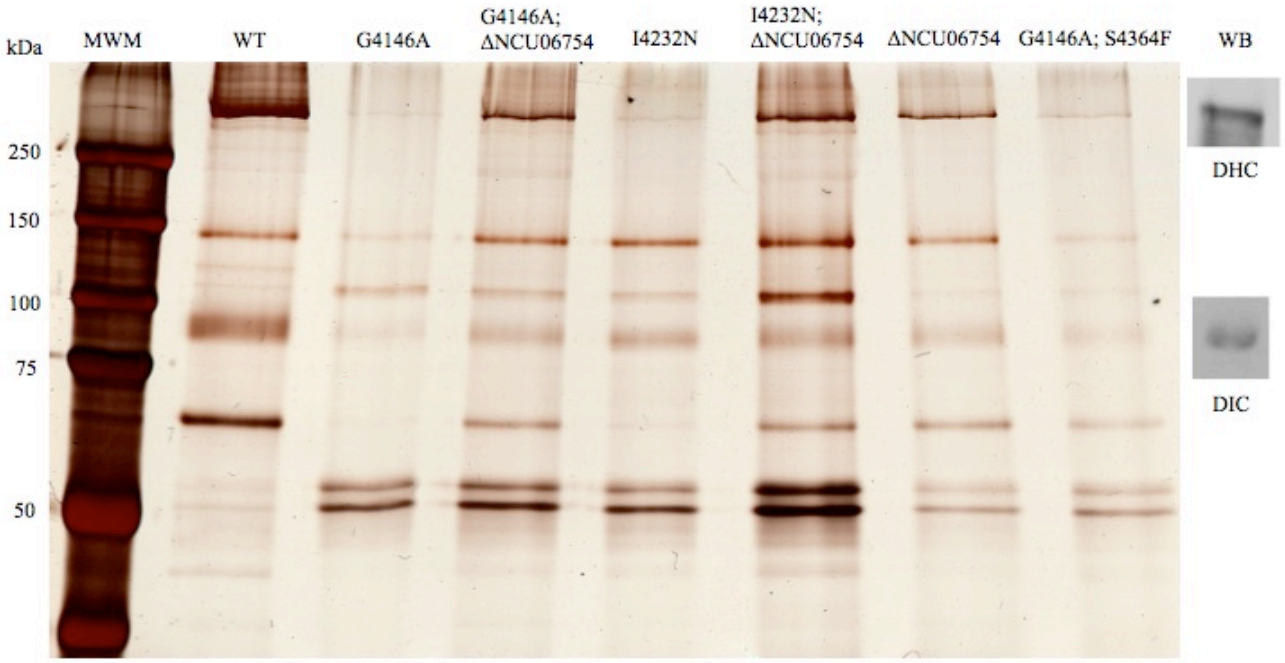

Figure 30. Silver stain gel comparison of *N. crassa* DHC protein levels. Both DHC and DIC were verified via western blot with results shown on the right. Various other bands exist and account for dynein related and interacting proteins that persist through the prep to the final elution. Of note is the G4146A and I4232N lanes with little DHC present compared to G4146A ; Δ6754 or I4232N ; Δ6754 with restored levels of DHC closer to WT.

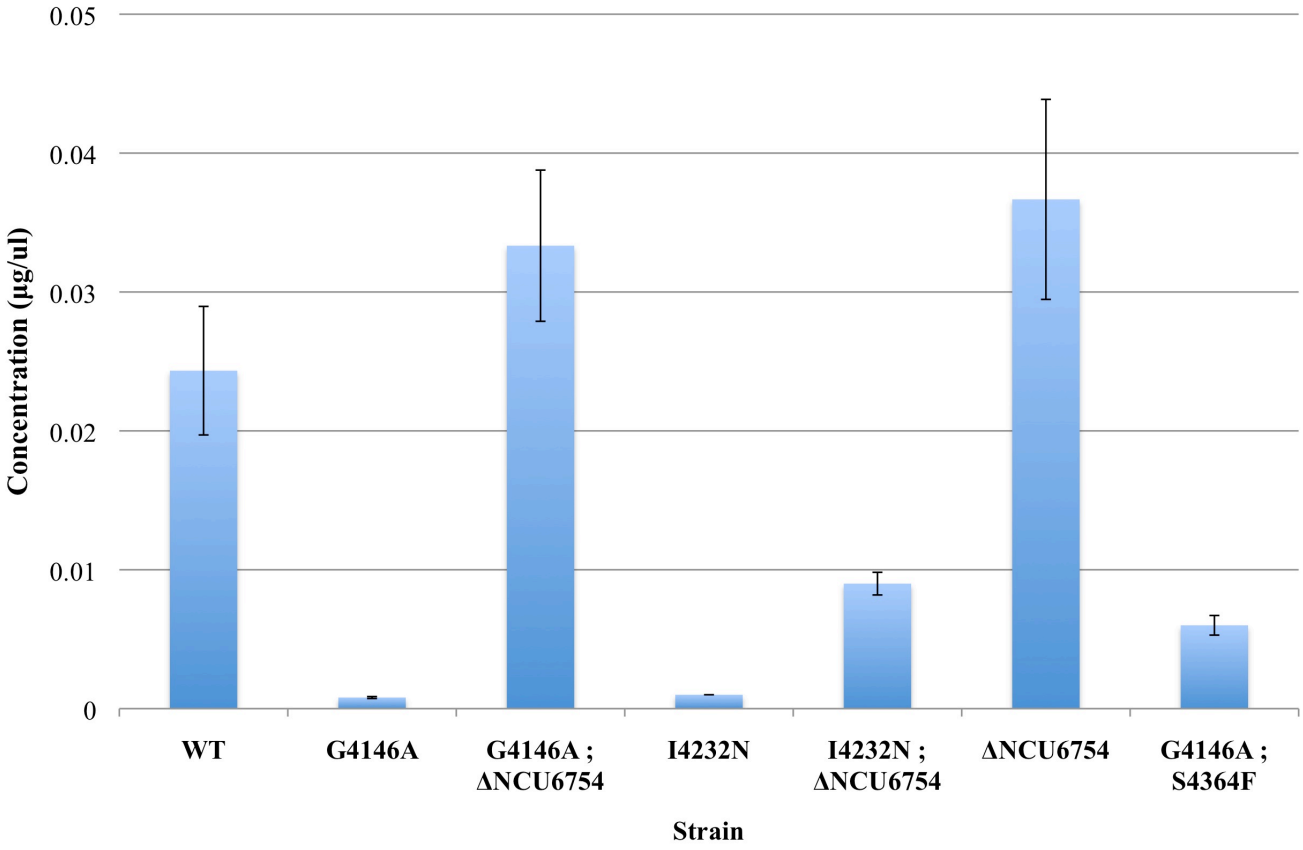

Figure 31. DHC concentration measured from DHC protein isolation preps from various *N. crassa* strains. When suppressed by a deletion of NCU06754, both C-terminal DHC mutants (G4146A and I4232N) show an increase in DHC protein concentration at or above wild-type levels. An intragenic suppressed strain (G4146A ; S4364F) has an increase in DHC concentration that is still below wild-type levels, yet the strain has a suppressed growth phenotype. Note: Concentrations were normalized to the initial wet weight used for purification of each strain.

Table 7. Summary of *In vitro* DHC single molecule results.

Strain	Velocity (µm/sec)	Distance (µm)	Microtubule Binding	n
Wild type	0.6 ± 0.2	2.6 ± 2.1	+	32
G4146A	---	---	+++	---
G4146A ; ΔNCU06754	0.8 ± 0.4	2.4 ± 1.8	+++	50
ΔNCU06754	1.0 ± 0.3	2.1 ± 1.7	+	51

level as other C-terminal DHC suppressed strains. An NCU06754 deletion strain has an average DHC protein level of 0.04 μg/μl, or a 30% increase above the average wild-type concentration.

Suppressed C-terminal DHC Mutant Strains Have Similar *In vitro* Velocities as Wild-type.

In vitro single molecule motility assays were preformed with purifed dynein protein sample from various strains. Wild-type *N. crasa* dynein motor had an average velocity of 0.6 μm/sec ± 0.2 μm/sec. A suppressed C-terminal DHC mutant strain had an average velocity of 0.8 μm/sec ± 0.4 μm/sec. The NCU06754 deletion strain had an average velocity of 1.0 μm/sec ± 0.3 μm/sec. Although both the C-terminal DHC mutant strain and the NCU06754 deletion strain displayed faster average velocities than wild-type, both fall within the standard deviation range of wild-type DHC (Table 7). Due to the low level of DHC protein isolated from the C-terminal DHC mutant strains, *in vitro* analysis could not be done for those particular strains. However, general results can be garnered for these strains from *in vitro* analysis. In comparison to both a wild-type and a NCU06754 deletion strain, strains with a C-terminal DHC mutation whether present alone or with an NCU06754 deletion, had much higher microtubule binding affinity *in vitro* (Table 7). Within about one minute of placing a slide with a C-terminal DHC mutant (G4146A) or suppressed mutant dynein (G4146A ; ΔNCU06754) sample under the microscope for inspection of motility, numerous beads with attached dynein were bound tightly to microtubules. Within a short period, visible microtubules were almost full of bound beads. This was not seen for wild-type or ΔNCU06754 dynein samples.

This result indicates that the C-terminal DHC mutants may have varying microtubule affinities in comparison to wild-type.

Suppressed C-terminal DHC Mutant Strain Have *In vitro* ATPase Activities Similar to Wild-type

In vitro ATPase assays were completed on wild-type, ΔNCU06754, G4146A ; ΔNCU06754, and I4232N ; ΔNCU06754 purified protein samples (Table 8). ATPase assays were unable to be completed on the C-terminal DHC strains lacking suppressing mutations due to low overall DHC protein yields. ATPase activity was determined by the overall cleavage of a radioactive isotope of ^{32}P incorporated into ATP by the various protein samples. Wild-type DHC had an ATPase activity of 100 ± 20 nmoles ATP/min/mg protein in the absence of tubulin and 125 ± 30 nmoles ATP/min/mg protein in the presence of 5 μM tubulin. ΔNCU06754 protein samples had an ATPase activity very close to wild-type, 90 ± 20 nmoles ATP/min/mg protein and 100 ± 30 nmoles ATP/min/mg protein, in the absence and presence of tubulin, respectively. G4146A ; ΔNCU06754 had an ATPase activity of 160 ± 30 nmoles ATP/min/mg protein and 170 ± 50 nmoles ATP/min/mg protein, in the absence and presence of tubulin, respectively. I4232N ; ΔNCU06754 had an ATPase activity of 110 ± 10 nmoles ATP/min/mg protein and 200 ± 10 nmoles ATP/min/mg protein, in the absence and presence of tubulin, respectively.

Table 8. ATPase activites of dynein from wild-type, suppressed C-terminal DHC mutants, and extragenic suppressor (NCU06754). Basal and microtubule-stimulated ATPase activities as the mean ± SD from multiple trials and the approximate fold change for basal versus microtubule-stimulated ATPase is shown.

Strain	**Basal ATPase (nmol/min/mg dynein)**	**MT-Stimulated ATPase (nmol/min/mg dynein**	**Fold Change**
Wild type	100 ± 20	125 ± 30	~1.3
G4146A ; ΔNCU6754	160 ± 30	170 ± 50	~1.1
I4232N ; ΔNCU6754	110 ± 10	200 ± 10	~1.8
ΔNCU6754	90 ± 20	100 ± 30	~1.1

C-terminal Mutant DHC Protein Levels Are Not Dependent Upon Kinesin, Dynactin, or Lis-1 Complex

Because DHC exists in complex with numerous accessory proteins, we wondered whether or not association of DHC in complex with DIC in our purification assay is dependent upon kinesin, dynactin, and/or the Lis-1 complex. Silver stain gel analysis indicated that strains without functional kinesin, dynactin, or Lis-1 complex have wild-type levels of DHC protein (*kin-1*) or an increased level of DHC protein (*Δro-3* and *Δro-11*) of 0.06 – 0.07 μg/μl, or about a 100% increase above the average wild-type concentration (Figures 32, 33). However, when these deletions are crossed into the C-terminal DHC mutant strain, there is no significant increase in DHC protein levels when compared to the C-terminal DHC mutant strain itself. As discussed previously, when the NCU06754 gene is deleted in a C-terminal DHC mutant strain, the DHC levels increase to that of wild-type or greater, in a C-terminal DHC mutant strain that lacks either kinesin, dynactin, or lis-1 complex, the levels of DHC protein are only restored to approximately 0.003 μg/μl, or about 10% of the average wild-type concentration. Additionally, these C-terminal DHC mutant strains that lack kinesin, dynactin, or lis-1 complex are not suppressed for ropy growth as is seen with C-terminal suppressed strains with modifications to NCU06754.

Heterokaryons of C-terminal DHC Mutants and Dynactin Mutants (Δ*ro-3*) Indicates Specificity of NCU06754 Action

To investigate if the action of suppression by mutation or deletion of NCU06754 is specific to mutant DHC or simply any DHC present in the hyphae, heterokaryons of a

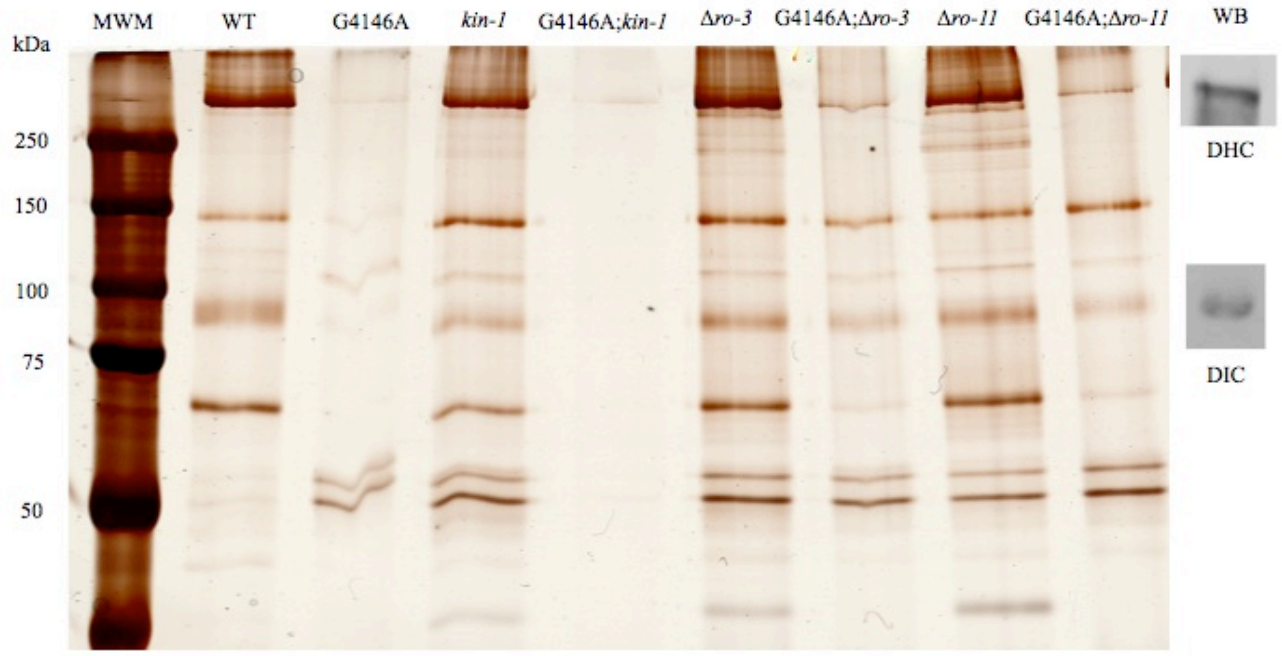

Figure 32. Silver stain gel comparison of *N. crassa* DHC protein levels in various strains. The presence of both DHC and DIC were confirmed via western blot as shown. DHC protein levels were compared for a C-terminal DHC mutant (G4146A) with wild-type (WT), a kinesin mutant (*kin-1*), dynactin p150 null (Δ*ro-3*), and Lis complex null (Δ*ro-11*) and the subsequent double mutant strains. No significant increase in DHC level is seen when a C-terminal mutant strain is in combination with a kinesin mutant, p150, or Lis null. Various other bands exist and account for dynein related and interacting proteins that persist through the prep to the final elution.

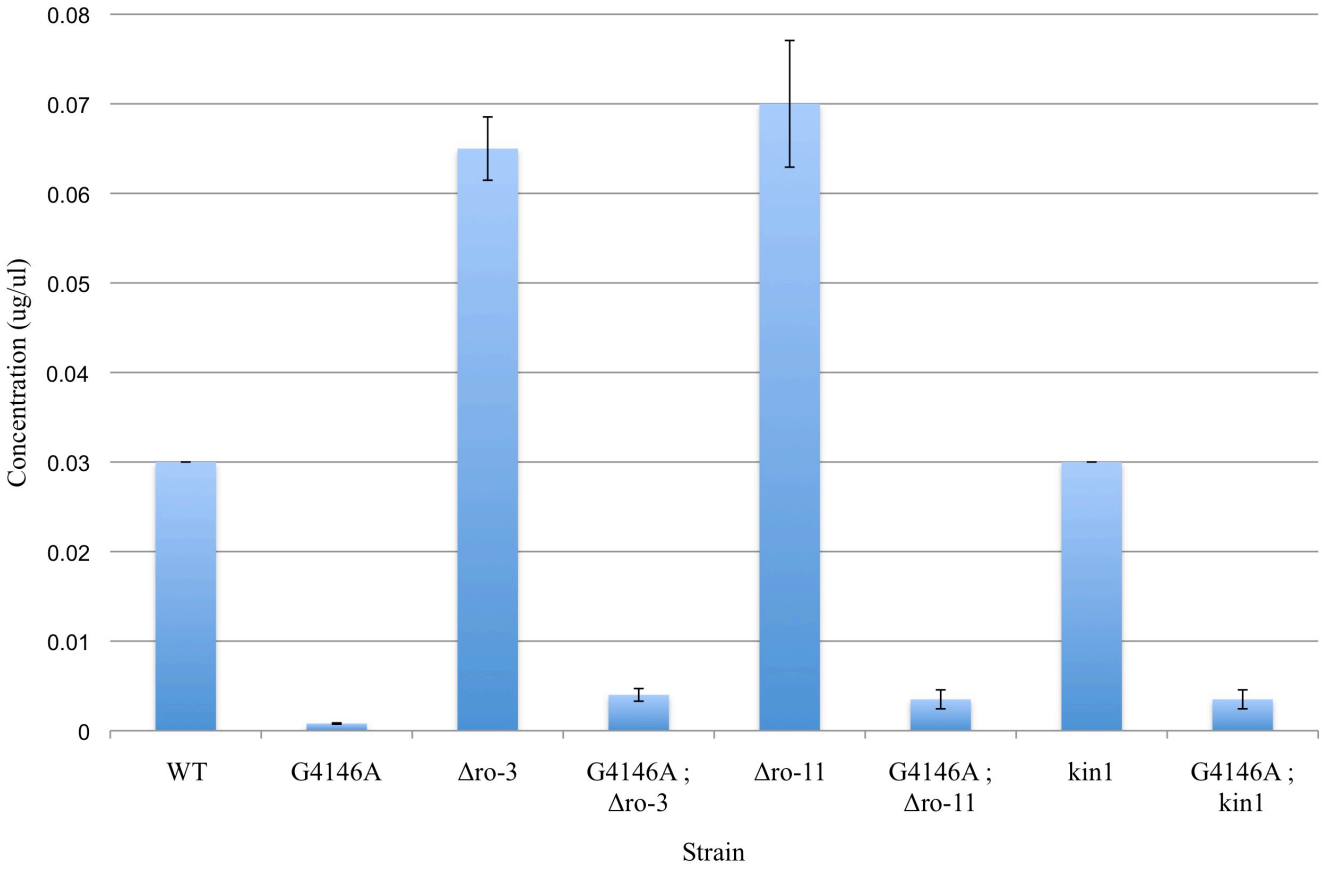

Figure 33. DHC concentration measured from DHC protein isolation preps from various *N. crassa* strains. In the presence of a kinesin mutant (*kin1*), dynactin mutant (Δ*ro-3*), or Lis1 mutant (Δ*ro-11*), no significant increase in DHC levels is seen for a C-terminal DHC mutant (G4146A). An increase in overall DHC level occurs in both single mutant strains, Δ*ro-3* and Δ*ro-11*, but not in a kinesin mutant. Note: Concentrations were normalized to the initial wet weight used for purification of each strain.

C-terminal DHC mutant and Δ*ro-3* were created. If functional NCU06754 targets any DHC present and not just mutant DHC, both growth and DIC mCherry phenotypes for the heterokaryon should be ropy (growth) or haze (DIC mCherry). However, the heterokaryons displayed wild-type growth and DIC mCherry distribution, indicating that the wild-type dynein present was not targeted by functional NCU06754 present in the heterokaryon.

Strains Used for Purification Contain Similar Levels of DHC Protein

Initial western blots indicated that C-terminal DHC strains contained similar levels of wild-type as well as to both intragenic and extragenic revertant strains (Figure 29). However, after purification was complete, DHC protein isolated from C-terminal DHC mutants was approximately 30 fold lower than wild-type (Figure 30). To verify that tagged DIC strains used for purification contained DHC and at levels near wild-type as were seen previously, western blots were completed. The results indicate that at the start of the purification process, each strain contains DHC protein at comparable levels to wild-type and to non-DIC tagged strains (Figure 34).

ΔNCU06754 Affects Non-C-terminal DHC Mutant Localization and Growth

To answer the question of what affect the lack of NCU06754 function has on other DHC mutants, all previously described DHC mutants with DIC mCherry were crossed with the ΔNCU06754 strain. Both *in vivo* dynein localization and growth were compared between the DHC mutant strain and the double mutant. Six DHC mutants were

WT
G414A
I423N
ΔNCU06754
G414A ; ΔNCU06754
I423N ; ΔNCU06754
Δro-3 (dynactin)
G414A ; Δro-3
Δro-11 (List)
G414A ; Δro-11
kin-1(kinesin)
G414A ; kin-1
G414A tr101
G414A ; ro-3 mCherry
G414A (no tag)
WT (no tag)

Figure 34. Western blot against DHC protein for purification strains. All strains contain the DIC-HMS (His-Myc-Strep) tagged for purification of dynein unless noted as "no tag". All strains contain similar levels of DHC before purification was carried out.

found to have changes in *in vivo* dynein localization pattern (Figure 35). Of these six mutants, two also had suppressed growth similar to G4146A ; ΔNCU06754 (Figure 22).

Five of the six mutants affected by loss of NCU06754 function had a haze distribution phenotype and the remaining one had a distal microtubule track decoration phenotype. Of the haze mutants, two had increased distal microtubule tracks, one had increased hyphal tip localization, and the remaining two had an increase in comet structures near the hyphal tip upon deletion of NCU06754. The distal microtubule track mutant simply had an increase in the signal seen on microtubules in distal regions. Two of the haze mutants had improved growth in the absence of NCU06754.

Summary of Results of C-terminal DHC Mutant Reversion Analysis

Previous work on dynein suggested that the C-terminal region might play a role in regulation of the ATPase activity of AAA1 (72). To further study the role and importance of this region of DHC, a dynein mutant screen was completed to identify numerous DHC mutants, including a set of four in the C-terminal region. Initial western blotting for DHC levels amongst the various DHC mutants revealed that the C-terminal DHC mutants, although having varying levels of DHC protein, were comparable to wild-type levels. However, these strains do display a ropy growth phenotype associated with DHC mutants while the nuclear distribution change is nominal. The *in vivo* distribution of the dynein motor in these C-terminal DHC mutants was hazy or diffuse with no distinct microtubule association. Suppressed C-terminal DHC mutants not only return to more wild-type growth, but the DIC mCherry signal is greatly increased in hyphal tip regions, almost identical to that of wild-type. DHC protein levels for suppressed strains

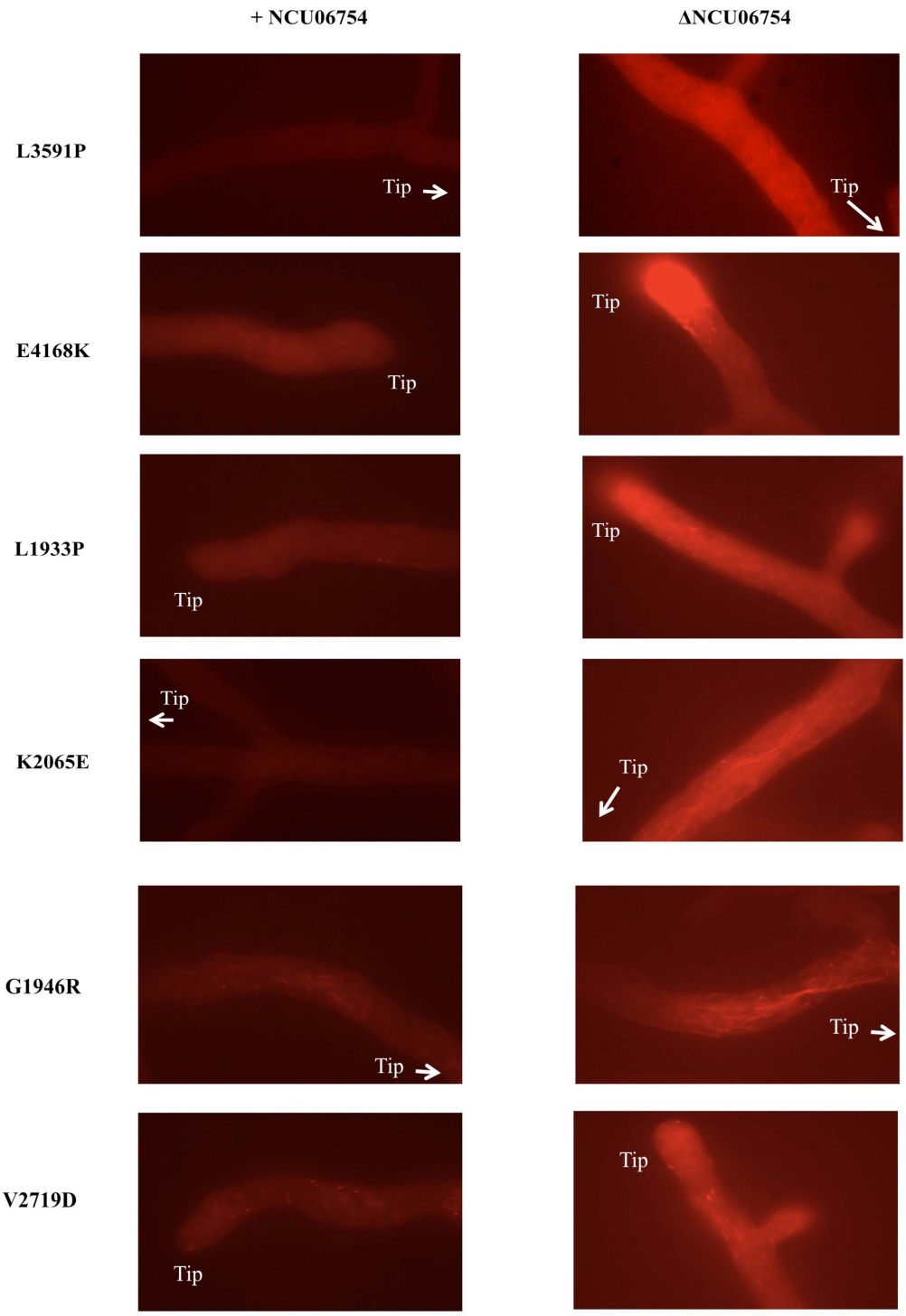
+ NCU06754
ΔNCU06754
L3591P
E4168K
L1933P
K2065E
G1946R
V2719D
Tip

Figure 35. Effects of ΔNCU06754 on *in vivo* dynein localization on other DHC mutants. DIC mCherry images of five haze mutants (L3591P, E4168K, L1933P, K2065E, V2719D) and one distal microtubule track mutant (G1946R) in the presence (left) or absence (right) of NCU06754. L3591P, K2065E, and G1946R mutants have increased distal microtubule tracks, E4168K has increased hyphal tip localization, and L1933P and V2719 have increased numbers of comet structures in the hyphal tip region, in the presence of ΔNCU06754. E4168K and V2719D had improved growth in the absence of NCU06754.

were also not significantly increased compared to the original mutant as shown via western blotting. However, upon completion of purification of dynein from C-terminal DHC mutants, the level of DHC protein was about 30-fold lower than wild-type, while the suppressed strains had a return to wild-type levels. Additionally, crosses with other DHC mutants and ΔNCU06754 resulted in suppressed growth and *in vivo* localization phenotype for two DHC mutants and suppressed *in vivo* localization phenotype for four other DHC mutants. In whole, these results suggest a role for the E3 ubiquitin ligase NCU06754 in the assembly of the dynein motor complex of numerous DHC mutants.

CHAPTER 4

DISCUSSION

Although many studies have been completed on the dynein motor complex, few have focused on the C-terminal region of the dynein heavy chain (DHC) and its role in the entire complex and overall dynein function in the cell. In one of the few studies, recombinant DHC proteins were constructed with portions of the ring structure missing, including the C-terminal region, and an increase in overall ATPase level was observed (72). A study using cryoelectron microscopy to gain information on the interaction of dynein with microtubules led to a proposed model where sliding occurs in the dynein heavy chain during the ATPase cycle and its movement along microtubules. (75) This sliding was projected to take place between the N-terminal tail, AAA1/2 domains (ATPases associated with diverse cellular activities), and the C-terminal domain, indicating changes in interactions between the C-terminal region and other nearby domains of the DHC (75). Little else is known about the role of the C-terminal region of the DHC, so this dissertation sought to address the following: 1) What are the differences, if any, in the biochemical properties of C-terminal DHC mutants relative to wild-type dynein? 2) How are DHC mutations present in the C-terminal region suppressed? 3) What model provides a likely explanation for the suppression of C-terminal DHC mutants by an extragenic source?

Discovery of Mutations in an E3 Ubiquitin Ligase Leading to Suppression of DHC Mutants

E3 ubiquitin ligases are known to be involved in numerous and diverse cellular activities (Table 3). Although these enzymes play key roles in regulation of membrane trafficking (Hochrainer 08), mitotic processes (1, 7), and cytoskeletal remodeling (149), until this work, no direct link between the dynein motor complex and E3 ubiquitin ligases has been discovered. Based on the knowledge of E3 ubiquitin ligases and data obtained through this research, models can be put forth to explain the role of the E3 ubiquitin ligase, NCU06754, in the dynein complex in *N. crassa*.

Since the major role of E3 ubiquitin ligases is to add ubiquitin groups to proteins thus marking them for proteasomal degradation, an initial model for the suppression of C-terminal DHC mutants by mutation or deletion of NCU06754 is that the original mutation leads to a large increase in degradation of DHC via NCU06754 activity and simply modifying this gene allows for a restoration of DHC protein level. Based on the DHC purification and *in vivo* DIC mCherry localization data, this theory holds some merit. DHC concentration after purification was determined to be about 30-fold lower in C-terminal DHC mutants than in wild-type (Figure 31) and a hazy, diffuse distribution was seen for *in vivo* localization (Figure 22). However, the initial western blot data indicated that DHC protein levels between C-terminal DHC mutants and revertants, both intragenic and extragenic, is relatively unchanged (Figure 29), undermining this model.

If mutations in the C-terminal region of DHC do not simply reduce the overall level of DHC protein in the cell via NCU06754 and the proteasomal pathway, some other problem must be occurring in the dynein complex brought about by the C-terminal

mutations leading to ropy growth, hazy *in vivo* localization, and inability to purify dynein from a DIC His-Myc-Strep (HMS) tagged strain. Because DHC protein concentration does not show drastic changes from strain to strain when the C-terminal DHC mutant strains are compared to revertant strains (Figure 29), yet *in vivo* localization, utilizing a DIC mCherry strain, results in a haze (Figure 22) and upon attempted purification in a DIC-HMS strain, DHC protein levels are near zero (Figure 31), DHC is unable to properly associate with the entire dynein complex, and more specifically with the DIC itself. In this model of suppression via mutation or deletion of NCU06754, the E3 ubiquitin ligase targets either an assembly factor for the dynein complex, "Factor X" for degradation or has direct contact with DHC or another dynein subunit or dynein-associated protein (Figure 36). In either scenario, when dynein has altered structure and/or function, the NCU06754 E3 ubiquitin ligase is activated and the dynein complex is unable to properly assemble. In one scenario, when NCU06754 activity is removed, assembly "Factor X" levels are restored and the dynein complex is able to assemble. In another scenario, NCU06754 makes a direct protein-protein interaction with DHC or another dynein-associated protein and during conditions of altered dynein structure and/or function this interaction may lead to changes which prevent proper dynein complex assembly.

Upon purification of dynein from either a Lis1 or p150/dynactin mutant strain, the level of DHC was measured at approximately double the concentration purified from a wild-type strain (Figure 33). Since assembled dynein, including DHC in complex with

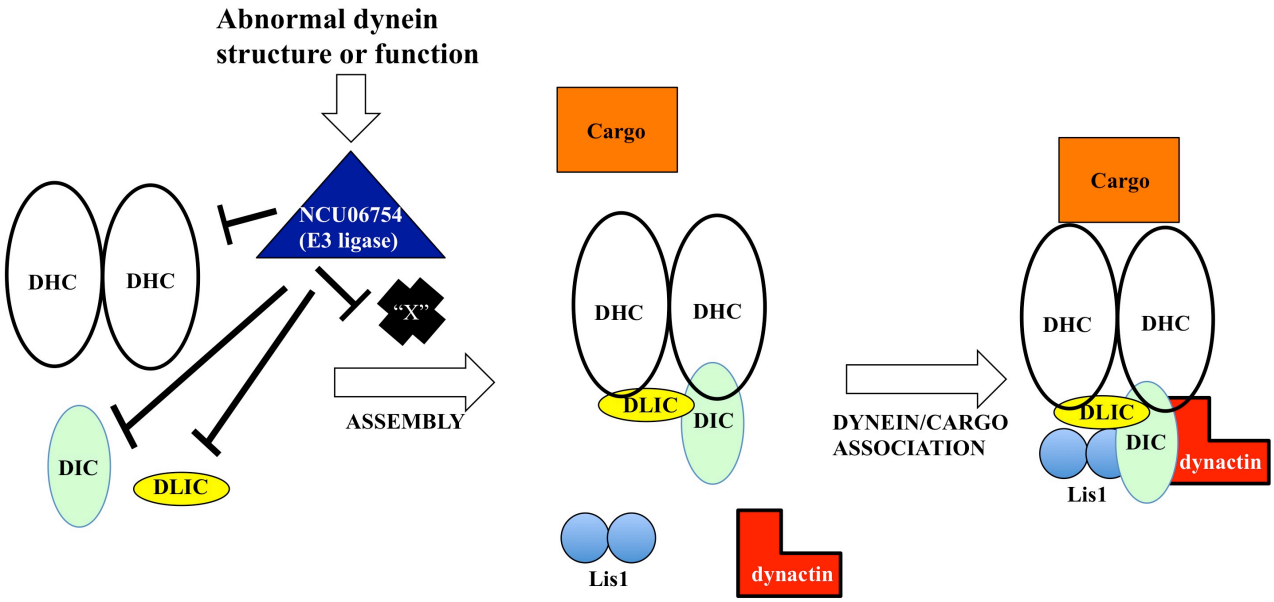

Figure 36. Model for the role of NCU06754 in dynein complex assembly. Dynein complex formation is shown in two steps, first being assembly of DHC with DIC and DLIC then dynein and cargo association along with the addition of Lis1 and dynactin. Under normal conditions, DHC is able to properly assemble first with DIC and DLIC because factor "X", an assembly factor for the dynein complex, is not polyubiquitinated by NCU06754, which would mark it for degradation. However, under adverse conditions in the cell where there is abnormal dynein structure and/or function, NCU06754 polyubiquitinates factor "X", marking it for degradation and hindering proper assembly of DHC with DIC and DLIC. Or, under normal conditions, DHC is able to properly assemble first with DIC and DLIC because NCU06754 does not interact with DHC, DIC, or DLIC and does not monoubiqutinate its target which would hinder proper dynein assembly. However, under adverse conditions in the cell where there is abnormal dynein structure and/or function, NCU06754 monoubiqutinates DHC, DIC, or DLIC, which prevents proper dynein assembly.

DIC, is collected from the purification, it is clear that the loss of Lis1 or p150/dynactin does not hinder the assembly of DIC with DHC and therefore Lis1 and dynactin are unlikely to components of the pre-assembled portion of either model.

Identification of Extragenic Suppressors of C-terminal DHC Mutants

Up to the point of this dissertation, no other group had attempted a genome wide scan in *N. crassa* utilizing the SNP differences between standard strains to identify suppressors of dynein genes. This novel screening method indicated a bracketed area on linkage group II that contained an extragenic suppressor of C-terminal DHC mutants. Although this method could only indicate a general area of the genome that included several hundred genes, this new method was deemed a success and could be used for future studies to help identify extragenic suppressors.

An effort by the Neurospora Genome Project to obtain targeted gene knockouts of almost all genes in the *N. crassa* genome was of great benefit to aid in the identification of the major extragenic suppressor of C-terminal DHC mutants (94). The use of multiple gene KOs in the area predicted to contain the suppressor by SNP mapping resulted in further definition of the region on linkage group II. Transformation of gene KO constructs was vital in determining that NCU06754, when knocked out, gave rise to suppressed growth of a C-terminal DHC strain. DNA sequencing of the NCU06754 ORF resulted in the identification of 19 unique changes to the NCU06754 sequence that lead to suppression of ropy growth of C-terminal DHC mutants (Table 6). Many of the mutations in NCU06754 are focused in a region of homology between NCU06754 and Pirh2 in humans (Figure 27). Multiple cysteine and histidine residues in this region are

conserved in this protein from various species, which are involved in the coordination of zinc in this domain of the N-terminal region of the protein. These residues are highly conserved between Pirh2 and NCU06754 and the suppressor mutations from this region of homology have been mapped onto the Pirh2 structure as reference (Figure 37). Further sequencing indicated that not only could this particular region of NCU06754 be modified to bring about suppression, but essentially eliminating the translation of a full-length product by introduction of nonsense mutations or deletions early in the sequence also could bring about growth suppression of C-terminal DHC mutants. This was not surprising since the ΔNCU06754 deletion strain on its own has no discernable difference in growth from wild-type.

Recently, a strain with an extragenic suppressor that was determined to be unlinked to NCU06754 was sent to Joint Genome Institute (JGI) for whole genome sequencing to identify the suppressor mutation(s) leading to reversion of the C-terminal DHC mutants. After mapping studies showed tight linkage between NCU02289 and the minor extragenic suppressor locus, experiments were conducted where C-terminal DHC mutants were transformed with wild-type NCU02289 DNA resulting in RNAi knockdown of the NCU02289 gene and restoration of near wild-type growth to the DHC mutants. Interestingly, the NCU02289 gene is predicted to encode an E2 ubiquitin conjugating enzyme and its homologous partner in humans, UBE2D2, has been shown to interact with Pirh2, the likely homolog to NCU06754 of *N. crassa* (Figure 38) (159). Thus far, only one mutation has been identified in NCU02289 that leads to suppression of C-terminal DHC mutant phenotypes, and it lies in a region known to be important for UBE2D2 and Pirh2 interaction (Figures 28, 38). Because a single E2 ubiquitin ligase has

multiple E3 ligase partners and is an essential gene for *N. crassa* viability, mutations resulting in the elimination of this gene, as was the case with NCU06754, are not expected and any other mutations likely result in the perturbation of interaction between NCU06754 and NCU02289 (159).

NCU06754 and NCU02289 human homologs Pirh2 and UBE2D2 are involved in p53 regulation

The tumor suppressor p53 has been shown to be involved in numerous cellular responses to stress. When activated, p53 can exert effects upon DNA synthesis, cell cycle arrest, apoptosis and transcription, amongst many others (190). Mutations in the p53 gene that render the protein incapable of carrying out its various functions have been identified in over 50% of cancer cases (193). The cellular levels of p53 are tightly controlled by numerous mechanisms including ubiquitination by E3 ubiquitin ligases (190, 89, 98). Pirh2 is an E3 ubiquitin ligase that along with MDM2, COP1, and ARF-BP1 regulates the level of p53 in the cell (89). Pirh2, human homolog of *N. crassa* NCU06754, is a RING finger family member and contains a RING-H2 motif ($Cys_3His_2Cys_3$) as its functional domain (190, 28) (Figures 27, 37). Pirh2 functions in the Pirh2-p53 feedback loop independent of other E3 ligases. Its major role is during DNA damage response when Pirh2 targets p53 for degradation due to the inability of MDM2 to carry out such a response (159).

It was recently discovered that the E2 ubiquitin-conjugating enzyme UBE2D2 is an E2 protein that interacts with Pirh2 to aid in regulation of p53 (159) (Figure 38).

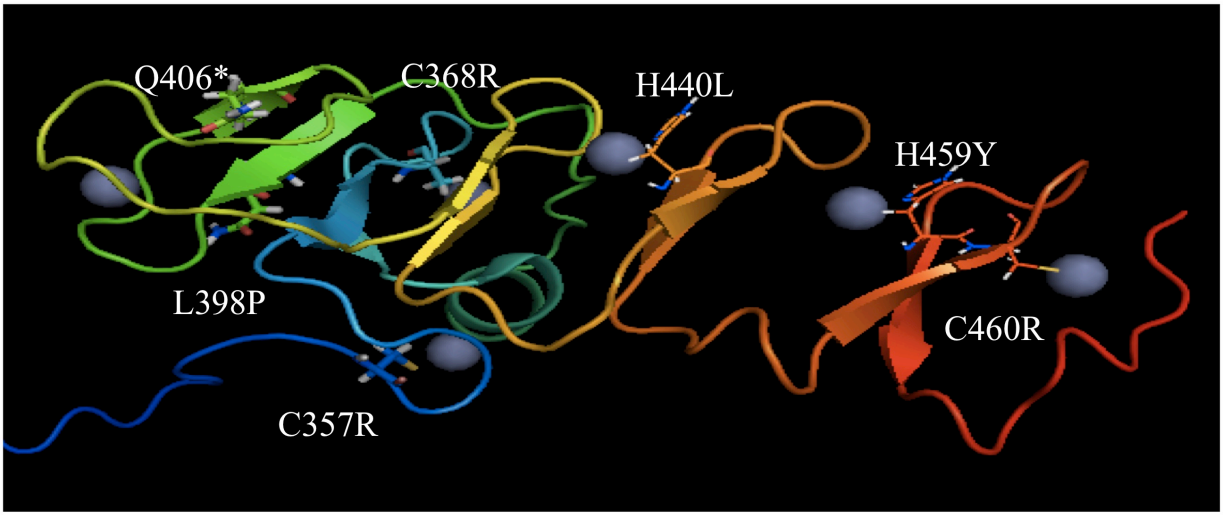

Figure 37. Pirh2 N-terminal domain structure with NCU06754 mutations. Labeled are the residues that when modified lead to suppression of C-terminal mutants in *N. crassa* DHC. In Pirh2, these residues are involved in coordination of zinc ions in the CHY-RING domain. (Pdb 2K2C)

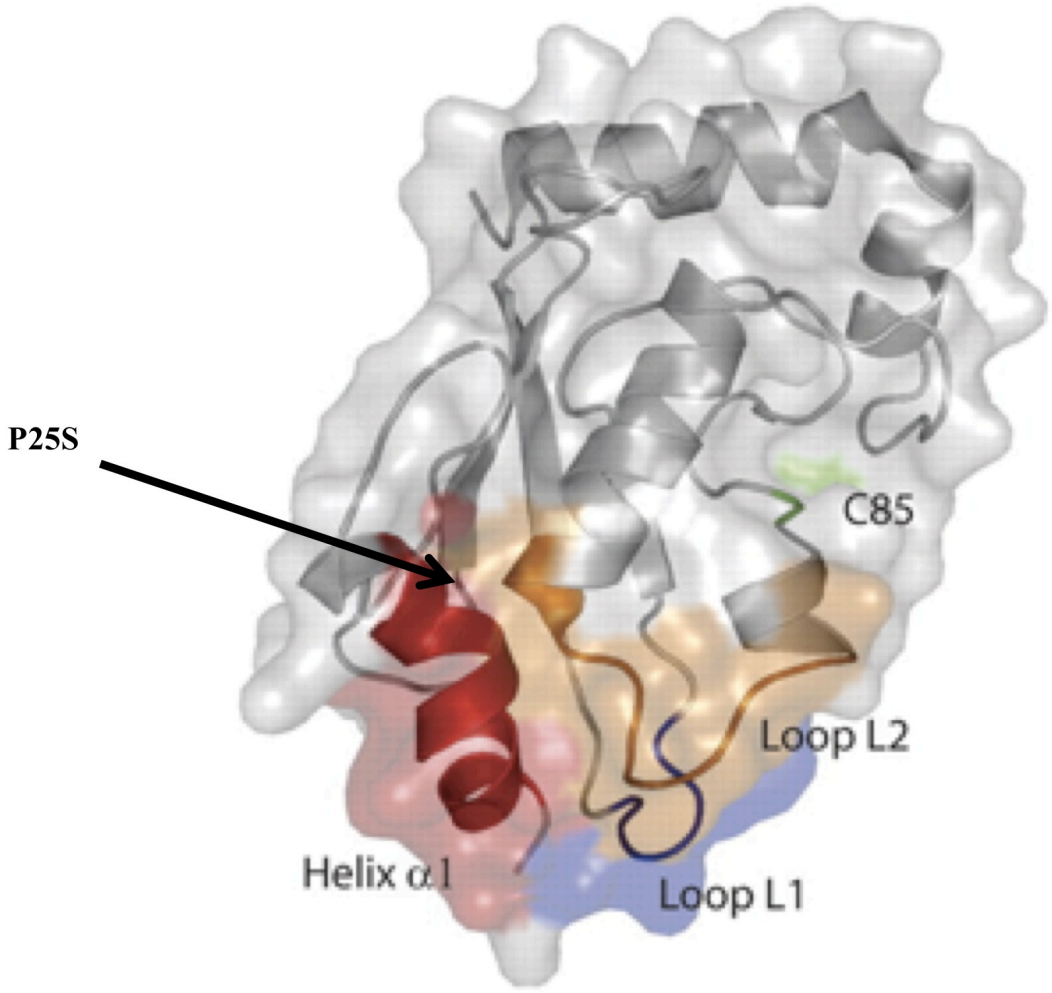

Figure 38. Structure of UBE2D2 with Pirh2 interaction site. In higher organisms, the E3 ligase Pirh2, homolog of NCU06754 in *Neurospora crassa*, interacts with ubiquitin conjugating enzyme E2 UBE2D2, homolog of NCU02289 in *Neurospora crassa*. The interaction site is color coded and includes portions of helix α1 and loops L1 and L2. The position of the suppressor mutation in NCU02289 is shown at the tip of the arrow. (Adapted from reference 159)

UBE2D2, human homolog of *N. crassa* NCU02289, is also an interacting partner with MDM2, another E3 ligase involved in p53 regulation (102). Although neither NCU06754 nor NCU02289 have been shown to be functional members of a ubiquitin ligase pathway in *N. crassa*, based on homology and data from other organisms, the two gene products most likely work in concert to carry out a regulatory role in the fungus and data from this research suggests that role is in the regulation of dynein complex assembly.

Commonalities of Intragenic and Extragenic Suppressors of C-terminal DHC Mutants

Mutants identified from the *cot-1* screen were classified on a scale of 1 to 5, with 1 being wild-type and 5 being a ΔDHC strain. C-terminal DHC mutants are near 3 on the phenotypic scale and are classified as "mild ropies". The fact that there was little change in nuclear distribution compared to wild-type further supports these mutants as mild. However, C-terminal mutants have adverse DICmCherry distribution, lacking strong signal near the hyphal tip, rather displaying a diffuse or hazy distribution throughout the hyphae (Figure 22). This was the first major difference seen compared to wild-type and seemingly suggested a reduced overall amount of dynein complex present near hyphal tips. Upon completion of reversion analysis, suppressor mutations were identified in the *ro-1* gene that brought about a return to more wild-type growth of C-terminal DHC mutants. The majority of these mutations were found to be located near the site of the original lesion, in and around the C-terminal region (Table 7). There were a few suppressor mutations found elsewhere, notably in the AAA1/2 region of the DHC. This is in agreement with previous work that suggested a relationship between the C-terminal

domain and AAA1/2 (72, 75). Because DHC is a ring and conformational changes are propagated throughout the entire ring structure, these suppressor mutations located in other areas may still occur in sites critical for overall dynein structural changes during the ATPase cycle and travel along microtubules. Although other suppressor mutations lie in AAA1 and AAA2 that conceivably interact with various side chains in the C-terminal domain, the vast majority lies in or directly around the end of the C-terminal region (Figures 23, 24). This helix or the regions near it appear to be of utmost importance in bringing about the phenotypic change seen in C-terminal DHC mutants. This suggests that after any of the initial C-terminal DHC mutations arises, the extreme end of the C-terminal domain has a negative activity imparted upon it. Perchance, a structural change occurs that causes poor assembly of the overall dynein complex through the activity of NCU06754. It is also possible that this region may be vital for recognition by the ubiquitin ligase system and perturbation of numerous residues and structures in the C-terminus causes DHC to be more preferentially bound by NCU06754, the E3 ubiquitin ligase. By altering this end of the peptide, wild-type like growth is seen. No matter the reason, in combination, the original C-terminal DHC mutation and an intragenic suppressor mutation bring about a return to more wild-type growth and an *in vivo* restoration of dynein localization signal to the hyphal tip (Figure 22) as well as an increase in the amount of DHC able to be purified from these suppressed strains (Figure 31).

Likewise to the intragenic suppressor pattern seen, the extragenic suppressors show commonality in their suppression. Not only does ΔNCU06754 bring about suppression of the C-terminal DHC mutants, but also individual isolated suppressors of

C-terminal DHC mutants identified in the NCU06754 gene are able to suppress each of the C-terminal DHC mutants. The same holds for the mutation found in the E2 ubiquitin conjugating enzyme, NCU02289, which was crossed with each of the C-terminal DHC mutants and was able to suppress the ropy growth phenotype for each one.

Role of NCU06754 on Dynein Function

Importance of Kinesin, Lis-1, and Dynactin in NCU06754 Suppression of DHC Mutants

Numerous studies have shown the importance of interaction between various proteins and the dynein heavy chain. Kinesin and dynein work together along microtubules to transport cargoes from one end to another, in opposing directions and function as carriers for each other along microtubules (48, 55, 93, 155). The Lis-1 complex has been shown to be an important enzymatic regulator of the dynein motor (113, 37), while the dynactin complex is involved in overall dynein processivity during its journey along microtubules (38, 97). Since these proteins have known function in relation to the dynein motor complex, we explored the possible influence they have on suppression of DHC mutants by NCU06754. Specifically, does the amount of dynein heavy chain purified from DIC-HMS tagged strains increase or decrease significantly in the absence of *kin-1*, *ro-11* (*lis-1*), or *ro-3* (dynactin) activities (Figure 33)? Levels of DHC in a *kin-1* mutant strain remained unchanged from wild-type, while DHC levels increased approximately 2 fold in both Δ*ro-11* and Δ*ro-3* strains in comparison to wild-type, which has been observed previously in the Plamann lab. When dynein was purified from a strain with a C-terminal DHC mutation and either *kin-1* mutation, Δ*ro-3*, or Δ*ro-11*, no significant increase in DHC levels was observed. Additionally, no growth

suppression is observed for these strains. Because there is no change in DHC levels in a *kin-1* mutant background, suppression of DHC mutants by NCU06754 is seemingly not dependent upon dynein interacting with, and being recycled back to hyphal tips, by kinesin. Thus, it appears that kinesin, Lis-1, and dynactin do not play a significant role in suppression of C-terminal DHC mutants via NCU06754. Because the lack of recycling back to the microtubule plus end (*kin-1* mutant) and elimination of either dynactin (Δ*ro-3*) or Lis1 (Δ*ro-11*) does not lead to a significant improvement in the levels of purifiable dynein from a C-terminal DHC mutant and DIC-HMS strain, this suggests that the presence of functional kinesin, Lis-1, or dynactin does not further hinder the C-terminal mutants ability to properly complete the overall dynein cycle of subunit assembly, cargo binding, travel along microtubules, and recycling back to the plus end of microtubules. The inability to complete this cycle leads to disassembly of the overall dynein complex.

Dynein Heavy Chain Mutant Nuclear Distribution and Localization Phenotypes

Because the C-terminal DHC mutants are not severe ropy growers overall, it is not surprising that nuclear distribution in these strains is also not severely impacted compared to wild-type. With that said, C-terminal DHC mutants do not have wild-type nuclear distribution. While wild-type strains will most often have even distribution of nuclei throughout the growing hyphal tube and either one or zero nuclei in the spore itself, C-terminal DHC mutants do have slightly less even distribution and often times have more than a single nucleus present in the spore. However, in comparison to a DHC null strain, C-terminal DHC mutants are quite mild for any nuclear distribution phenotype (Figure 22).

Due to the fact that the C-terminal DHC mutants have a mild ropy growth phenotype and fairly well distributed nuclei in growing hyphae, it could be postulated that the *in vivo* distribution of dynein should be relatively close to wild-type. However, what was observed was very much unlike wild-type. DICmCherry distribution in C-terminal DHC mutant hyphae is hazy and diffuse. Gone is the heavy red signal near the hyphal tip, replaced with a diffuse haze throughout the hypha. When this information is compared with initial western blot and purification results, the *in vivo* data further suggests that C-terminal mutant DHC is unable to properly assemble in a functional dynein complex.

When NCU06754 is mutated or deleted, both nuclear distribution and *in vivo* dynein localization are restored to a more wild-type phenotype (Figure 22). If the absence of NCU06754 allows the dynein complex to properly assemble, it is not surprising that both distribution of nuclei and dynein complex again resembles wild-type for both properties.

Biochemical Properties of C-terminal DHC Mutants

Various mutations around the DHC bring about different changes to the overall biochemical properties of the dynein motor in regards to ATPase and motility along the microtubules. Initial data indicates that these mutants may not be as severely affected for ATPase activity and microtubule motility. Because little protein can be purified from C-terminal DHC mutants, their biochemical properties cannot be determined at this time. However, some information can be garnered from suppressed C-terminal DHC mutant strains. There is a slight increase in activity for a suppressed C-terminal DHC mutant in

comparison to wild-type, however, the range of values observed for the suppressed C-terminal DHC mutant strain is similar to wild-type (Table 9). Unlike other mutants observed previously, the suppressed C-terminal DHC mutant does not have ATPase activity that is substantially higher than WT (161).

Changes to motility from wild-type to C-terminal DHC mutants were more pronounced than changes to ATPase activity. As with the ATPase assays, due to low levels of protein for C-terminal DHC mutants, few if any motility events were seen. However, a striking difference was observed for these mutants: that is the rapid and strong binding to microtubules. After a minute of observation under the microscope, beads coated with either C-terminal DHC mutant protein or suppressed C-terminal DHC mutant protein rapidly bound to the microtubules. In comparison, after several minutes of observation of wild-type or ΔNCU06754 samples, few beads were bound and stuck to microtubules. This data indicates a change in microtubule affinity for C-terminal DHC mutants and even in the presence of an extragenic suppressor that property of the motors does not change. It is possible that the phenotypes seen in C-terminal DHC mutants may be in part due to the change in microtubule affinity for these mutants, leading to dynein complex assembly issues.

Although dynein from a C-terminal DHC mutant lacking NCU06754 activity does retain strong microtubule affinity, both the motility and ATPase activities of these motors is similar to wild-type (Tables 8, 9). In addition, dynein purified from the ΔNCU06754 strain also had biochemical properties comparable to wild-type. This data suggests that dynein from these C-terminal DHC mutants, whether in the presence or absence of NCU06754, does not change in terms of its overall biochemical properties.

Affects of Mutation or Deletion of NCU06754 on Non-C-terminal DHC Mutants

The ability of NCU06754 mutation or deletion to suppress DHC mutants was discovered through the reversion analysis screen of C-terminal DHC mutants. Up until that point in the screens, no extragenic lesions were found that suppressed other DHC mutants. Since there was found to be commonality amongst intragenic suppressors of C-terminal DHC mutants and because suppression screens have not been completed on all of the DHC mutants, it was important to look at any possible affects of NCU06754 mutation or deletion on non-C-terminal DHC mutants. The ΔNCU06754 deletion was crossed into other DHC mutants and both growth and *in vivo* localization of dynein were analyzed for each (Figure 34). Upon comparison of growth and localization studies, it was concluded that deletion of NCU06754 did bring about growth suppression for two of the mutants with hazy distribution of DICmCherry signal as seen with the C-terminal DHC mutants. Furthermore, although unable to bring about growth suppression for all mutants studied, the absence of NCU06754 did affect *in vivo* localization of certain DHC mutants. Those mutants that retain ropy growth when combined with ΔNCU06754 mutations would be expected to have DHC mutations that still impart a more negative activity on the dynein complex leading to ropy growth, even if the absence of NCU06754 allows better overall dynein complex assembly.

Additional Experiments with NCU06754

Combination of C-terminal DHC Suppressor Mutation and ΔNCU06754

To test whether or not the combination of a DHC intragenic suppressor mutation and lack of NCU06754 on a C-terminal DHC mutant was possibly helpful or harmful, a G4146A ; S4364F strain and a ΔNCU06754 strain were crossed and progeny plated.

Upon visual inspection, no changes were seen for growth phenotype of progeny. In combination, lack of NCU06754 and the intragenic suppressor S4364F do not enhance nor worsen growth of a C-terminal DHC mutant strain.

In vivo NCU06754 mCherry Studies

An mCherry NCU06754 construct was completed in a similar fashion to those constructs shown in Figure 14. In addition, a hygromycin resistance marker was added to the plasmid to aid in identification of positive transformants by plating on media with hygromycin. After transformation, positive matches were found for strains able to grow on hygromycin media. Visualization under the fluorescence microscope revealed little overall mCherry signal and no distinct region in the hyphae where higher amounts of signal could be seen. Based on this experiment, it appears NCU06754 may not be localized to a particular area of the hyphae or may not be present in high enough concentration to be properly visualized by this method.

Western Blot Against Ubiquitinated Protein from Dynein Purifications

Western blots were completed to attempt to determine if DHC was in fact either mono-ubiquinated or poly-ubiquitinated. No ubiquitinated DHC was seen on any of the blots using purified dynein samples. Regardless, if DHC is the target of the E3 ubiquitin ligase, it is possible that the marked protein would be rapidly eliminated from the cell and would not be identified in a Western blot. Likewise, if a protein is simply mono-ubiquitinated or if only a small amount of the protein is modified, then this technique may not be a sensitive enough assay to identify it.

New Dynein Mutant Screen for Mutants in an ΔNCU06754 Background

A new screen was completed to isolate dynein mutants starting from an ΔNCU06754, *cot-1*^{ts} strain in hopes of one or more of the following occurring: 1) discovery of possible new ropy mutants with different phenotypes than those previously isolated, 2) isolation of mutants with dependency upon the absence of NCU06754 (i.e. synthetic ropies), 3) the identification of new C-terminal DHC mutants, if it was even possible to identify these in a screen such as this, or 4) the isolation of mutants in the pathway leading to NCU06754 activity upon the dynein complex. The screen was carried out in a similar fashion as the original dynein mutant screen.

Over 150 ropy mutants were isolated, purified and examined for growth and DIC mCherry distribution. Preliminary results indicate that although there were no mutants with a dependence on the absence of NCU06754 function (i.e., synthetic ropy mutants), three new classes of *in vivo* localization mutants were discovered (Figure 38). The first class is a mutant with bright spots of mCherry signal focused primarily at septa. The second has numerous sports of mCherry signal scattered throughout the hyphae with no apparent order. The final class displays a brighter haze of mCherry signal near hyphal tips while lacking any discernable structures like dots or comets as have been observed in previous classes. No mutants were identified from this screen that define other genes likely to function in the NCU06754 activation pathway.

NCU06754 Functions in Dynein Complex Assembly and Not Dynein Function

C-terminal DHC mutants have levels of DHC protein similar to wild-type (Figure 28) and those same strains used for dynein purification also have DHC protein levels

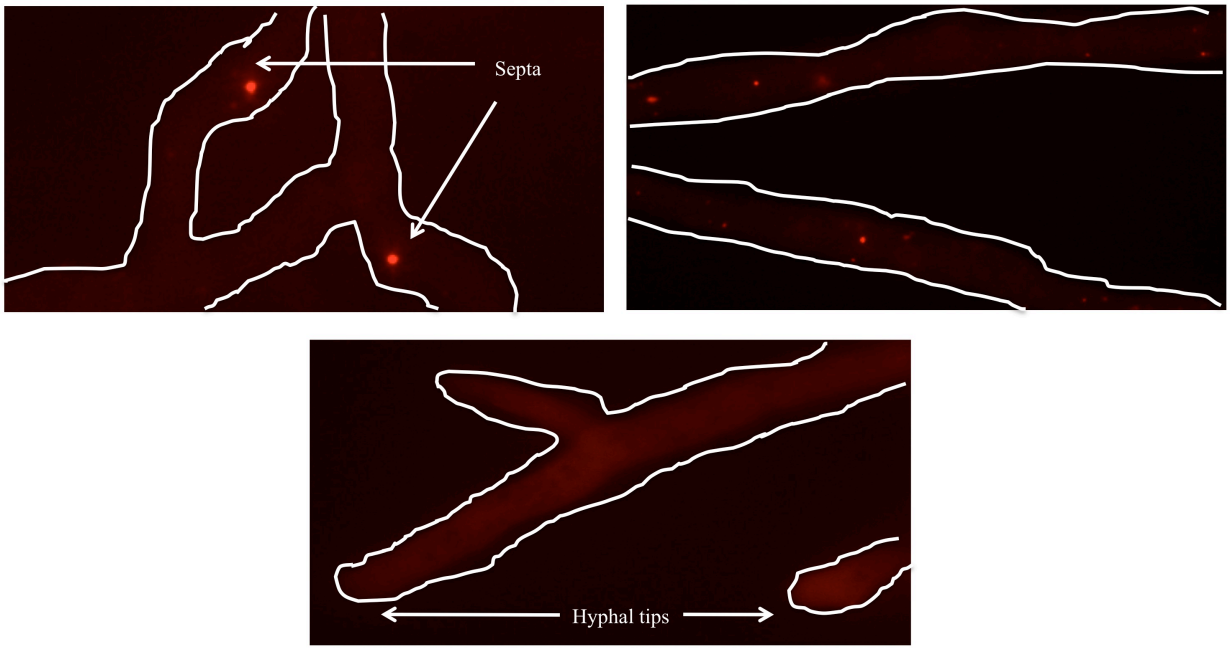

Figure 39. New classes of *in vivo* dynein localization isolated from dynein mutant screen in ΔNCU06754 background. Three new classes of *in vivo* localization mutants have been discovered from a recent dynein screen. The first class has bright mCherry spots located at septa (top left), the second bright mCherry spots scattered throughout the hyphae, and the third a brighter haze of mCherry signal near the hyphal tip with no identifiable structures. White lines were added to identify the hyphal walls.

similar to wild-type (Figure 34). These mutants also have a mild ropy growth phenotype and almost wild-type nuclear distribution (Figure 22). However, *in vivo* DIC mCherry localization is a diffuse haze of signal (Figure 22) and after purification is carried out, the DHC levels of C-terminal DHC proteins is about 30 fold lower than wild-type (Figure 31). Upon removal of NCU06754 activity, DHC C-terminal mutants return to more wild-type phenotypes for each of these properties. For both proper purification and DIC mCherry *in vivo* localization, DHC must associate with DIC. For C-terminal DHC mutants, this does not occur. However, when NCU06754 function is eliminated, this association of DIC and DHC can occur once again as indicated by the return to more wild-type like phenotypes. Loss of kinesin, Lis1, or dynactin activity does not bring about significant changes to DHC levels in a C-terminal mutant (Figure 33). This indicates that the negative impact of C-terminal DHC mutants occurs before the dynein cycle can begin. The cycle cannot begin because the dynein complex cannot properly assemble. NCU06754 activity in certain DHC mutants causes this lack of assembly. When this activity of NCU06754 is removed by either mutation or deletion, dynein is again able to assemble and carry out its cellular function as needed. Thus far, the cellular target of NCU06754 is unknown and the identity of this protein is critical for better understanding of the role of NCU06754 on the dynein complex.

REFERENCES

1. Ban KH, Torres JZ, Miller JJ, Mikhailov A, Nachury MV, Tung JJ, Rieder CL, Jackson PK. The END network couples spindle pole assembly to inhibition of the anaphase-promoting complex/cyclosome in early mitosis. Dev Cell 2007;13(1):29-42.

2. Banks GT, Haas MA, Line S, Shepherd HL, Alqatari M, Stewart S, Rishal I, Philpott A, Kalmar B, Kuta A and others. Behavioral and other phenotypes in a cytoplasmic Dynein light intermediate chain 1 mutant mouse. J Neurosci 2011;31(14):5483-94.

3. Benashski SE, Harrison A, Patel-King RS, King SM. Dimerization of the highly conserved light chain shared by dynein and myosin V. J Biol Chem 1997;272(33):20929-35.

4. Bielli A, Thornqvist PO, Hendrick AG, Finn R, Fitzgerald K, McCaffrey MW. The small GTPase Rab4A interacts with the central region of cytoplasmic dynein light intermediate chain-1. Biochem Biophys Res Commun 2001;281(5):1141-53.

5. Bonifacino JS, Weissman AM. Ubiquitin and the control of protein fate in the secretory and endocytic pathways. Annu Rev Cell Dev Biol 1998;14:19-57.

6. Borkovich KA, Alex LA, Yarden O, Freitag M, Turner GE, Read ND, Seiler S, Bell-Pedersen D, Paietta J, Plesofsky N and others. Lessons from the genome sequence of Neurospora crassa: tracing the path from genomic blueprint to multicellular organism. Microbiol Mol Biol Rev 2004;68(1):1-108.

7. Bothos J, Summers MK, Venere M, Scolnick DM, Halazonetis TD. The Chfr mitotic checkpoint protein functions with Ubc13-Mms2 to form Lys63-linked polyubiquitin chains. Oncogene 2003;22(46):7101-7.

8. Brault JB, Kudelko M, Vidalain PO, Tangy F, Despres P, Pardigon N. The interaction of flavivirus M protein with light chain Tctex-1 of human dynein plays a role in late stages of virus replication. Virology 2011;417(2):369-78.

9. Bruno KS, Aramayo R, Minke PF, Metzenberg RL, Plamann M. Loss of growth polarity and mislocalization of septa in a Neurospora mutant altered in the regulatory subunit of cAMP-dependent protein kinase. EMBO J 1996;15(21):5772-82.

10. Bruno KS, Tinsley JH, Minke PF, Plamann M. Genetic interactions among cytoplasmic dynein, dynactin, and nuclear distribution mutants of Neurospora crassa. Proc Natl Acad Sci U S A 1996;93(10):4775-80.

11. Brust-Mascher I, Scholey JM. Mitotic motors and chromosome segregation: the mechanism of anaphase B. Biochem Soc Trans 2011;39(5):1149-53.

12. Bullock SL, Ish-Horowicz D. Conserved signals and machinery for RNA transport in Drosophila oogenesis and embryogenesis. Nature 2001;414(6864):611-6.

13. Burgess SA, Knight PJ. Is the dynein motor a winch? Curr Opin Struct Biol 2004;14(2):138-46.

14. Burgess SA, Walker ML, Sakakibara H, Knight PJ, Oiwa K. Dynein structure and power stroke. Nature 2003;421(6924):715-8.

15. Burgess SA, Walker ML, White HD, Trinick J. Flexibility within myosin heads revealed by negative stain and single-particle analysis. J Cell Biol 1997;139(3):675-81.

16. Burroughs AM, Jaffee M, Iyer LM, Aravind L. Anatomy of the E2 ligase fold: implications for enzymology and evolution of ubiquitin/Ub-like protein conjugation. J Struct Biol 2008;162(2):205-18.

17. Busch H, Goldknopf IL. Ubiquitin - protein conjugates. Mol Cell Biochem 1981;40(3):173-87.

18. Cabeen MT, Jacobs-Wagner C. The bacterial cytoskeleton. Annu Rev Genet 2010;44:365-92.

19. Cappello S, Monzo P, Vallee RB. NudC is required for interkinetic nuclear migration and neuronal migration during neocortical development. Dev Biol 2011;357(2):326-35.

20. Carter AP, Cho C, Jin L, Vale RD. Crystal structure of the dynein motor domain. Science 2011;331(6021):1159-65.

21. Carter AP, Garbarino JE, Wilson-Kubalek EM, Shipley WE, Cho C, Milligan RA, Vale RD, Gibbons IR. Structure and functional role of dynein's microtubule-binding domain. Science 2008;322(5908):1691-5.

22. Carter AP, Vale RD. Communication between the AAA+ ring and microtubule-binding domain of dynein. Biochem Cell Biol 2010;88(1):15-21.

23. Caughey B, Baron GS, Chesebro B, Jeffrey M. Getting a grip on prions: oligomers, amyloids, and pathological membrane interactions. Annu Rev Biochem 2009;78:177-204.

24. Caviston JP, Ross JL, Antony SM, Tokito M, Holzbaur EL. Huntingtin facilitates dynein/dynactin-mediated vesicle transport. Proc Natl Acad Sci U S A 2007;104(24):10045-50.

25. Chen X-J, Levedakou EN, Millen KJ, Wollmann RL, Soliven B, Popko B. Proprioceptive Sensory Neuropathy in Mice with a Mutation in the Cytoplasmic Dynein Heavy Chain 1 Gene. The Journal of Neuroscience 2007;27(52):14515-14524.

26. Cho C, Reck-Peterson SL, Vale RD. Regulatory ATPase sites of cytoplasmic dynein affect processivity and force generation. J Biol Chem 2008;283(38):25839-45.

27. Ciechanover A, Schwartz AL. The ubiquitin-proteasome pathway: The complexity and myriad functions of proteins death. Proceedings of the National Academy of Sciences 1998;95(6):2727-2730.

28. Corcoran CA, Montalbano J, Sun H, He Q, Huang Y, Sheikh MS. Identification and characterization of two novel isoforms of Pirh2 ubiquitin ligase that negatively regulate p53 independent of RING finger domains. J Biol Chem 2009;284(33):21955-70.

29. Culver-Hanlon TL, Lex SA, Stephens AD, Quintyne NJ, King SJ. A microtubule-binding domain in dynactin increases dynein processivity by skating along microtubules. Nat Cell Biol 2006;8(3):264-70.

30. Deacon SW, Serpinskaya AS, Vaughan PS, Lopez Fanarraga M, Vernos I, Vaughan KT, Gelfand VI. Dynactin is required for bidirectional organelle transport. J Cell Biol 2003;160(3):297-301.

31. Deshaies RJ, Joazeiro CA. RING domain E3 ubiquitin ligases. Annu Rev Biochem 2009;78:399-434.

32. Dillman JF, 3rd, Pfister KK. Differential phosphorylation in vivo of cytoplasmic dynein associated with anterogradely moving organelles. J Cell Biol 1994;127(6 Pt 1):1671-81.

33. Ding C, Liang X, Ma L, Yuan X, Zhu X. Opposing effects of Ndel1 and alpha1 or alpha2 on cytoplasmic dynein through competitive binding to Lis1. J Cell Sci 2009;122(Pt 16):2820-7.

34. Dornan D, Shimizu H, Mah A, Dudhela T, Eby M, O'Rourke K, Seshagiri S, Dixit VM. ATM engages autodegradation of the E3 ubiquitin ligase COP1 after DNA damage. Science 2006;313(5790):1122-6.

35. Duan W, Gao L, Wu X, Zhang Y, Otterson GA, Villalona-Calero MA. Differential response between the p53 ubiquitin-protein ligases Pirh2 and MdM2 following DNA damage in human cancer cells. Exp Cell Res 2006;312(17):3370-8.

36. Eckley DM, Gill SR, Melkonian KA, Bingham JB, Goodson HV, Heuser JE, Schroer TA. Analysis of dynactin subcomplexes reveals a novel actin-related protein associated with the arp1 minifilament pointed end. J Cell Biol 1999;147(2):307-20.

37. Egan MJ, Tan K, Reck-Peterson SL. Lis1 is an initiation factor for dynein-driven organelle transport. J Cell Biol 2012.

38. Encalada SE, Szpankowski L, Xia CH, Goldstein LS. Stable kinesin and dynein assemblies drive the axonal transport of mammalian prion protein vesicles. Cell 2011;144(4):551-65.

39. Eshel D, Urrestarazu LA, Vissers S, Jauniaux JC, van Vliet-Reedijk JC, Planta RJ, Gibbons IR. Cytoplasmic dynein is required for normal nuclear segregation in yeast. Proc Natl Acad Sci U S A 1993;90(23):11172-6.

40. Espindola FS, Suter DM, Partata LB, Cao T, Wolenski JS, Cheney RE, King SM, Mooseker MS. The light chain composition of chicken brain myosin-Va: calmodulin, myosin-II essential light chains, and 8-kDa dynein light chain/PIN. Cell Motil Cytoskeleton 2000;47(4):269-81.

41. Feng Y, Olson EC, Stukenberg PT, Flanagan LA, Kirschner MW, Walsh CA. LIS1 regulates CNS lamination by interacting with mNudE, a central component of the centrosome. Neuron 2000;28(3):665-79.

42. Finley KR, Bouchonville KJ, Quick A, Berman J. Dynein-dependent nuclear dynamics affect morphogenesis in Candida albicans by means of the Bub2p spindle checkpoint. J Cell Sci 2008;121(Pt 4):466-76.

43. Freitag M, Hickey PC, Raju NB, Selker EU, Read ND. GFP as a tool to analyze the organization, dynamics and function of nuclei and microtubules in Neurospora crassa. Fungal Genet Biol 2004;41(10):897-910.

44. Gagnon JA, Mowry KL. Molecular motors: directing traffic during RNA localization. Crit Rev Biochem Mol Biol 2011;46(3):229-39.

45. Gao S, Alarcon C, Sapkota G, Rahman S, Chen PY, Goerner N, Macias MJ, Erdjument-Bromage H, Tempst P, Massague J. Ubiquitin ligase Nedd4L targets activated Smad2/3 to limit TGF-beta signaling. Mol Cell 2009;36(3):457-68.

46. Garcia-Mata R, Bebok Z, Sorscher EJ, Sztul ES. Characterization and dynamics of aggresome formation by a cytosolic GFP-chimera. J Cell Biol 1999;146(6):1239-54.

47. Gee MA, Heuser JE, Vallee RB. An extended microtubule-binding structure within the dynein motor domain. Nature 1997;390(6660):636-9.

48. Gennerich A, Vale RD. Walking the walk: how kinesin and dynein coordinate their steps. Curr Opin Cell Biol 2009;21(1):59-67.

49. Gibbons IR, Garbarino JE, Tan CE, Reck-Peterson SL, Vale RD, Carter AP. The affinity of the dynein microtubule-binding domain is modulated by the conformation of its coiled-coil stalk. J Biol Chem 2005;280(25):23960-5.

50. Gibbons IR, Garbarino JE, Tan CE, Reck-Peterson SL, Vale RD, Carter AP. The Affinity of the Dynein Microtubule-binding Domain Is Modulated by the Conformation of Its Coiled-coil Stalk. Journal of Biological Chemistry 2012;280(25):23960-23965.

51. Gibbons IR, Gibbons BH, Mocz G, Asai DJ. Multiple nucleotide-binding sites in the sequence of dynein beta heavy chain. Nature 1991;352(6336):640-3.

52. Gibbons IR, Lee-Eiford A, Mocz G, Phillipson CA, Tang WJ, Gibbons BH. Photosensitized cleavage of dynein heavy chains. Cleavage at the "V1 site" by irradiation at 365 nm in the presence of ATP and vanadate. J Biol Chem 1987;262(6):2780-6.

53. Gill SR, Cleveland DW, Schroer TA. Characterization of DLC-A and DLC-B, two families of cytoplasmic dynein light chain subunits. Mol Biol Cell 1994;5(6):645-54.

54. Glickman MH, Ciechanover A. The ubiquitin-proteasome proteolytic pathway: destruction for the sake of construction. Physiol Rev 2002;82(2):373-428.

55. Goldstein LS, Yang Z. Microtubule-based transport systems in neurons: the roles of kinesins and dyneins. Annu Rev Neurosci 2000;23:39-71.

56. Grava S, Keller M, Voegeli S, Seger S, Lang C, Philippsen P. Clustering of nuclei in multinucleated hyphae is prevented by dynein-driven bidirectional nuclear movements and microtubule growth control in Ashbya gossypii. Eukaryot Cell 2011;10(7):902-15.

57. Guo J, Yang Z, Song W, Chen Q, Wang F, Zhang Q, Zhu X. Nudel contributes to microtubule anchoring at the mother centriole and is involved in both dynein-dependent and -independent centrosomal protein assembly. Mol Biol Cell 2006;17(2):680-9.

58. Habura A, Tikhonenko I, Chisholm RL, Koonce MP. Interaction mapping of a dynein heavy chain. Identification of dimerization and intermediate-chain binding domains. J Biol Chem 1999;274(22):15447-53.

59. Hafezparast M, Klocke R, Ruhrberg C, Marquardt A, Ahmad-Annuar A, Bowen S, Lalli G, Witherden AS, Hummerich H, Nicholson S and others. Mutations in dynein link

motor neuron degeneration to defects in retrograde transport. Science 2003;300(5620):808-12.

60. Hall J, Song Y, Karplus PA, Barbar E. The crystal structure of dynein intermediate chain-light chain roadblock complex gives new insights into dynein assembly. J Biol Chem 2010;285(29):22566-75.

61. Hammer JA, Sellers JR. Walking to work: roles for class V myosins as cargo transporters. Nat Rev Mol Cell Biol 2012;13(1):13-26.

62. Hanson PI, Whiteheart SW. AAA+ proteins: have engine, will work. Nat Rev Mol Cell Biol 2005;6(7):519-29.

63. Harris SD, Momany M. Polarity in filamentous fungi: moving beyond the yeast paradigm. Fungal Genet Biol 2004;41(4):391-400.

64. Hattendorf DA, Lindquist SL. Analysis of the AAA sensor-2 motif in the C-terminal ATPase domain of Hsp104 with a site-specific fluorescent probe of nucleotide binding. Proc Natl Acad Sci U S A 2002;99(5):2732-7.

65. Hattendorf DA, Lindquist SL. Cooperative kinetics of both Hsp104 ATPase domains and interdomain communication revealed by AAA sensor-1 mutants. EMBO J 2002;21(1-2):12-21.

66. Hershko A, Ciechanover A. The ubiquitin system. Annu Rev Biochem 1998;67:425-79.

67. Hicke L. Gettin' down with ubiquitin: turning off cell-surface receptors, transporters and channels. Trends Cell Biol 1999;9(3):107-12.

68. Hirokawa N, Noda Y. Intracellular transport and kinesin superfamily proteins, KIFs: structure, function, and dynamics. Physiol Rev 2008;88(3):1089-118.

69. Hochrainer K, Kroismayr R, Baranyi U, Binder BR, Lipp J. Highly homologous HERC proteins localize to endosomes and exhibit specific interactions with hPLIC and Nm23B. Cell Mol Life Sci 2008;65(13):2105-17.

70. Hofmann RM, Pickart CM. In vitro assembly and recognition of Lys-63 polyubiquitin chains. J Biol Chem 2001;276(30):27936-43.

71. Hook P. The mechanical components of the dynein motor. ScientificWorldJournal 2010;10:857-64.

72. Hook P, Mikami A, Shafer B, Chait BT, Rosenfeld SS, Vallee RB. Long range allosteric control of cytoplasmic dynein ATPase activity by the stalk and C-terminal domains. J Biol Chem 2005;280(38):33045-54.

73. Hunt SD, Stephens DJ. The role of motor proteins in endosomal sorting. Biochem Soc Trans 2011;39(5):1179-84.

74. Igawa T, Fujiwara M, Takahashi H, Sawasaki T, Endo Y, Seki M, Shinozaki K, Fukao Y, Yanagawa Y. Isolation and identification of ubiquitin-related proteins from Arabidopsis seedlings. J Exp Bot 2009;60(11):3067-73.

75. Imamula K, Kon T, Ohkura R, Sutoh K. The coordination of cyclic microtubule association/dissociation and tail swing of cytoplasmic dynein. Proc Natl Acad Sci U S A 2007;104(41):16134-9.

76. Inoue S, Turgeon BG, Yoder OC, Aist JR. Role of fungal dynein in hyphal growth, microtubule organization, spindle pole body motility and nuclear migration. J Cell Sci 1998;111 (Pt 11):1555-66.

77. Iyadurai SJ, Li MG, Gilbert SP, Hays TS. Evidence for cooperative interactions between the two motor domains of cytoplasmic dynein. Curr Biol 1999;9(14):771-4.

78. Iyer LM, Leipe DD, Koonin EV, Aravind L. Evolutionary history and higher order classification of AAA+ ATPases. J Struct Biol 2004;146(1-2):11-31.

79. Johansson M, Rocha N, Zwart W, Jordens I, Janssen L, Kuijl C, Olkkonen VM, Neefjes J. Activation of endosomal dynein motors by stepwise assembly of Rab7-RILP-p150Glued, ORP1L, and the receptor betalll spectrin. J Cell Biol 2007;176(4):459-71.

80. Jung YS, Hakem A, Hakem R, Chen X. Pirh2 e3 ubiquitin ligase monoubiquitinates DNA polymerase eta to suppress translesion DNA synthesis. Mol Cell Biol 2011;31(19):3997-4006.

81. Jung YS, Qian Y, Chen X. The p73 tumor suppressor is targeted by Pirh2 RING finger E3 ubiquitin ligase for the proteasome-dependent degradation. J Biol Chem 2011.

82. Kapitein LC, Hoogenraad CC. Which way to go? Cytoskeletal organization and polarized transport in neurons. Mol Cell Neurosci 2011;46(1):9-20.

83. Karata K, Inagawa T, Wilkinson AJ, Tatsuta T, Ogura T. Dissecting the role of a conserved motif (the second region of homology) in the AAA family of ATPases. Site-directed mutagenesis of the ATP-dependent protease FtsH. J Biol Chem 1999;274(37):26225-32.

84. Kimura N, Inoue M, Okabayashi S, Ono F, Negishi T. Dynein dysfunction induces endocytic pathology accompanied by an increase in Rab GTPases: a potential mechanism underlying age-dependent endocytic dysfunction. J Biol Chem 2009;284(45):31291-302.

85. Kimura N, Okabayashi S, Ono F. Dynein dysfunction disrupts intracellular vesicle trafficking bidirectionally and perturbs synaptic vesicle docking via endocytic disturbances a potential mechanism underlying age-dependent impairment of cognitive function. Am J Pathol 2012;180(2):550-61.

86. King ML, Messitt TJ, Mowry KL. Putting RNAs in the right place at the right time: RNA localization in the frog oocyte. Biol Cell 2005;97(1):19-33.

87. King SJ, Bonilla M, Rodgers ME, Schroer TA. Subunit organization in cytoplasmic dynein subcomplexes. Protein Sci 2002;11(5):1239-50.

88. King SJ, Brown CL, Maier KC, Quintyne NJ, Schroer TA. Analysis of the dynein-dynactin interaction in vitro and in vivo. Mol Biol Cell 2003;14(12):5089-97.

89. Kitagawa K, Kotake Y, Kitagawa M. Ubiquitin-mediated control of oncogene and tumor suppressor gene products. Cancer Sci 2009;100(8):1374-81.

90. Kon T, Sutoh K, Kurisu G. X-ray structure of a functional full-length dynein motor domain. Nat Struct Mol Biol 2011;18(6):638-42.

91. Kon T, Oyama T, Shimo-Kon R, Imamula K, Shima T, Sutoh K, Kurisu G. The 2.8[thinsp]A crystal structure of the dynein motor domain. Nature 2012;advance online publication.

92. Koonce MP, Grissom PM, McIntosh JR. Dynein from Dictyostelium: primary structure comparisons between a cytoplasmic motor enzyme and flagellar dynein. J Cell Biol 1992;119(6):1597-604.

93. Kulikova S, Abatis M, Heng C, Lelievre V. Interkinetic nuclear migration: Reciprocal activities of dynein and kinesin. Cell Adh Migr 2011;5(4):277-9.

94. Lambreghts R, Shi M, Belden WJ, Decaprio D, Park D, Henn MR, Galagan JE, Basturkmen M, Birren BW, Sachs MS and others. A high-density single nucleotide polymorphism map for Neurospora crassa. Genetics 2009;181(2):767-81.

95. Lee MY, Ajjappala BS, Kim MS, Oh YK, Baek KH. DUB-1, a fate determinant of dynein heavy chain in B-lymphocytes, is regulated by the ubiquitin-proteasome pathway. J Cell Biochem 2008;105(6):1420-9.

96. Lees-Miller JP, Helfman DM, Schroer TA. A vertebrate actin-related protein is a component of a multisubunit complex involved in microtubule-based vesicle motility. Nature 1992;359(6392):244-6.

97. Lenartowska M, Walczewski J. [Myosin VI: the unique motor protein of the actin cytoskeleton]. Postepy Biochem 2011;57(1):63-73.

98. Leng RP, Lin Y, Ma W, Wu H, Lemmers B, Chung S, Parant JM, Lozano G, Hakem R, Benchimol S. Pirh2, a p53-induced ubiquitin-protein ligase, promotes p53 degradation. Cell 2003;112(6):779-91.

99. Liang J, Jaffrey SR, Guo W, Snyder SH, Clardy J. Structure of the PIN/LC8 dimer with a bound peptide. Nat Struct Biol 1999;6(8):735-40.

100. Liang Y, Yu W, Li Y, Yu L, Zhang Q, Wang F, Yang Z, Du J, Huang Q, Yao X and others. Nudel modulates kinetochore association and function of cytoplasmic dynein in M phase. Mol Biol Cell 2007;18(7):2656-66.

101. Lo KW, Kogoy JM, Pfister KK. The DYNLT3 light chain directly links cytoplasmic dynein to a spindle checkpoint protein, Bub3. J Biol Chem 2007;282(15):11205-12.

102. Logan IR, Sapountzi V, Gaughan L, Neal DE, Robson CN. Control of human PIRH2 protein stability: involvement of TIP60 and the proteosome. J Biol Chem 2004;279(12):11696-704.

103. Lopez-Franco R, Bartnicki-Garcia S, Bracker CE. Pulsed growth of fungal hyphal tips. Proc Natl Acad Sci U S A 1994;91(25):12228-32.

104. Kapitein LC, Kwok BH, Weinger JS, Schmidt CF, Kapoor TM, Peterman EJG. Microtubule cross-linking triggers the directional motility of kinesin-5. The Journal of Cell Biology 2008;182(3):421-428.

105. Ali MY, Lu H, Bookwalter CS, Warshaw DM, Trybus KM. Myosin V and Kinesin act as tethers to enhance each others' processivity. Proceedings of the National Academy of Sciences 2008;105(12):4691-4696.

106. Malone CJ, Misner L, Le Bot N, Tsai MC, Campbell JM, Ahringer J, White JG. The C. elegans hook protein, ZYG-12, mediates the essential attachment between the centrosome and nucleus. Cell 2003;115(7):825-36.

107. McKenney RJ, Weil SJ, Scherer J, Vallee RB. Mutually exclusive cytoplasmic dynein regulation by nude-LIS1 and dynactin. J Biol Chem 2011.

108. Merino-Gracia J, Garcia-Mayoral MF, Rodriguez-Crespo I. The association of viral proteins with host cell dynein components during virus infection. FEBS J 2011;278(17):2997-3011.

109. Mesngon MT, Tarricone C, Hebbar S, Guillotte AM, Schmitt EW, Lanier L, Musacchio A, King SJ, Smith DS. Regulation of cytoplasmic dynein ATPase by Lis1. J Neurosci 2006;26(7):2132-9.

110. Miki H, Setou M, Kaneshiro K, Hirokawa N. All kinesin superfamily protein, KIF, genes in mouse and human. Proc Natl Acad Sci U S A 2001;98(13):7004-11.

111. Minakhina S, Steward R. Axes formation and RNA localization. Curr Opin Genet Dev 2005;15(4):416-21.

112. Minke PF, Lee IH, Tinsley JH, Bruno KS, Plamann M. Neurospora crassa ro-10 and ro-11 genes encode novel proteins required for nuclear distribution. Mol Microbiol 1999;32(5):1065-76.

113. Mizuno N, Narita A, Kon T, Sutoh K, Kikkawa M. Three-dimensional structure of cytoplasmic dynein bound to microtubules. Proc Natl Acad Sci U S A 2007;104(52):20832-7.

114. Mocz G, Gibbons IR. Phase partition analysis of nucleotide binding to axonemal dynein. Biochemistry 1996;35(28):9204-11.

115. Mocz G, Gibbons IR. Model for the motor component of dynein heavy chain based on homology to the AAA family of oligomeric ATPases. Structure 2001;9(2):93-103.

116. Mok YK, Lo KW, Zhang M. Structure of Tctex-1 and its interaction with cytoplasmic dynein intermediate chain. J Biol Chem 2001;276(17):14067-74.

117. Morel M, Heraud C, Nicaise C, Suain V, Brion JP. Levels of kinesin light chain and dynein intermediate chain are reduced in the frontal cortex in Alzheimer's disease: implications for axoplasmic transport. Acta Neuropathol 2012;123(1):71-84.

118. Mori T, Li Y, Hata H, Kochi H. NIRF is a ubiquitin ligase that is capable of ubiquitinating PCNP, a PEST-containing nuclear protein. FEBS Lett 2004;557(1-3):209-14.

119. Mourino-Perez RR, Roberson RW, Bartnicki-Garcia S. Microtubule dynamics and organization during hyphal growth and branching in Neurospora crassa. Fungal Genet Biol 2006;43(6):389-400.

120. Munoz MA, Saunders DN, Henderson MJ, Clancy JL, Russell AJ, Lehrbach G, Musgrove EA, Watts CK, Sutherland RL. The E3 ubiquitin ligase EDD regulates S-phase and G(2)/M DNA damage checkpoints. Cell Cycle 2007;6(24):3070-7.

121. Muresan V, Stankewich MC, Steffen W, Morrow JS, Holzbaur EL, Schnapp BJ. Dynactin-dependent, dynein-driven vesicle transport in the absence of membrane proteins: a role for spectrin and acidic phospholipids. Mol Cell 2001;7(1):173-83.

122. Nakamura N, Fukuda H, Kato A, Hirose S. MARCH-II is a syntaxin-6-binding protein involved in endosomal trafficking. Mol Biol Cell 2005;16(4):1696-710.

123. Neely MD, Erickson HP, Boekelheide K. HMW-2, the Sertoli cell cytoplasmic dynein from rat testis, is a dimer composed of nearly identical subunits. Journal of Biological Chemistry 2012;265(15):8691-8698.

124. Neuwald AF, Aravind L, Spouge JL, Koonin EV. AAA+: A class of chaperone-like ATPases associated with the assembly, operation, and disassembly of protein complexes. Genome Res 1999;9(1):27-43.

125. Nurminsky DI, Nurminskaya MV, Benevolenskaya EV, Shevelyov YY, Hartl DL, Gvozdev VA. Cytoplasmic dynein intermediate-chain isoforms with different targeting properties created by tissue-specific alternative splicing. Mol Cell Biol 1998;18(11):6816-25.

126. Nyarko A, Hare M, Hays TS, Barbar E. The intermediate chain of cytoplasmic dynein is partially disordered and gains structure upon binding to light-chain LC8. Biochemistry 2004;43(49):15595-603.

127. Oakley BR, Oakley CE, Yoon Y, Jung MK. Gamma-tubulin is a component of the spindle pole body that is essential for microtubule function in Aspergillus nidulans. Cell 1990;61(7):1289-301.

128. Ochiai K, Watanabe M, Ueki H, Huang P, Fujii Y, Nasu Y, Noguchi H, Hirata T, Sakaguchi M, Huh NH and others. Tumor suppressor REIC/Dkk-3 interacts with the dynein light chain, Tctex-1. Biochem Biophys Res Commun 2011;412(2):391-5.

129. Ogawa K. Four ATP-binding sites in the midregion of the beta heavy chain of dynein. Nature 1991;352(6336):643-5.

130. Ogawa K, Mohri H. A dynein motor superfamily. Cell Struct Funct 1996;21(5):343-9.

131. Ogura T, Whiteheart SW, Wilkinson AJ. Conserved arginine residues implicated in ATP hydrolysis, nucleotide-sensing, and inter-subunit interactions in AAA and AAA+ ATPases. J Struct Biol 2004;146(1-2):106-12.

132. Osmani AH, Osmani SA, Morris NR. The molecular cloning and identification of a gene product specifically required for nuclear movement in Aspergillus nidulans. J Cell Biol 1990;111(2):543-51.

133. Paschal BM, Shpetner HS, Vallee RB. MAP 1C is a microtubule-activated ATPase which translocates microtubules in vitro and has dynein-like properties. J Cell Biol 1987;105(3):1273-82.

134. Paschal BM, Vallee RB. Retrograde transport by the microtubule-associated protein MAP 1C. Nature 1987;330(6144):181-183.

135. Pfister KK, Shah PR, Hummerich H, Russ A, Cotton J, Annuar AA, King SM, Fisher EM. Genetic analysis of the cytoplasmic dynein subunit families. PLoS Genet 2006;2(1):e1.

136. Plamann M, Minke PF, Tinsley JH, Bruno KS. Cytoplasmic dynein and actin-related protein Arp1 are required for normal nuclear distribution in filamentous fungi. J Cell Biol 1994;127(1):139-149.

137. Pulipati NR, Jin Q, Liu X, Sun B, Pandey MK, Huber JP, Ding W, Mulder KM. Overexpression of the dynein light chain km23-1 in human ovarian carcinoma cells inhibits tumor formation in vivo and causes mitotic delay at prometaphase/metaphase. Int J Cancer 2011;129(3):553-64.

138. Quintyne NJ, Gill SR, Eckley DM, Crego CL, Compton DA, Schroer TA. Dynactin is required for microtubule anchoring at centrosomes. J Cell Biol 1999;147(2):321-34.

139. Ramos-Garcia SL, Roberson RW, Freitag M, Bartnicki-Garcia S, Mourino-Perez RR. Cytoplasmic bulk flow propels nuclei in mature hyphae of Neurospora crassa. Eukaryot Cell 2009;8(12):1880-90.

140. Raux H, Flamand A, Blondel D. Interaction of the rabies virus P protein with the LC8 dynein light chain. J Virol 2000;74(21):10212-6.

141. Reiner O, Carrozzo R, Shen Y, Wehnert M, Faustinella F, Dobyns WB, Caskey CT, Ledbetter DH. Isolation of a Miller-Dieker lissencephaly gene containing G protein beta-subunit-like repeats. Nature 1993;364(6439):717-21.

142. Riehemann K, Sorg C. Sequence homologies between four cytoskeleton-associated proteins. Trends Biochem Sci 1993;18(3):82-3.

143. Riquelme M, Gierz G, Bartnicki-Garcia S. Dynein and dynactin deficiencies affect the formation and function of the Spitzenkorper and distort hyphal morphogenesis of Neurospora crassa. Microbiology 2000;146 (Pt 7):1743-52.

144. Riquelme M, Roberson RW, McDaniel DP, Bartnicki-Garcia S. The effects of ropy-1 mutation on cytoplasmic organization and intracellular motility in mature hyphae of Neurospora crassa. Fungal Genet Biol 2002;37(2):171-9.

145. Riquelme M, Yarden O, Bartnicki-Garcia S, Bowman B, Castro-Longoria E, Free SJ, Fleissner A, Freitag M, Lew RR, Mourino-Perez R and others. Architecture and development of the Neurospora crassa hypha -- a model cell for polarized growth. Fungal Biol 2011;115(6):446-74.

146. Roberts AJ, Numata N, Walker ML, Kato YS, Malkova B, Kon T, Ohkura R, Arisaka F, Knight PJ, Sutoh K and others. AAA+ Ring and linker swing mechanism in the dynein motor. Cell 2009;136(3):485-95.

147. Robzyk K, Recht J, Osley MA. Rad6-dependent ubiquitination of histone H2B in yeast. Science 2000;287(5452):501-4.

148. Roca MG, Kuo HC, Lichius A, Freitag M, Read ND. Nuclear dynamics, mitosis, and the cytoskeleton during the early stages of colony initiation in Neurospora crassa. Eukaryot Cell 2010;9(8):1171-83.

149. Rogel MR, Jaitovich A, Ridge KM. The role of the ubiquitin proteasome pathway in keratin intermediate filament protein degradation. Proc Am Thorac Soc 2010;7(1):71-6.

150. Roper M, Ellison C, Taylor JW, Glass NL. Nuclear and genome dynamics in multinucleate ascomycete fungi. Curr Biol 2011;21(18):R786-93.

151. Schmit JC, Brody S. Biochemical genetics of Neurospora crassa conidial germination. Bacteriol Rev 1976;40(1):1-41.

152. Schnyder T, Castello A, Feest C, Harwood NE, Oellerich T, Urlaub H, Engelke M, Wienands J, Bruckbauer A, Batista FD. B cell receptor-mediated antigen gathering requires ubiquitin ligase Cbl and adaptors Grb2 and Dok-3 to recruit dynein to the signaling microcluster. Immunity 2011;34(6):905-18.

153. Schoch CL, Aist JR, Yoder OC, Gillian Turgeon B. A complete inventory of fungal kinesins in representative filamentous ascomycetes. Fungal Genet Biol 2003;39(1):1-15.

154. Schroer TA. Dynactin. Annu Rev Cell Dev Biol 2004;20:759-79.

155. Schuster M, Kilaru S, Fink G, Collemare J, Roger Y, Steinberg G. Kinesin-3 and dynein cooperate in long-range retrograde endosome motility along a non-uniform microtubule array. Mol Biol Cell 2011.

156. Seiler S, Plamann M, Schliwa M. Kinesin and dynein mutants provide novel insights into the roles of vesicle traffic during cell morphogenesis in Neurospora. Curr Biol 1999;9(15):779-85.

157. Seiler S, Vogt N, Ziv C, Gorovits R, Yarden O. The STE20/germinal center kinase POD6 interacts with the NDR kinase COT1 and is involved in polar tip extension in Neurospora crassa. Mol Biol Cell 2006;17(9):4080-92.

158. Shaw SL, Yeh E, Maddox P, Salmon ED, Bloom K. Astral microtubule dynamics in yeast: a microtubule-based searching mechanism for spindle orientation and nuclear migration into the bud. J Cell Biol 1997;139(4):985-94.

159. Shloush J, Vlassov JE, Engson I, Duan S, Saridakis V, Dhe-Paganon S, Raught B, Sheng Y, Arrowsmith CH. Structural and functional comparison of the RING domains of two p53 E3 ligases, Mdm2 and Pirh2. J Biol Chem 2011;286(6):4796-808.

160. Silvanovich A, Li MG, Serr M, Mische S, Hays TS. The third P-loop domain in cytoplasmic dynein heavy chain is essential for dynein motor function and ATP-sensitive microtubule binding. Mol Biol Cell 2003;14(4):1355-65.

161. Sivagurunathan S, Schnittker RR, Razafsky DS, Nandini S, Plamann MD, King SJ. Analyses of Dynein Heavy Chain Mutations Reveal Complex Interactions between Dynein Motor Domains and Cellular Dynein Functions. Genetics 2012.

162. Smith DS, Niethammer M, Ayala R, Zhou Y, Gambello MJ, Wynshaw-Boris A, Tsai LH. Regulation of cytoplasmic dynein behaviour and microtubule organization by mammalian Lis1. Nat Cell Biol 2000;2(11):767-75.

163. Soltes G, Muller, Eric , D'Aversa, Teresa G. Ubiquitin, Ubiquitination, and Proteasomal Degradation in the Eukaryotic Cell: A Review. BIOS 2011.

164. Stangl K, Stangl V. The ubiquitin-proteasome pathway and endothelial (dys)function. Cardiovasc Res 2010;85(2):281-90.

165. Starr DA, Williams BC, Hays TS, Goldberg ML. ZW10 helps recruit dynactin and dynein to the kinetochore. J Cell Biol 1998;142(3):763-74.

166. Klumpp S, Lipowsky R. Cooperative cargo transport by several molecular motors. Proceedings of the National Academy of Sciences of the United States of America 2005;102(48):17284-17289.

167. Steffen W, Karki S, Vaughan KT, Vallee RB, Holzbaur EL, Weiss DG, Kuznetsov SA. The involvement of the intermediate chain of cytoplasmic dynein in binding the motor complex to membranous organelles of Xenopus oocytes. Mol Biol Cell 1997;8(10):2077-88.

168. Stehman SA, Chen Y, McKenney RJ, Vallee RB. NudE and NudEL are required for mitotic progression and are involved in dynein recruitment to kinetochores. J Cell Biol 2007;178(4):583-94.

169. Steinberg G. On the move: endosomes in fungal growth and pathogenicity. Nat Rev Microbiol 2007;5(4):309-16.

170. Stiess M, Bradke F. Neuronal polarization: the cytoskeleton leads the way. Dev Neurobiol 2011;71(6):430-44.

171. Su J, Liu YC. Foxp3 positive regulatory T cells: a functional regulation by the E3 ubiquitin ligase Itch. Semin Immunopathol 2010;32(2):149-56.

172. Su SB, Fang J, Fang D, Silver PB, Wen F, Li B, Ren X, Lin Q, Caspi RR. The role of TLR2, TRL3, TRL4, and TRL9 signaling in the pathogenesis of autoimmune disease in a retinal autoimmunity model. Invest Ophthalmol Vis Sci 2010;51(6):3092-9.

173. Suelmann R, Sievers N, Fischer R. Nuclear traffic in fungal hyphae: in vivo study of nuclear migration and positioning in Aspergillus nidulans. Mol Microbiol 1997;25(4):757-69.

174. Tai AW, Chuang JZ, Bode C, Wolfrum U, Sung CH. Rhodopsin's carboxy-terminal cytoplasmic tail acts as a membrane receptor for cytoplasmic dynein by binding to the dynein light chain Tctex-1. Cell 1999;97(7):877-87.

175. Tai CY, Dujardin DL, Faulkner NE, Vallee RB. Role of dynein, dynactin, and CLIP-170 interactions in LIS1 kinetochore function. J Cell Biol 2002;156(6):959-68.

176. Takahashi Y, Edamatsu M, Toyoshima YY. Multiple ATP-hydrolyzing sites that potentially function in cytoplasmic dynein. Proc Natl Acad Sci U S A 2004;101(35):12865-9.

177. Tan JM, Wong ES, Lim KL. Protein misfolding and aggregation in Parkinson's disease. Antioxid Redox Signal 2009;11(9):2119-34.

178. Tarricone C, Perrina F, Monzani S, Massimiliano L, Kim MH, Derewenda ZS, Knapp S, Tsai LH, Musacchio A. Coupling PAF signaling to dynein regulation: structure of LIS1 in complex with PAF-acetylhydrolase. Neuron 2004;44(5):809-21.

179. Uchida M, Mourino-Perez RR, Freitag M, Bartnicki-Garcia S, Roberson RW. Microtubule dynamics and the role of molecular motors in Neurospora crassa. Fungal Genet Biol 2008;45(5):683-92.

180. Vale RD. The molecular motor toolbox for intracellular transport. Cell 2003;112(4):467-80.

181. van Wijk SJL, Timmers HTM. The family of ubiquitin-conjugating enzymes (E2s): deciding between life and death of proteins. The FASEB Journal 2010;24(4):981-993.

182. Varma D, Dujardin DL, Stehman SA, Vallee RB. Role of the kinetochore/cell cycle checkpoint protein ZW10 in interphase cytoplasmic dynein function. J Cell Biol 2006;172(5):655-62.

183. Vaughan KT, Vallee RB. Cytoplasmic dynein binds dynactin through a direct interaction between the intermediate chains and p150Glued. J Cell Biol 1995;131(6 Pt 1):1507-16.

184. Allan VJ. Cytoplasmic dynein. Biochemical Society Transactions 2012;39(5):1169-1178.

185. Efimov VP, Morris NR. The Lis1-Related Nudf Protein of Aspergillus nidulans Interacts with the Coiled-Coil Domain of the Nude/Ro11 Protein. The Journal of Cell Biology 2000;150(3):681-688.

186. Wakana Y, Takai S, Nakajima K, Tani K, Yamamoto A, Watson P, Stephens DJ, Hauri HP, Tagaya M. Bap31 is an itinerant protein that moves between the peripheral endoplasmic reticulum (ER) and a juxtanuclear compartment related to ER-associated Degradation. Mol Biol Cell 2008;19(5):1825-36.

187. Walker ML, Burgess SA, Sellers JR, Wang F, Hammer JA, 3rd, Trinick J, Knight PJ. Two-headed binding of a processive myosin to F-actin. Nature 2000;405(6788):804-7.

188. Wan Y, Yang Z, Guo J, Zhang Q, Zeng L, Song W, Xiao Y, Zhu X. Misfolded Gbeta is recruited to cytoplasmic dynein by Nudel for efficient clearance. Cell Res 2012.

189. Wang Q, Song C, Irizarry L, Dai R, Zhang X, Li CC. Multifunctional roles of the conserved Arg residues in the second region of homology of p97/valosin-containing protein. J Biol Chem 2005;280(49):40515-23.

190. Wang Z, Yang B, Dong L, Peng B, He X, Liu W. A novel oncoprotein Pirh2: rising from the shadow of MDM2. Cancer Sci 2011;102(5):909-17.

191. Wanschers B, van de Vorstenbosch R, Wijers M, Wieringa B, King SM, Fransen J. Rab6 family proteins interact with the dynein light chain protein DYNLRB1. Cell Motil Cytoskeleton 2008;65(3):183-96.

192. Weedon MN, Hastings R, Caswell R, Xie W, Paszkiewicz K, Antoniadi T, Williams M, King C, Greenhalgh L, Newbury-Ecob R and others. Exome Sequencing Identifies a

DYNC1H1 Mutation in a Large Pedigree with Dominant Axonal Charcot-Marie-Tooth Disease. Am J Hum Genet 2011;89(2):308-12.

193. Whibley C, Pharoah PD, Hollstein M. p53 polymorphisms: cancer implications. Nat Rev Cancer 2009;9(2):95-107.

194. Wilkerson CG, King SM, Koutoulis A, Pazour GJ, Witman GB. The 78,000 M(r) intermediate chain of Chlamydomonas outer arm dynein isa WD-repeat protein required for arm assembly. J Cell Biol 1995;129(1):169-78.

195. Williams JC, Roulhac PL, Roy AG, Vallee RB, Fitzgerald MC, Hendrickson WA. Structural and thermodynamic characterization of a cytoplasmic dynein light chain-intermediate chain complex. Proc Natl Acad Sci U S A 2007;104(24):10028-33.

196. Wu G, Sun M, Zhang L, Zhou J, Wang Y, Huo K. A novel hPirh2 splicing variant without ubiquitin protein ligase activity interacts with p53 and is down-regulated in hepatocellular carcinoma. FEBS Lett 2010;584(13):2772-8.

197. Xiang X, Fischer R. Nuclear migration and positioning in filamentous fungi. Fungal Genet Biol 2004;41(4):411-9.

198. Xiang X, Roghi C, Morris NR. Characterization and localization of the cytoplasmic dynein heavy chain in Aspergillus nidulans. Proc Natl Acad Sci U S A 1995;92(21):9890-4.

199. Yang X, Li H, Zhou Z, Wang WH, Deng A, Andrisani O, Liu X. Plk1-mediated phosphorylation of Topors regulates p53 stability. J Biol Chem 2009;284(28):18588-92.

200. Yarden O, Plamann M, Ebbole DJ, Yanofsky C. cot-1, a gene required for hyphal elongation in Neurospora crassa, encodes a protein kinase. EMBO J 1992;11(6):2159-66.

201. Yoshida H, Kitagishi Y, Okumura N, Murakami M, Nishimura Y, Matsuda S. How do you RUN on? FEBS Lett 2011;585(12):1707-10.

202. Zhang L, Anglesio MS, O'Sullivan M, Zhang F, Yang G, Sarao R, Mai PN, Cronin S, Hara H, Melnyk N and others. The E3 ligase HACE1 is a critical chromosome 6q21 tumor suppressor involved in multiple cancers. Nat Med 2007;13(9):1060-9.

203. Zhong Q, Gao W, Du F, Wang X. Mule/ARF-BP1, a BH3-only E3 ubiquitin ligase, catalyzes the polyubiquitination of Mcl-1 and regulates apoptosis. Cell 2005;121(7):1085-95.

VITA

Ryan Lee Elsenpeter was born January 11th, 1982 in Coon Rapids, Minnesota. He graduated from Anoka High School in Anoka, Minnesota in 2000. In May 2005, Ryan graduated from the University of Wisconsin – La Crosse in La Crosse, Wisconsin with a Bachelor of Science in both Cell and Molecular Biology and Biochemistry. In August 2005, Ryan started graduate studies at the University of Missouri – Kansas City in Kansas City, Missouri. He received a Master's degree in Cell and Molecular Biology in 2007.